OPTIMIZATION OF A PAVEMENT INSTRUMENTATION PLAN FOR A FULL-SCALE TEST ROAD: EVALUATION

BDV31-977-04

Final Report

Submitted by:

Jennifer A. Rice, Ph.D.
Principal Investigator
Department of Civil and Coastal Engineering
University of Florida
jrice@ce.ufl.edu

Submitted to:

Sandra Bell
Business Systems Coordinator
FDOT Research Center
sandra.bell@dot.state.fl.us

April 30, 2014

Disclaimer

The opinions, findings, and conclusions expressed in this publication are those of the authors and not necessarily those of the State of Florida Department of Transportation.

Approximate Conversion to SI Units

SYMBOL	WHEN YOU KNOW	MULTIPLY BY	TO FIND	SYMBOL
LENGTH				
in	inches	25.4	millimeters	mm
ft	feet	0.305	meters	m
yd	yards	0.914	meters	m
mi	miles	1.61	kilometers	km

SYMBOL	WHEN YOU KNOW	MULTIPLY BY	TO FIND	SYMBOL
AREA				
in^2	square inches	645.2	square millimeters	mm^2
ft^2	square feet	0.093	square meters	m^2
yd^2	square yard	0.836	square meters	m^2
ac	acres	0.405	hectares	ha
mi^2	square miles	2.59	square kilometers	km^2

SYMBOL	WHEN YOU KNOW	MULTIPLY BY	TO FIND	SYMBOL
VOLUME				
fl oz	fluid ounces	29.57	milliliters	mL
gal	gallons	3.785	liters	L
ft^3	cubic feet	0.028	cubic meters	m^3
yd^3	cubic yards	0.765	cubic meters	m^3
NOTE: volumes greater than 1000 L shall be shown in m^3				

SYMBOL	WHEN YOU KNOW	MULTIPLY BY	TO FIND	SYMBOL
MASS				
oz	ounces	28.35	grams	g
lb	pounds	0.454	kilograms	kg
T	short tons (2000 lb)	0.907	megagrams (or "metric ton")	Mg (or "t")

SYMBOL	WHEN YOU KNOW	MULTIPLY BY	TO FIND	SYMBOL
TEMPERATURE (exact degrees)				
°F	Fahrenheit	5 (F-32)/9 or (F-32)/1.8	Celsius	°C

SYMBOL	WHEN YOU KNOW	MULTIPLY BY	TO FIND	SYMBOL
ILLUMINATION				
fc	foot-candles	10.76	lux	lx
fl	foot-Lamberts	3.426	candela/m^2	cd/m^2

SYMBOL	WHEN YOU KNOW	MULTIPLY BY	TO FIND	SYMBOL
FORCE and PRESSURE or STRESS				
lbf	pound force	4.45	newtons	N
lbf/in^2	pound force per square inch	6.89	kilopascals	kPa

Approximate Conversion to SI Units

SYMBOL	WHEN YOU KNOW	MULTIPLY BY	TO FIND	SYMBOL
LENGTH				
mm	millimeters	0.039	inches	in
m	meters	3.28	feet	ft
m	meters	1.09	yards	yd
km	kilometers	0.621	miles	mi

SYMBOL	WHEN YOU KNOW	MULTIPLY BY	TO FIND	SYMBOL
AREA				
mm^2	square millimeters	0.0016	square inches	in^2
m^2	square meters	10.764	square feet	ft^2
m^2	square meters	1.195	square yards	yd^2
ha	hectares	2.47	acres	ac
km^2	square kilometers	0.386	square miles	mi^2

SYMBOL	WHEN YOU KNOW	MULTIPLY BY	TO FIND	SYMBOL
VOLUME				
mL	milliliters	0.034	fluid ounces	fl oz
L	liters	0.264	gallons	gal
m^3	cubic meters	35.314	cubic feet	ft^3
m^3	cubic meters	1.307	cubic yards	yd^3

SYMBOL	WHEN YOU KNOW	MULTIPLY BY	TO FIND	SYMBOL
MASS				
g	grams	0.035	ounces	oz
kg	kilograms	2.202	pounds	lb
Mg (or "t")	megagrams (or "metric ton")	1.103	short tons (2000 lb)	T

SYMBOL	WHEN YOU KNOW	MULTIPLY BY	TO FIND	SYMBOL
TEMPERATURE (exact degrees)				
°C	Celsius	1.8C+32	Fahrenheit	°F

SYMBOL	WHEN YOU KNOW	MULTIPLY BY	TO FIND	SYMBOL
ILLUMINATION				
lx	lux	0.0929	foot-candles	fc
cd/m^2	candela/m^2	0.2919	foot-Lamberts	fl

SYMBOL	WHEN YOU KNOW	MULTIPLY BY	TO FIND	SYMBOL
FORCE and PRESSURE or STRESS				
N	newtons	0.225	poundforce	lbf
kPa	kilopascals	0.145	poundforce per square inch	lbf/in^2

1. Report No.	2. Government Accession No.	3. Recipient's Catalog No.
4. Title and Subtitle OPTIMIZATION OF A PAVEMENT INSTRUMENTATION PLAN FOR A FULL-SCALE TEST ROAD: EVALUATION		5. Report Date April 2014 6. Performing Organization Code
7. Author(s) Jennifer A. Rice, Ph.D., James Lloyd		8. Performing Organization Report No.
9. Performing Organization Name and Address University of Florida Engineering School of Sustainable Infrastructure & Environment University of Florida 365 Weil Hall / PO Box 116550 Gainesville, FL 32611		10. Work Unit No. (TRAIS) 11. Contract or Grant No. BDV31-977-04
12. Sponsoring Agency Name and Address Florida Department of Transportation 605 Suwannee Street, MS 30 Tallahassee, FL 32399		13. Type of Report and Period Covered Draft Final Report 5/28/2013 – 04/30/2014 14. Sponsoring Agency Code
15. Supplementary Notes		

16. Abstract

A 2.5-mile, concrete test road is planned for construction by the Florida Department of Transportation (FDOT) in 2016. To support the goals of the test road, a comprehensive instrumentation system is required to provide reliable data over a long period. The unique challenges posed by the geographical location and configuration of the test pavement require sensors that can employ long sensor cables without compromising data quality and have limited susceptibility to damage from lightning strike. The research conducted for this report investigated the availability and performance of traditional and emerging instrumentation approaches for the embedded measurement of concrete strains and temperatures. Fiber optic sensors possess features that overcome the specific challenges of the proposed test pavement and were chosen for experimental evaluation alongside the copper-based sensors that have been routinely employed by the State Materials Office (SMO). The candidate strain sensors were initially evaluated in a series of non-embedded tests to assess their measurement capabilities, noise susceptibility, temperature sensitivity, and ease of installation and use. A small concrete test slab was then constructed for longer-term evaluation of the various sensor types in conditions similar to those of the proposed test road. The duration of the test slab experiments (several weeks) exposed the slab to environmentally-induced loads and dynamic wheel loads imposed by a Heavy Vehicle Simulator. The resulting strain and temperature measurements were analyzed to assess the accuracy, repeatability, and robustness of the sensors. The copper and fiber optic strain sensors yielded similar measurement results; however, the fiber optic sensors provided a more streamlined installation and setup process. The cost of the individual fiber optic sensors is higher than the copper sensors; however, the fiber optic sensors require fewer data acquisition (DAQ) units. A hybrid instrumentation plan (copper/fiber optic) is suggested to optimize instrumentation costs while ensuring the measurement needs and data quality requirements of the test pavement are met.

17. Key Word	18. Distribution Statement
Test pavement, embedded strain sensor, fiber optic sensor, data acquisition	No restrictions

19. Security Classif. (of this report)	20. Security Classif. (of this page)	21. No. of Pages	22. Price
Unclassified	Unclassified	143	

Executive Summary

A 2.5-mile, concrete test road is planned for construction by the Florida Department of Transportation (FDOT) in 2016, which will result in the largest experimental pavement in the southeastern U.S. The test pavement will enable the evaluation of a range of materials and construction practices to improve the performance and economics of future pavement designs in the state of Florida. To support the goals of the test road, a comprehensive instrumentation system is required. This instrumentation system must meet the measurement needs of the pavement analysis project by providing reliable data over a long time period (up to ten years). The unique challenges posed by the geographical location and configuration of the test pavement require sensors that can employ long sensor cables without compromising data quality and have limited susceptibility to damage from lightning strike.

The research conducted for this report investigated the availability and performance of traditional and emerging instrumentation approaches for the embedded measurement of concrete strains and temperatures. Fiber optic sensors provide an alternative to commonly used copper-based sensors and possess features that overcome the specific challenges of the proposed test pavement. A preliminary background investigation indicated that the sensors and data acquisition (DAQ) components offered by Micron Optics, Inc., provide the functionality and reliability required for the test road evaluation. These sensors were chosen for experimental evaluation alongside the copper-based sensors that have been routinely employed by the State Materials Office (SMO) in their Accelerated Pavement Testing program.

The candidate strain sensors were initially evaluated in a series of non-embedded tests to assess their measurement capabilities, noise susceptibility, temperature sensitivity, and ease of installation and use. These preliminary tests demonstrated the viability of the fiber optic sensors for data collection in a range of measurement conditions. A small concrete test slab was constructed for longer-term evaluation of the various sensor types in conditions similar to those of the proposed test road. The duration of the test slab experiments (several weeks) exposed the slab to environmentally-induced loads and dynamic wheel loads imposed by a Heavy Vehicle Simulator. The resulting strain and temperature measurements were analyzed to assess the accuracy, repeatability, and robustness of the sensors. The copper and fiber optic strain sensors

yielded similar measurement results; however, the Micron Optic sensors provided a more streamlined installation and setup process.

The costs of the candidate sensors and DAQ systems are a critical aspect of the selection and design of the instrumentation plan for the test road. The cost of the individual fiber optic sensors is higher than the copper sensors; however, the fiber optic sensors require fewer data collection units as a result of their sensing mechanism. Maintaining a lower DAQ unit count lowers the overall instrumentation system costs and future maintenance. A hybrid instrumentation plan (copper/fiber optic) is suggested to optimize instrumentation costs while ensuring the measurement needs and data quality requirements of the project are met.

Table of Contents

Disclaimer ii

Approximate Conversion to SI Units iii

Technical Report Documentation Page v

Executive Summary vi

Table of Contents viii

List of Figures xii

List of Tables xvii

1 Introduction 1

1.1 Project Description 1
1.2 Objective 2
1.3 Challenges 2
1.4 Potential Solutions 3
1.5 Report Organization 3

2 Pavement Instrumentation Background 5

2.1 Test Pavements 5
2.1.1 Auburn Case Study 5
2.1.2 MnROAD Case Study 6
2.2 Data Acquisition and Sensing Fundamentals 8
2.3 Traditional/Electronic Sensors 8
2.3.1 Available Sensors 9
2.3.2 Data Acquisition 13
2.3.3 Advantages 13
2.3.4 Disadvantages 14

2.4 Fiber Optic Sensors 14
2.4.1 Terminology 15
2.4.2 Available Sensors 16
2.4.3 Data Acquisition 19
2.4.4 Case Studies 21
2.4.5 Advantages 22
2.4.6 Disadvantages 23
2.5 System Comparison 23
2.6 Cost Analysis 24
2.7 Background Summary 25

3 Initial Testing and Evaluation 27

3.1 Data Acquisition and Archiving 28
3.2 Compression Test 51
3.2.1 Specimen Description 51
3.2.2 Testing Equipment 53
3.2.3 Procedure 53
3.2.4 Results 54
3.3 Sensor Extraction 58
3.4 Tension Test 60
3.4.1 Specimen Description and Sensor Layout 60
3.4.2 Testing Equipment 63
3.4.3 Procedure 64
3.4.4 Results 65
3.5 Temperature Test 71
3.5.1 Specimen Description 72
3.5.2 Testing Equipment 72
3.5.3 Procedure 73
3.5.4 Results 74
3.6 Noise Test 77
3.6.1 Specimen Description 77

3.6.2 Testing Equipment....77
3.6.3 Procedure....78
3.6.4 Results....78
3.7 Initial Testing Conclusion....83

4 Embedded Testing....85

4.1 Introduction....85
4.2 Test Setup....86
4.2.1 Slab Description....86
4.2.2 Sensor Layout....86
4.2.3 Installation Considerations....90
4.2.4 Data Acquisition....91
4.2.5 Heavy Vehicle Simulator....93
4.3 Tests....94
4.3.1 Curing Tests....94
4.3.2 Dynamic Tests....101
4.3.3 National Instruments PXI Tests....113
4.3.4 Geokon Data....116
4.4 Embedded Testing Conclusions....118

5 Conclusions and Recommendations....121

5.1 Summary....121
5.2 Recommendations....122

References....124

Appendix A: Out of Pavement Raw Data....128

Cylinder Compression Data....128
Tension Data....129
Temperature Data....130

Appendix B: Additional Embedded Dynamic Analysis....133

Raw Data 133
Peak Analysis.....138
Data Repeatability Analysis – Peaks 141
Strain Distribution 144

List of Figures

Figure 1-1. FDOT US-301 concrete test road location. 1
Figure 2-1. NCAT test track at Auburn, AL (NCAT, 2013). 6
Figure 2-2. MnROAD at Albertville, MN (Jensen, 2011). 6
Figure 2-3. Results from phase I research 1994-2006 (Jensen, 2011). 7
Figure 2-4. Vishay EGP-5-120 embeddable dynamic strain gauge. 10
Figure 2-5. Tokyo Sokki KM-100BT embeddable static strain gauge. 10
Figure 2-6. Tokyo Sokki PML-60-2L embeddable dynamic strain gauge. 10
Figure 2-7. Geokon 4200A-2 embeddable vibrating wire sensor. 11
Figure 2-8. Geokon 3900 embeddable dynamic strain gauge. 11
Figure 2-9. Illustration of Irrometer Watermark 200SS soil moisture sensors. 13
Figure 2-10. Working/Operating Principle of FBG sensors (Botsis et al., 2005). 15
Figure 2-11. os3600 embeddable strain sensor. 17
Figure 2-12. os3610 surface mount strain sensor. 18
Figure 2-13. os4350 non-metallic temperature sensor. 19
Figure 2-14. sm130 interrogator field module. 20
Figure 2-15. sm230 rack mount interrogator. 20
Figure 2-16. ENLIGHT acquisition tab. 21
Figure 3-1. Electric hum noise aliased into measured signal. 48
Figure 3-2. Measured electrical hum noise in the time domain using NI Compact DAQ and foil strain gauges. 49
Figure 3-3. Measured electrical hum noise in the frequency domain using NI Compact DAQ and foil strain gauges. 49
Figure 3-4. FIR filter to reduce 60-Hz noise in strain measurements. 50
Figure 3-5. Sensor layout for formwork of the concrete cylinder specimen. 52
Figure 3-6. Finished concrete cylinder specimen. 52
Figure 3-7. Instron UTM being used for concrete cylinder compression test. 53
Figure 3-8. 5 k compression strain measurements and sensor measurement difference. 55
Figure 3-9. 20 k compression strain measurements and sensor measurement difference. 56
Figure 3-10. Ramp and hold compression strain measurements. 57

Figure 3-11. Dynamic compression strain measurements. 58
Figure 3-12. Transverse cut along top and bottom. 59
Figure 3-13. Longitudinal cut. 59
Figure 3-14. Prying technique used for sensor removal. 60
Figure 3-15. Micron Optics os3600 after extraction. 60
Figure 3-16 Steel plate sensor layout. 62
Figure 3-17. Sensor layout before installation of os3610. 62
Figure 3-18. Sensor layout after installation of os3610. 63
Figure 3-19. Instron UTM being used for steel plate tension test. 64
Figure 3-20. 2 k tension strain measurements and sensor measurement differences. 66
Figure 3-21. 20 k tension strain measurements and sensor measurement differences. 67
Figure 3-22. Dynamic compression strain measurements. 70
Figure 3-23. Blue M CEO9xx-4 test chamber. 72
Figure 3-24. Temperature test setup inside environmental chamber. 73
Figure 3-25. Strain readings during heating: temperature (top), strain (middle) and strain vs. temperature (bottom). 75
Figure 3-26. Strain readings during cooling: temperature (top), strain (middle) and strain vs. temperature (bottom). 76
Figure 3-27. 1 Hz noise tests: Fiber optic (top), foil gauge (middle), and thermocouple (bottom). 79
Figure 3-28. 100 Hz noise tests: Fiber optic (top), foil gauge (middle), and thermocouple (bottom). 80
Figure 3-29. 500 Hz noise tests: Fiber optic (top), foil gauge (middle), and thermocouple (bottom). 81
Figure 3-30. 500 Hz noise analysis frequency responses. 82
Figure 4-1. Thermocouple tree. 87
Figure 4-2. Sensor layout – bottom. 89
Figure 4-3. Sensor layout – top. 89
Figure 4-4. Strain gauge tree. 90
Figure 4-5. Sensor layout – full. 90
Figure 4-6. HVS exterior. 93

Figure 4-7. HVS interior. 94
Figure 4-8. Slab and ambient temperatures during and after curing. 95
Figure 4-9. Temperature vs. strain response. 97
Figure 4-10. Slab temperatures corresponding to the minimum measured temperature gradient (left), the average ambient temperature (middle), and the maximum measured temperature gradient (right). 99
Figure 4-11. Minimum simplified temperature and strain gradients. 100
Figure 4-12. Maximum simplified temperature and strain gradients. 100
Figure 4-13. Representative dynamic plot. 102
Figure 4-14. Representative dynamic plot – zoomed view. 103
Figure 4-15. Sensory summary graph. 104
Figure 4-16. Strain vs. time of day – 15 kip. 105
Figure 4-17. Strain vs. ambient temperature – 15 kip. 106
Figure 4-18. Peak strain vs. slab temperature – 15 kip. 106
Figure 4-19. Micron Optics repeatability plot – 15 kip. 107
Figure 4-20. Tokyo Sokki repeatability plot – 15 kip. 108
Figure 4-21. Vishay repeatability plot – 15 kip. 108
Figure 4-22. Micron Optics noise plot. 109
Figure 4-23. Tokyo Sokki noise plot. 110
Figure 4-24. Vishay noise plot. 110
Figure 4-25. Micron Optics strain distribution – 15 kip. 112
Figure 4-26. Tokyo Sokki strain distribution – 15 kip. 112
Figure 4-27. Vishay strain distribution – 15 kip. 113
Figure 4-28. Micron Optics temperatures using PXIe-4844 interrogator. 114
Figure 4-29. Representative dynamic plot. 115
Figure 4-30. Dynamic data from the PXIe-4844 interrogator, sampled at 10 Hz. 116
Figure 4-31. Dynamic data from the sm-130 interrogator, sampled at 500 Hz. 116
Figure 4-32. Geokon ensemble temperatures. 117
Figure 4-33. Geokon individual strain. 118
Figure 4-34. Geokon ensemble strain. 118
Figure A-1. Compression strain results. 128

Figure A-2. Tension strain results. 129
Figure A-3. Cooling strain readings. 130
Figure A-4. Heating strain readings. 131
Figure A-5. Hot (left) and cold (right) strain readings. 131
Figure A-6. Room temperature strain readings. 132
Figure B-1. November 4th 3:00 PM 9-kip dynamic test along row 1, separate plot for each row of sensors. 133
Figure B-2. November 4th 3:00 PM 12-kip dynamic test along row 1, separate plot for each row of sensors. 134
Figure B-3. November 4th 3:00 PM 15-kip dynamic test along row 1, separate plot for each row of sensors. 135
Figure B-4. November 4th 3:00 PM 15-kip dynamic test along row 1, top sensors. 136
Figure B-5. November 4th 3:00 PM 15-kip dynamic test along row 1, top sensors – zoomed view. 136
Figure B-6. November 4th 3:00 PM 15-kip dynamic test along row 1, unfiltered data without detrending. 137
Figure B-7. November 4th 3:00 PM 15-kip dynamic test along row 1, unfiltered data without detrending – zoomed view. 137
Figure B-8. Strain vs. time of day – 9 kip. 138
Figure B-9. Strain vs. ambient temperature – 9 kip. 138
Figure B-10. Strain vs. slab temperature – 9 kip. 139
Figure B-11. Strain vs. time of day – 12 kip. 139
Figure B-12. Strain vs. ambient temperature – 12 kip. 140
Figure B-13. Strain vs. slab temperature – 12 kip. 140
Figure B-14. Micron Optics repeatability plot – 9 kip. 141
Figure B-15. Tokyo Sokki repeatability plot – 9 kip. 141
Figure B-16. Vishay repeatability plot – 9 kip. 142
Figure B-17. Micron Optics repeatability plot – 12 kip. 142
Figure B-18. Tokyo Sokki repeatability plot – 12 kip. 143
Figure B-19. Vishay repeatability plot – 12 kip. 143
Figure B-20. Micron Optics strain distribution – 9 kip. 144

Figure B-21. Tokyo Sokki strain distribution – 9 kip. 144
Figure B-22. Vishay strain distribution – 9 kip. 145
Figure B-23. Micron Optics strain distribution – 12 kip. 145
Figure B-24. Tokyo Sokki strain distribution – 12 kip. 146
Figure B-25. Vishay strain distribution – 12 kip. 146

List of Tables

Table 2-1. Summary of technical specifications for electronic strain sensors. 12
Table 2-2. Unit price cost summary. 25
Table 3-1. Compression load cases. 54
Table 3-2. Static hold compression load results. 57
Table 3-3 Static tensile load cases. 64
Table 3-4. Static hold tension load results for os3610 compared to the foil strain gauge. 68
Table 3-5. Static hold tension load results for os3110 compared to the foil strain gauge. 68
Table 3-6. Static hold tension load results for os3610 compared to the os3110. 69
Table 3-7. Noise during tension test. 69
Table 3-8. Dynamic tension test results compared to the foil gauge readings. 71
Table 3-9. Various temperatures tested. 74
Table 3-10. Noise analysis results. 82
Table 4-1. Slab sensors. 87
Table 4-2. Temperature and strain gradient summary table. 101
Table 4-3. Sensor analysis table 104
Table 4-4. Peak strain variations due to ambient and slab temperatures. 107

1 Introduction

1.1 Project Description

The Florida Department of Transportation (FDOT) is planning to construct a 2.5-mile concrete test road starting in 2016. This test road will be located just off US-301 in Clay County, Florida, as shown in Figure 1-1. Traffic will be periodically diverted from the test highway back to the existing roadway to monitor performance and characterize the structural response of the test roadway pavement. The State Materials Office (SMO) will be responsible for planning and conducting all monitoring and evaluation activities. Upon completion of the test road, FDOT will possess the only full-scale concrete pavement test facility in the southeastern United States.

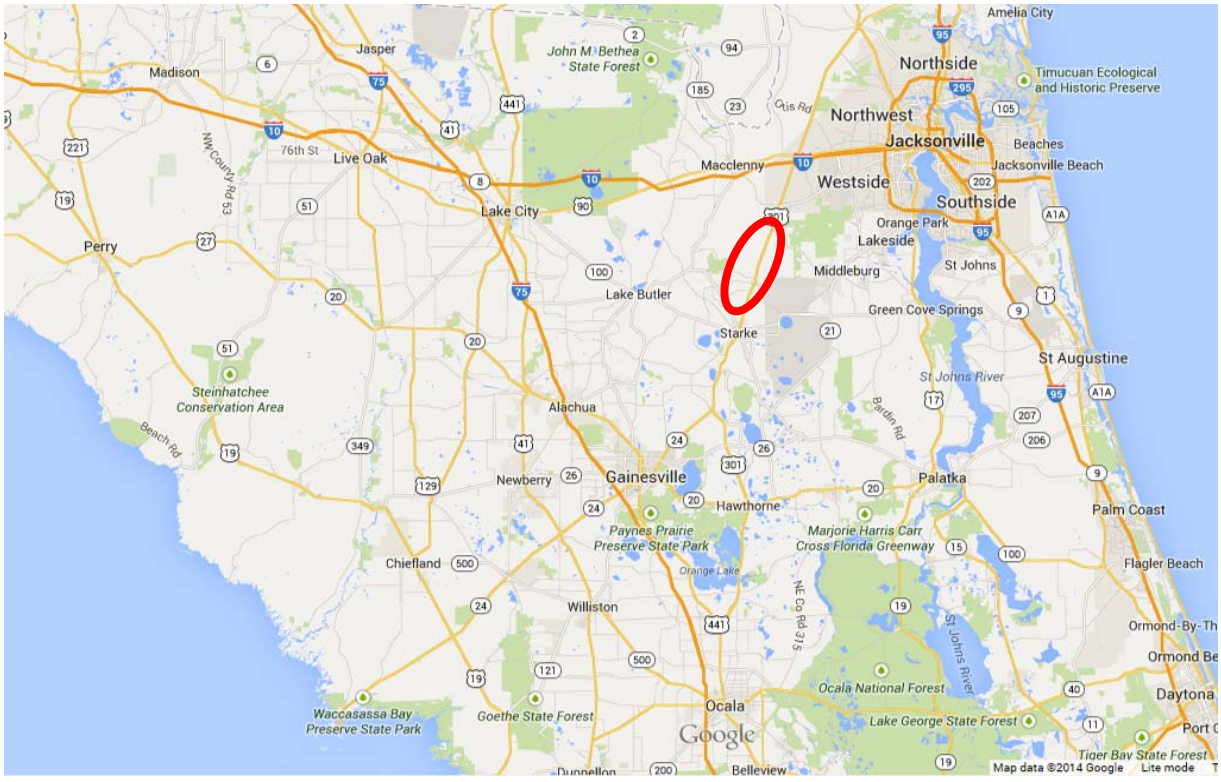

Figure 1-1. FDOT US-301 concrete test road location.

The test road will feature 52 individual test segments, each approximately 225 feet long, to provide a real-world testing ground to measure critical pavement responses to traffic (dynamic) and environmental loads (static) as well as pavement distresses that accumulate over the life of the road. Data from the test road will be used to develop new construction, rehabilitation, and maintenance strategies, as well as to analyze new cost-effective materials and

design methods. To achieve these goals, a portion of each segment will be instrumented with embedded strain and temperature sensors, among others, resulting in a very large number of sensors, data channels, and supporting data acquisition (DAQ) components. The necessity for such a complex and large-scale instrumentation program, coupled with the significant investment it will require, makes a thorough assessment of available sensing and DAQ technology critical to the overall success of the proposed test pavement.

1.2 Objective

The primary objective of this study is to evaluate available sensors and DAQ systems for their suitability to overcome the constraints and meet the objectives of the US-301 test road. Specifically, this study will evaluate and compare traditional copper-based sensors and fiber optic sensors. The results of this study will be the foundation for a comprehensive instrumentation plan for the test road. The evaluation will identify the most appropriate and cost-effective sensor system components based on extensive literature review, vendor engagement, as well as experimental testing and analyses. The results will be recommendations for sensors and DAQ system(s).

1.3 Challenges

The proposed test pavement creates three primary challenges related to sensing and data acquisition: 1) lightning strike susceptibility, 2) potentially long sensor lead lengths, and 3) a high sensor channel count.

The geographic area of the test pavement is known to be a high lighting strike area, which can have potentially catastrophic impacts on copper-based sensor systems (University of Florida, 2013). In addition, there is a large ditch planned along the edge of the roadway that requires some of the DAQ systems that retrieve and store data to be located over 100 feet from the embedded sensors. In traditional copper-based sensing systems, long lead lengths can result in noisy measurements, with the noise levels proportional to the lead length. Finally, because of the size of the test road, there will potentially be thousands of sensors that require extensive planning and units for data collection.

1.4 Potential Solutions

To address the challenges of acquiring data from the proposed test pavement, FDOT is considering the implementation of fiber optic sensors (FOS) due to their low level of measurement noise over long distances and immunity to electromagnetic interference from lightning strikes.

FDOT will have a large economic investment in the test road facility, therefore the implications of the sensing technologies' cost analysis is significant. Because the DAQ units are an expensive component of the overall sensor system due to initial cost and long-term maintenance, it is economically advantageous to limit the number of DAQ units for the test road. FOS technology allows for multiplexing, which offers the ability of a single optical fiber line to support a large amount of sensors (Yu & Yin, 2002). Multiplexing combines data from several sensors into one measurement channel (Udd, 1995). Multiplexing would reduce the quantity of DAQ units required for the test road, thereby reducing overall costs; however, higher rates of multiplexing reduce potential sampling rates, creating the need to balance the cost of the DAQ units and the desired sampling rate.

The test road sensors must to last 5-10 years, and though some sensor failure is expected, it should be minimized to protect the investment and ensure data availability over the duration of the project. While the test road has the potential to produce data that can be implemented to save a large amount of money in the future by creating more effective design, construction and maintenance methods, the cost of the instrumentation project is a critical factor in the selection of the sensor and data acquisition components.

1.5 Report Organization

Three phases of research were conducted to meet the goals of this project, as outlined in the sections of this report. Section 2 provides background information and a literature review on pavement testing and embedded sensing technology. In addition, Section 2 provides information gained from discussions with various sensor and DAQ vendors to assess the availability and cost of potential sensor and sensor system technologies. The work completed for Section 2 resulted in a number of candidate sensors with accompanying DAQ technology to be experimentally investigated in subsequent phases of the research. Section 3 presents the results of a series of

preliminary tests conducted with the candidate sensors, where their basic performance, robustness, and ease of use were evaluated. Section 4 presents the results of data acquired from strain and temperature sensors (copper and FOS) embedded in a small test pavement subjected to both dynamic wheel loads and fluctuating environmental conditions. Finally, Section 5 provides overall conclusions and recommendations based on the work conducted for this project. Following a list of references, additional data plots can be found in Appendices A and B.

2 Pavement Instrumentation Background

2.1 Test Pavements

Roadway pavement durability is affected by material, construction and curing practices, in situ soils, ambient and pavement temperatures, moisture, and loading from traffic. The proposed test road will analyze these factors through the evaluation of unique sections of roadway constructed using specific materials and thicknesses, various drainage features, and different construction methods. These "test pavements" or "test cells" will be approximately 225 feet in length. Sensors will be installed in two slabs at one end of each test section to monitor the structural effects of the environment and traffic loads on the pavement. The following sections describe some existing test pavements to illustrate typical test pavement data collection and outcomes.

2.1.1 Auburn Case Study

Auburn University is home to the National Center for Asphalt Technology (NCAT) Pavement Test Track. The NCAT test track, which opened in 2000, is asphalt-based, as the name of NCAT suggests. The track spans 1.7 miles with 46 different 200-foot test sections that mainly use copper-based sensing solutions. Test sections are trafficked using triple trailers to provide 10 million equivalent single axle loads (ESAL) in two years. The test track continues to yield many innovative results from its various research projects (NCAT, 2010). Figure 2-1 gives an aerial view of the NCAT test track.

Figure 2-1. NCAT test track at Auburn, AL (NCAT, 2013).

2.1.2 MnROAD Case Study

In 1990, the Minnesota Department of Transportation (MnDOT) began construction of a $25 million test road facility named MnROAD (Worel, 2006). MnROAD has two test road segments: a closed loop Low Volume Road (LVR) which is 2.5 miles and a 3.5 mile long mainline (ML) roadway parallel to I-94 near Albertville, Minnesota. Live traffic from I-94 is diverted to the ML roadway while controlled traffic is applied to the LVR. Figure 2-2 is a picture of the MnROAD test facility.

Figure 2-2. MnROAD at Albertville, MN (Jensen, 2011).

Despite significant differences in climate and local materials, MnROAD is very relevant to the US-301 concrete test road since the FDOT project will be of a similar scale and will use live traffic. MnROAD provides a good example of the potential benefits of the research opportunities a test road would provide as well as sensing options for testing both statically and dynamically. MnROAD has used over 9,500 sensors in the past 17 years. The dynamic sampling rate is 2,000 Hz and the environmental or static sampling rate captures data every 15 minutes. The dynamic sensors being used for Phase II are LVDTs, concrete embedment strain gauges, steel strain gauges, dynamic soil pressure cells, and bituminous strain gauges. The static sensors being used in Phase II are horizontal clip gauges, moisture gauges, thermocouples, resistivity probes, tipping buckets, and vibrating wires.

Phase I of the research at MnROAD spanned from 1994-2006 and is estimated to have saved the state of Minnesota $33 million/year and potentially $749 million/year nationally by creating new construction methods, rehabilitation and maintenance techniques, as well as new materials for roadways. The estimated annual savings resulting from Phase I are detailed in Figure 2-3. Phase II began in 2007 with similar goals to transform the materials, maintenance, and rehabilitation of roadways (Jensen, 2011).

Phase I (MN) Implemented Research	Annual Savings
Spring Load Restriction Policy	$14 Million
Winter Load Increase Policy	$7 Million
Low Temperature Cracking Reduction	$5.7 Million
ME Flexible Design Method	$4 Million
ME Rigid Design Method	$1.2 Million
Sealing Pavement/ Shoulder Joints	$1.2 Million

Figure 2-3. Results from phase I research 1994-2006 (Jensen, 2011).

2.2 Data Acquisition and Sensing Fundamentals

There are various sensor types used in structural evaluations, depending on the requirements of the project. Based on this project, the focus will be placed on sensors that analyze concrete strain, pavement deformation, concrete temperature, soil moisture, and joint, deflection. There will be added emphasis on the system comparison and cost analysis (see Section 2.6) of the sensor and data acquisition technology used in traditional sensing systems and that of optical fibers.

Data acquisition (DAQ) is the process by which sensor output, such as current, voltage, light, temperature, or sound, is captured and digitized by a computer for storage and further processing. A DAQ system consists of sensors, measurement hardware, and programmable software (National Instruments, 2013a). The DAQ hardware may include a power supply, sensor excitation, amplifiers, or other signal conditioning components. The DAQ software is used to define the measurement parameters, such as the sampling rates and test duration, in addition to the application of data filters if necessary.

The strain measured in a length of concrete is the ratio of the change in length under applied load divided by the original length. Pavement deformation is captured by concrete strain measurements to evaluate the deformation or the change in the pavement's profile. Deformations can either be elastic (temporary) or plastic (permanent). However, concrete pavement is considered to not have permanent deformations or rutting like asphalt pavement does. The tendency of the pavement profile to curl and warp when subjected to environmental impacts eventually compromises its structural integrity.

The temperature gradient within the slab due to seasonal and daily variations in temperature results in expansion and curling of the concrete slab due. These volume changes and deformations can create critical stresses which may result in joint spalling and cracks.

2.3 Traditional/Electronic Sensors

Traditionally, most sensors for structural and material testing have been copper-based. These copper-based sensors remain the most common sensor type for experimental structural and pavement studies today, and as a result, their behavior is well-understood, and they are widely available. Copper-based sensors are the core of the sensor systems used at most pavement testing

facilities. The following section, while not a comprehensive list of all the available sensors, describes many of the copper-based sensors that have been identified as candidates for FDOT test pavement.

2.3.1 Available Sensors

To measure the effects of traffic and environmental loading on the test road, the sensors must be placed in the concrete pavement prior to construction. The construction process is very harsh and potentially damaging to sensors if embedded in the concrete without proper planning and protection. There are copper-based sensors for all of the project's pertinent measurement types: concrete strain, pavement deformation, concrete temperature, and soil moisture.

Strain

Concrete strain can be measured using foil strain gauges, which convert a change in resistance resulting from strain to a measured voltage change. Foil strain gauges are inexpensive but are susceptible to noise and require lengthy mounting processes when surface mounted (Rice, 2009). The need for embedment makes bare foil strain gauges impractical because of their installation and durability issues.

The Vishay EGP-5-120 embeddable dynamic strain gauge functions similarly to foil strain gauges but has an encasing that adheres to the concrete as it cures, protecting the sensor and ensuring accurate measurements. The gauge is intended to measure strains exactly as the concrete experiences environmental and dynamic impacts (Vishay, 2011). Using similar principles as the Vishay gauge, Tokyo Sokki makes the KM-100BT embeddable static strain gauge and the PML-60-2L embeddable dynamic strain gauge (Tokyo Sokki, 2013a and Tokyo Sokki, 2013b). The Vishay and Tokyo Sokki gauges are depicted in Figure 2-4, Figure 2-5, and Figure 2-6, respectively.

Figure 2-4. Vishay EGP-5-120 embeddable dynamic strain gauge.

Figure 2-5. Tokyo Sokki KM-100BT embeddable static strain gauge.

Figure 2-6. Tokyo Sokki PML-60-2L embeddable dynamic strain gauge.

Strain can also be measured by Geokon's 4200A-2 vibrating wire strain sensor, which is made for embedment in concrete. Vibrating wire sensors are commonly applied for static measurements in pavements. However, vibrating wire sensors require additional programming code to convert the vibration frequency to strain. Vibrating wire sensors are also not suitable for higher frequency dynamic strain measurements due to limitations in the sampling rates they can

achieve (Geokon, 2013a). The Geokon 3900 embeddable dynamic strain gauge is similar to that of Vishay and Tokyo Sokki (Geokon, 2013b). The Geokon 4200 and 3900 series are shown in Figure 2-7 and Figure 2-8, respectively.

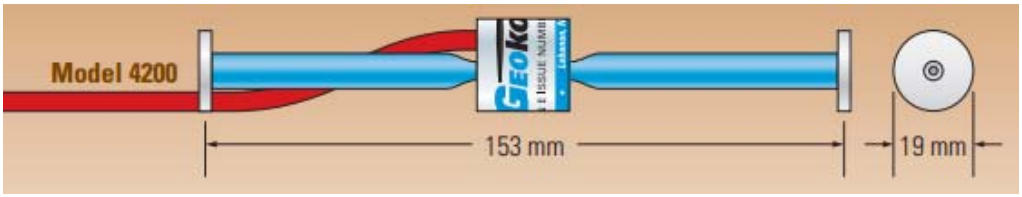

Figure 2-7. Geokon 4200A-2 embeddable vibrating wire sensor.

Figure 2-8. Geokon 3900 embeddable dynamic strain gauge.

The technical capabilities of the sensors from this section are found in their individual data sheets. A summary of the sensor characteristics is compiled below in **Error! Reference source not found.**. The cost of the sensors is discussed in Section 2.6 of this report.

Table 2-1. Summary of technical specifications for electronic strain sensors.

Specification	Vishay EGP-5-120 (dynamic)	Tokyo Sokki KM-100BT (static)	Tokyo Sokki PML-60-2L (dynamic)	Geokon 4200A-2 (static)	Geokon 3900 (dynamic)
Range (με)	-----	5000	-----	3000	5000
Resistance (Ω)	120	350	120	180	-----
Gage Length (mm)	100	100	125	153	203
Temperature Range (°C)	-30 - +60	-20 - +80	-20 - +60	-20 - +80	-20 - +80

Temperature

Electronic thermocouples can measure the temperature of the concrete. Thermocouples are extremely inexpensive and can easily be dispersed throughout the concrete test road. Omega's TT-K-24-100 thermocouple wire is duplex insulated for protection and has a maximum temperature of 260°C with a nominal size of 1.4 x 2.4 mm and weight of 6 lb/1000 ft (Omega, 2013).

Soil Moisture

Soil moisture is often measured using sensors which use the time domain reflectometry (TDR) method. Though the SMO is familiar with this method of soil moisture sensing, the size of the test road facility causes concern for the extensive calibration it often requires (Hammons et al., 2007). Several moisture sensors are under consideration for this project. The Campbell Scientific CS616-L water content probe is based on TDR and outputs a square wave with a frequency dependent on water content. The Decagon Devices GS3 is a capacitive sensor that provides soil moisture, electrical conductivity, and temperature in a ruggedized package. The Stevens' Hydra Probe II impedance-based sensor also provides electrical conductivity and temperature in addition to the moisture content of the soil and requires custom calibration for non-mineral soils. The Irrometer Watermark 200SS is a resistance-based sensor that requires minimal calibration. The 200SS has plastic caps with a stainless steel body over a hydrophilic fabric covered granular matrix (Irrometer, 2010), as illustrated in Figure 2-9.

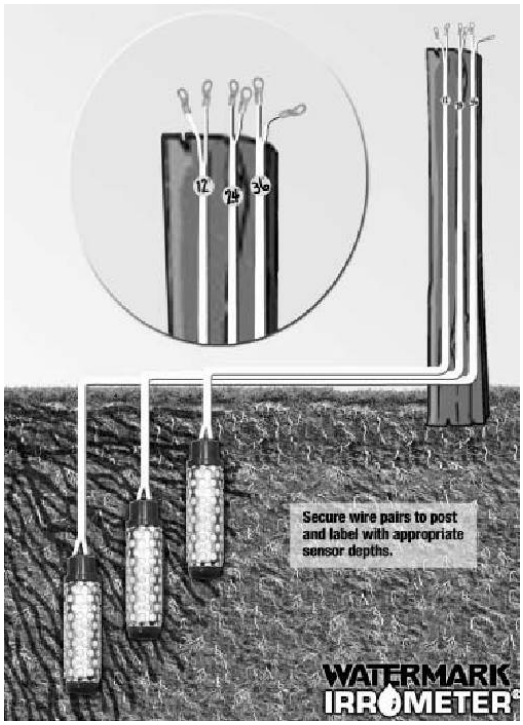

Figure 2-9. Illustration of Irrometer Watermark 200SS soil moisture sensors.

2.3.2 Data Acquisition

Efficient handing of data acquisition is a critical aspect of this project. For a copper-based system to achieve the necessary channel count with anticipated long cable lengths, each of the 52 test segments will require an individual DAQ cabinet. Within each DAQ cabinet there will be a DAQ chassis containing slots for measurement modules (National Instruments, 2013b).

It was determined that this project would focus on the use of National Instruments (NI) DAQ systems based on the SMO's extensive experience with their use and the ability of NI to provide the necessary technical support for such a large-scale instrumentation project.

2.3.3 Advantages

The availability of copper-based sensors is a large advantage over other sensor technologies; all of the necessary measurements for this study can be realized with readily available sensors and many of the sensors are inexpensive. In addition, FDOT has extensive experience with these types of sensors and the corresponding NI DAQ equipment, and would be

well-equipped to implement them in the US-301 concrete test road, especially with the available examples from other test road instrumentation plans.

2.3.4 Disadvantages

There are several disadvantages to using copper detection and characterization systems. Copper wire connects the sensor to its DAQ cabinet where the data is digitized and recorded. Given the long distance of wire between the embedded sensors and the DAQ units, a large amount of noise is expected to occur. MnROAD was constructed with DAQ cabinets directly next to the road, but the test road for FDOT will require several DAQ cabinets to be over 100 feet from the roadway sensors, making noise susceptibility particularly challenging. The large scale of this project may lead to the need to employ a high number of DAQ cabinets. Finally, the systems are susceptible to electromagnetic interference from lightning strikes, and the impact from lightning strikes would catastrophically damage the sensors.

2.4 Fiber Optic Sensors

In comparison to traditional sensor systems, the SMO has limited experience with fiber optic sensors (FOS). This section will detail the technology behind FOS, describing the fundamental terminology, availability, and capabilities to meet the needs of the US-301 concrete test road.

The basis of FOS technology is the optical fibers used to detect environmental changes. These clear glass fibers transmit light waves along their length and have the ability to act as both information carriers and sensors. Information is transmitted along the fiber length to a detector in the form of a light beam. The fiber acts as a sensor when the light beam is modulated by property changes in the fiber as a result of an environmental action (Udd and Spillman, 2011).

Though FOS technology is less familiar to the instrumentation community than copper-based sensing, its technology is beneficial in several ways, many of which resolve the limitations of traditional systems. Advantages that FOS systems have are multiplexing capabilities, durability, immunity to electromagnetic interference (e.g., lightning strike), and long range signal transmission.

2.4.1 Terminology

Though optical fibers may be used as sensors in a number of ways, the fundamental concept involves the modulation of the light waves due to changes in the fiber at the sensor locations. FOS can be done by either using discrete sensors similar to electronic sensors or by using distributed sensing along the optical fiber. Distributed sensing provides hundreds of measurement locations per meter of fiber, rather than just a few key locations.

FOS systems require a light source and a detector, often combined in a single unit called an interrogator. The light source is transmitted with a particular wavelength range, with each sensor along the length of the fiber operating in a predetermined portion of the wavelength range. As each sensor experiences a change due to a physical change, the properties of the wavelength shift within its portion of the total range. In FOS systems, the DAQ capacity is controlled by the wavelength range and the portion of the range required by each sensor.

Fiber Bragg grating (FBG) sensors are made up of a fiber core, which is surrounded by a fiber cladding for protection. FBG sensors operate by modulating the incident spectrum or wavelength (λ) through the sensor's core, resulting in a slightly altered transmitted wavelength. The difference in the incident wavelength and the transmitted wavelength is the reflected or refractive wavelength. The refractive wavelength represents the structural impact of a particular phenomenon. Figure 2-10 shows the operating principle of FBG sensors.

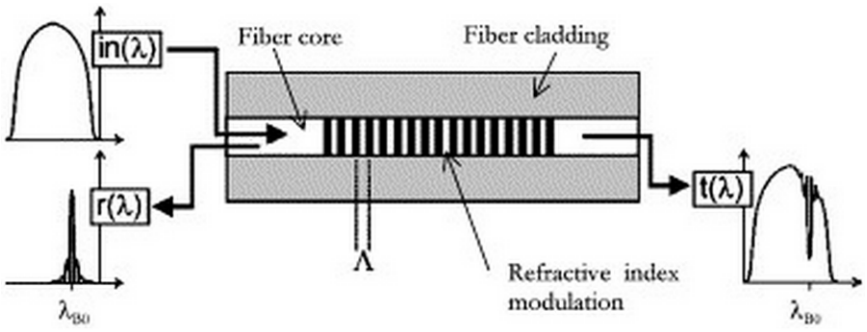

Figure 2-10. Working/Operating Principle of FBG sensors (Botsis et al., 2005).

2.4.2 Available Sensors

While there are many companies that specialize in the sales and manufacturing of fiber optic sensors and/or DAQ components, most were found not to meet the specific needs of the US-301 concrete test road instrumentation project. This project requires rugged, discrete, embeddable concrete strain and temperature sensors. These sensors and their supporting DAQ components must be available off-the-shelf (i.e., ready for use without the need to "build" a system from scratch). The supplier of these sensors must have a history of successful application in large-scale instrumentation deployments and must have the ability to provide the necessary training and technical support throughout the project. After research and interaction with multiple FOS companies, the SMO determined many FOS vendors lack the necessary breadth and experience to support the activities of the proposed test pavement. Many manufacturers and distributors are from foreign locations and have insufficient customer services for a project this size.

The focus of many FOS companies is on distributed sensing applications (as described earlier) that are primarily used in mechanical and aerospace applications (Luna, 2013). An example of this type of company is Luna Technologies, which was investigated as an option for this project. Though Luna's technology is advanced for accurately capturing an object's strain distribution, the practical installation of the technology has not been thoroughly tested for concrete embedment. The DAQ unit for Luna utilizes swept-wavelength interferometry and is relatively inexpensive at $4,000 per unit (Luna, 2012). Despite these beneficial attributes of the Luna technology, the difficulties of installation and lack of previous application in civil structures are undesirable for this project. Thus, Luna Technologies was not further investigated in this study.

There are only a handful of companies providing discrete, embeddable concrete strain sensors. FiberSensing, Inc., based in Portugal, is a fairly new company that provides embeddable concrete strain sensors. Micron Optics, Inc., is a very established company based in the U.S., and provides a range of embeddable sensors for direct application at specific locations throughout a structure. Micron Optics has been used for many large-scale projects in civil engineering (Micron Optics, 2013). The Micron Optics products were selected for further investigation based on the company's experience in applications similar to the US-301 test

pavement project and their ability to provide the necessary technical support throughout the project.

Currently, vendors in the U.S. do not offer fiber optic soil moisture gauges. Although the technology for these sensors is available and the sensors are manufactured in other countries, the demand in the U.S. has been inadequate to support their commercial availability. As a result, FOS technology for these measurements will not be evaluated in this study. Therefore, for these measurements, the use of FOS technology would need to be accompanied by the electronic sensors in a hybrid sensing system.

The following sections outline the sensors available from Micron Optics that will be evaluated for use in the test pavement.

Strain

Concrete strain will be analyzed by the FBG model os3600. Similar to the electronic concrete strain gauges, the os3600 is designed to be embedded in concrete and adhere during the curing process and maintain an accurate measurement of the impacts of static and dynamic loads on the structure. The os3600 is made of stainless steel and a Teflon encasing, and its gauge length is either 25 or 100 cm. The strain sensitivity is 1.2 pm/με, and the temperature sensitivity is 23.8 pm/°C. The sensor's operating temperature range is -40°C to +80°C with a strain limit (or range) of 2,500 με. According to the data sheet for the os3600, its fatigue life is 100 million cycles at 2,000 με (Micron Optics, 2012a). Figure 2-11 shows the os3600 FBG model with disk ends (top) and universal ends (bottom).

Figure 2-11. os3600 embeddable strain sensor.

For the out-of-pavement testing to be conducted in this study, Micron Optics recommends employing the os3610 FBG which is made for mounted testing similar to the use for the steel specimen that will be used for strain analysis. The os3610 is solely stainless steel, which is more appropriate for instrumenting the steel specimen than the Teflon encasing of the os3600. The gauge length, strain sensitivity, operating temperature, and fatigue life are the same as the os3600 model. However, the strain limit for the os3610 is 5,000 με, and the temperature sensitivity is 22 pm/°C (Micron Optics, 2012b). Figure 2-12 shows the os3610 FBG model.

Figure 2-12. os3610 surface mount strain sensor.

Temperature

FBGs temperature sensing instruments, although beneficial in some areas, are expensive when employed in the vast quantities required by the test road. Experimentation will confirm whether the benefits of FBG temperature sensing validate the extra expense over thermocouples.

Concrete temperature will be measured using the os4350 FBG. The os4350 is much more expensive than the aforementioned thermocouples but its anodized aluminum housing material is much more rugged and would adjust well to the construction process of the concrete test road. The os4350 has a response time of 4.2 seconds, an operating temperature range of -40°C to +120°C, and a sensitivity of 10 pm/°C (±1.7 pm/°C). The standard calibration for the sensor provides long term accuracy of 1.0°C and typical short term accuracy of 0.6°C. The premium calibration option increases those accuracies to 0.5°C and 0.2°C, respectively (Micron Optics, 2009a). Figure 2-13 shows the os4350 FBG model.

os4350 - Armored Cable, Flange Mount

Figure 2-13. os4350 non-metallic temperature sensor.

2.4.3 Data Acquisition

Simplification of data acquisition is one of the largest advantages of FOS systems. DAQ is expensive, and a system of the magnitude FDOT is designing would require 52 DAQ cabinets if solely copper-based. By contrast, the same test road employing an FOS system would require much fewer interrogators because of the ability of the FOS system to use long lead distances without noise. Interrogators do not require calibration, making them easier to operate while reducing installation time and cost. Additionally, the use of multiplexing techniques would also reduce the channel counts, resulting in the need for fewer interrogators. The electronic DAQ cabinet and FOS interrogator are of comparable unit cost so the analysis between the two systems' DAQ will be based on their ability to collect data efficiently with as few DAQ units as possible.

The Micron Optics sm130-500 interrogator will be investigated for FOS DAQ. For the purpose of this sensor evaluation project, the interrogator may be rented from Micron Optics at a rate of $2,199.20/month. The interrogator outputs sensor wavelength data through an Ethernet port which is then connected to an external computer where software is used to analyze and archive the data. The sm130-500 has four optical channels and a scan frequency of 500 Hz. The wavelength range for this model is 1510-1590 nm, with a typical FBG sensor capacity of 80. The operating temperature is 0°C to 50°C, and the operating humidity is 0 to 80% non-condensing (Micron Optics, 2010a). Figure 2-14 shows the sm130 interrogator.

Figure 2-14. sm130 interrogator field module.

For the large-scale instrumentation of the test road, it may be advantageous to invest in Micron Optics rack mount interrogators, which have the channel multiplexer installed directly into the interrogator. For example, the sm230-500 has a scan frequency of 500 Hz and a typical FBG sensor capacity of 80. The wavelength range, operating temperature, and humidity are the same as the sm130-500 interrogator (Micron Optics, 2010b). Figure 2-15 shows the sm230 interrogator.

Figure 2-15. sm230 rack mount interrogator.

ENLIGHT, the sensing analysis software developed by Micron Optics, is included with the sm130-500 and sm230-800 interrogator models. This software acquires, stores, and analyzes the sensor data. ENLIGHT can be used to generate data tables, graphs, and other visual aids for analysis. Figure 2-16 is a screenshot of the acquisition tab in the ENLIGHT software. Each peak represents an FBG sensor output where the optical wavelength measured from each sensor is indicated on the horizontal axis. These wavelength values are converted to strain values within the software (Micron Optics, 2012c).

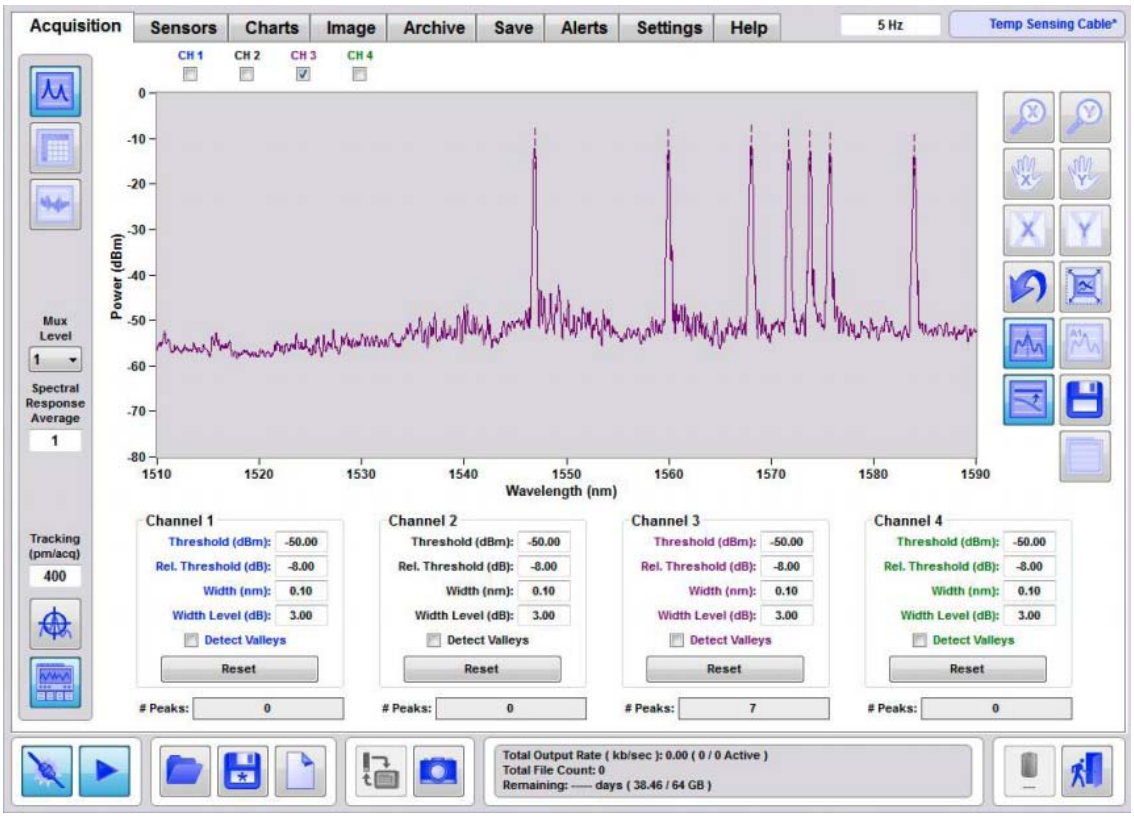

Figure 2-16. ENLIGHT acquisition tab.

2.4.4 Case Studies

There are many case studies that demonstrate the implementation of fiber optic sensors for civil applications. Although few involve test pavements and/or concrete embedment, there are studies available that evaluate FOS system fundamentals by means of other applications. The first case study discussed in this section illustrates the accuracy of FOS technology, and the second case study details the durability of these sensors. These studies help form a foundation for the out-of-pavement and embedded testing studies that will be done for FDOT's test road on US-301.

Internal Strain Measurements in Concrete Specimens in Compression

In Bologna, Italy, strain in the core of concrete cylinders was successfully evaluated without disrupting the nature of the core's reaction to physical phenomena. Traditional methods measured the external strain rather than internal strain. To achieve the internal strain measurements without a disruption to the material loading response, fiber optic strain sensors

were inserted into the specimen. The hypothesis was that FOS could measure the concrete strain experienced internally without influencing the concrete's behavior.

Two concrete cylinders were tested in compression. In order to protect the optical fiber sensor cable, a very small steel pipe was used. Strain was observed in the two different specimens with agreement. The study concluded that the FOS accurately measured the internal strain state without disturbance to the stress state of the specimen. This was previously unattainable by foil strain gauges, with FOS offering an improvement in the detection and characterization of strain in structures (Bonfiglioli & Pascale, 2003).

FOS Sensor Durability in Concrete Embedment

Nanyang Technological University (Singapore) reported its design and experimental evaluations of FBG sensors, focusing particularly on the packaging for embedded concrete applications.

A concrete beam was constructed with two FBG temperature sensors connected to top and bottom reinforcing bars. Three FBG sensors were embedded and installed with minimum protection, and consequently, one of those sensors was damaged during curing. Four FBG sensors and four electrical strain gauges were installed on the surface of the specimen. The dynamic sampling rates for the sensors were 17.5 Hz for FBG sensors and 100Hz for strain gauges. At the mid-span of the beam, the strain gauge recorded a maximum strain of 58 microstrain, while the FBG sensor recorded 55 microstrain.

The study concluded that FBG sensors can survive the harsh construction and curing environments associated with concrete structures and measure strain and temperature accurately during embedment (Moyo, et al., 2005).

2.4.5 Advantages

Some of the advantages of optical fibers are their flexibility, ruggedness, and immunity to electromagnetic interference. Additionally, an appealing feature of FOS is its inherent ability to serve as both the sensing element and the signal transmission medium, allowing the instrumentation to be located remotely from the measurement site without noise and its multiplexing ability (Ansari, 1997).

Specifically for this project, there are three key advantages of FOS technology: 1) resistance to electromagnetic interference, 2) ability to achieve long lead lengths and remote DAQ, and 3) fewer DAQ units required relative to copper-based sensing systems. As a consequence of a heightened probability of lightning in the area, there is a vested interest in the FOS system's resistance to the electromagnetic interference and its resulting protection from lightning strikes. The remote location from the measurement site is also a large factor to consider. The potential for noise in the electronic sensors is a concern for the long cable lengths required by the topography of the test road site, but this could be remedied by the use of a FOS system. Multiplexing coupled with the high channel count per interrogator would also minimize the amount of DAQ units necessary for the facility's sensing system.

2.4.6 Disadvantages

There are several measurements that FOS cannot evaluate, such as soil moisture. One solution to this is a hybrid system consisting of FOS for concrete strain and temperature while using the more familiar copper-based sensing technologies for the other necessary measurements. FOS can be easy to install but to avoid the need to field-splice of optical fibers (requiring special skill and training) expensive extension cables and connectors may be required. FOS sensors are expensive relative to copper-base sensors, but the money saved in DAQ may outweigh the increased sensor and installation cost. For a smaller project without the lightning and topography constraints, the copper-based system would be a more economical solution.

2.5 System Comparison

It has been widely demonstrated in recent years that FBG sensors can replace electrical strain gauges for structural engineering applications with similar sensitivities (Annamdas, 2011). Additionally, optical fibers experience lower noise levels over long distances and will not be affected by the electromagnetic interference of lightning strikes. The interrogators' multiplexing and the high channel count capability lower the required number of DAQ units.

This section of the report detailed the availability and capability of the sensor technologies. The ease and practicality of installation and robustness will be addressed in the later sections of the report that will describe the experimental procedures and findings of both out-of-pavement and embedded testing of the sensors.

2.6 Cost Analysis

Advancements in optical fiber technology have improved its availability in recent years. However, copper-based products still dominate the instrumentation community. Thus, a closer look at the economic benefits of each is vital to the evaluation of the sensor systems for this particular project.

As mentioned earlier, the sensor price is higher with FBG sensors, but the DAQ cost may be lower depending on the quantity of DAQ units required for an FOS system. Since the DAQ unit price is similar for copper and optical fibers, the total DAQ cost is solely influenced by the number of required DAQ units for the system. There is high economic motivation for fewer DAQ locations for a project the size of the US-301 concrete test road.

The cost of the optical fiber itself is substantially less expensive than copper wire. Optical interrogators do not require calibration resulting in greater longevity of the accuracy of the system. Finally, the optical sensing solution is simpler and more unified. The cost of maintaining the system is likely to be lower than electrical instrumentation. More hardware can be located within a climate controlled on-site facility rather than housed in enclosures located adjacent to the test road.

Table 2-2 shows preliminary unit prices for the components of a hybrid sensing system for the US-301 concrete test road. At this time, the use of all of these components and the quantity of these components are still under consideration. The necessary quantities of the sensors and DAQ units are to be determined by FDOT. The final quantities will dictate the cost benefit analysis for this particular project.

Table 2-2. Unit price cost summary.

Sensor/Material Type	Copper-based		Optical Fibers	
			Micron Optics	
	Model	Unit Price	Model	Unit Price
Concrete Strain	Vishay EGP-5-120 (dynamic)	$ 44.20	os3600	$ 649.00
	Tokyo Sokki PML-60-2L (dynamic)	$ 143.00		
	Tokyo Sokki KM-100BT (static)	-----		
	Geokon 4200A-2 (static)	$ 126.00		
	Geokon 3900 (dynamic)	$ 605.00		
Data Acquisition	National Instruments cRIO-9074	$ 2,929.00	sm130-700	$ 23,992.00
	Campbell Scientific CR1000-ST-SW-NC (soil moisture and vibrating wire data logger)	$ 1,465.00		
	Campbell Scientific AVW200-ST (module for temperature and strain)	$ 450.00		
Gap Displacement	Macrosensors GHSD-750-5000	-----	os5100	$ 3,349.00
Temperature	Omega TT-K-24-100 (T/C Wire)	$78.00 / 100 ft	os4350	$ 249.00
Soil Pressure	Geokon 3500	$ 720.00	-----	-----
Soil Moisture	Decagon Devices GS3	$ 259.00	-----	-----
	Irrometer Watermark 200SS	$ 91.00		
	Campbell Scientific CS616-L25	$ 139.75		
	Stevens Hydraprobe II	$ 359.00		

2.7 Background Summary

The measurements required for this project are concrete strain, pavement deformation, concrete temperature, soil moisture, and joint deflection. There are several constraints for the US-301 concrete test road that other test roads in the U.S. have not experienced, which makes an in-depth sensor evaluation advantageous. FDOT's concrete test road at US-301 has three major

challenges: a high propensity for lightning strike, a topography that requires several DAQ units to be over 100 feet from the embedded sensors, and the need for a high sensor channel count. All of these challenges create significant problems for traditional electronic sensors due to their susceptibility to electromagnetic interference experienced during lightning strikes and in long lead distances between sensors and DAQ locations which creates noisy data, as well as their low channel count per DAQ unit resulting from the limitations of lead lengths.

FOS systems address all of these major challenges. FBG sensors are immune to the electromagnetic interference of lightning strikes. They behave well over long lead distances without noise. Multiplexing capabilities and high channels counts for their DAQ interrogators provide a means to minimize the amount of DAQ units required for the test road. FBG sensors available in the U.S. do not address all of the required measurements for the project. Therefore, the FBG sensors will be studied to analyze their ability to detect concrete strain and concrete temperature. All other measurements will be accomplished with electronic sensors to create a hybrid sensor system. An investigation of FOS suppliers led to the selection of Micron Optics products for further experimental investigation.

The next sections of this study will detail experimental procedures and findings that will either confirm or reject the ability of FBG technology to meet the needs of this project while providing adequate measurement accuracy for the pertinent measurements.

3 Initial Testing and Evaluation

This section focuses on the initial sensor testing conducted in the second phase of the project. In preparation for the embedded evaluations of the sensors, a series of smaller-scale tests were designed and conducted to evaluate the performance of the candidate sensors in a range of measurement conditions. These tests provided experience with the installation processes, data acquisition procedures, and sensing capabilities. This initial testing and evaluation allowed preliminary comparisons to be made between the candidate sensors in a controlled testing environment, while future embedded tests more closely resembled the use-case of the sensors in the proposed test pavement and offer comparisons of the sensors in the harsh conditions of embedment in the heterogeneous concrete pavement.

This section describes the findings from the initial, out-of-pavement tests, which all took place at the SMO. The goal of the tests was to characterize and assess the performance of the candidate sensors (Vishay and Tokyo Sokki foil strain gauges, thermocouples, and Micron Optics fiber optic strain and temperature sensors). The tests performed for this report include concrete cylinder compression tests (dynamic and static), tensile tests (dynamic and static), temperature sensitivity tests, and noise tests. The measurement results from each sensor type were analyzed and compared.

The final application of the sensors that will be selected based on the research findings of this project is long-term embedment in concrete pavement; however the embedded environment is not ideal for direct comparison of sensor performance. Concrete's nonhomogeneous nature coupled with non-uniform loading and boundary conditions result in inconsistency in the pavement's behavior over its volume. Therefore the sensors may experience different strains and temperatures once embedded in the heterogeneous material – even when they are installed close to one another. In addition, it is imperative that all installation and data acquisition procedures are assessed prior to embedding these expensive sensors in order to prevent errors and increase efficiency. The initial testing and evaluation presented in this report provides a consistent baseline for sensor characterization and comparison, which were further evaluated when the sensors are embedded in the pavement.

Section 3.1 of this report discusses the means by which data was acquired and archived for the various tests. The sections thereafter describe the materials, methods, and results for each experimental setup. The order of the tests discussed in this section is: compression, tension, temperature, and noise. This portion of the report closed by a conclusion that summarize the findings and details the outcomes from the initial testing and evaluation phase of this project.

3.1 Data Acquisition and Archiving

All sensors require DAQ hardware to supply power and convert analog signals to digital data streams for archiving. National Instruments (NI) DAQ hardware was utilized to collect data from the copper sensors strain sensors and thermocouples. Specifically, an NI CompactDAQ eight-slot chasses with interchangeable sensor modules was used. Strain measurements used an NI 9235 eight-channel, 120-ohm quarter-bridge module capable of sampling rates up to 10 kHz. The thermocouples interfaced with an NI 9213 16-channel thermocouple module. Data was collected from the fiber optic sensors using the four-channel sm130-500 interrogator. The interrogator can sample data up to 500 Hz with a capacity of up to 80 sensors (20 sensors per channel using multiplexing).

Data acquisition and archiving requires appropriate software configured for each experimental setup. The software configuration usually determines the data sampling rate, the length of each test, and the file location for data storage. The data acquisition software is typically coupled with the acquisition hardware being employed. Depending on the desired format of the collected data, a combination of acquisition and post-processing software may be used. For the tests presented in this section, LabVIEW, ENLIGHT, Excel, and MATLAB are the software programs used in the collection and analysis of data. This section describes the operation of the DAQ software and the challenges associated with using the heterogeneous DAQ setup required for a hybrid copper/FOS sensor system.

Data acquisition for the copper-based sensor connected to the NI CompactDAQ hardware was supported by NI LabVIEW DAQ software to read and record the data streams. ENLIGHT is the DAQ software provided by Micron Optics to acquire data from the interrogator capturing data from the fiber optic sensors. ENLIGHT can be fully integrated into a LabVIEW application to streamline the data acquisition of different sensor types; however, given the short timeframe for the initial testing phase of this project, the integrated feature was not utilized. Rather, the two

programs (LabVIEW and ENLIGHT) were run separately to collect data, resulting in a slight time difference between the initiations of data collection on each system. A second LabVIEW application was used to join and align the data files, resulting in a single synchronized data file containing the output of all sensors used in a given test. Further data post processing and analysis was conducted in MATLAB to generate data plots and statistics for the various tests in this phase.

The effective sampling rate used for each of the tests described in this section was selected based on the anticipated length of the test and whether any dynamic features that were intended to be captured. A sampling rate of 100 Hz was used for the compression and tension tests. Since the temperature tests were conducted over an extended period of time and the data were not expected to change rapidly, the effective sampling rate was decreased to one sample per second (1 Hz). The noise evaluation tests were conducted at different sampling rates to capture the impact of the sampling rate on the measured noise levels.

One of the anticipated noise sources for the copper-based sensors is “electric hum,” which occurs at the power line frequency of 60 Hz. The source of this noise can either be from electromagnetic interference from nearby electrical components or a differential between the ground of the measurement signal and the ground of the power source. While certain measures can be taken to reduce these noise sources, such as cable shielding and careful grounding procedures, it is often difficult to completely eliminate them. Preliminary tests on the steel specimen (described in detail below) demonstrated the presence of 60-Hz noise in the measured signals. In signal sampling and digitization, the Nyquist frequency is the highest detectable frequency in the measured signal and is half of the sampling rate. For a sampling rate of 100 Hz the Nyquist frequency is 50 Hz. If significant energy exists in the signal above the Nyquist frequency, as is the case for electric hum noise at 60 Hz being sampled at 100 Hz with a Nyquist frequency of 50 Hz, it will be “folded” back into the measured signal through a process called “aliasing”. For example, a 60-Hz noise will be mirrored about a 50-Hz Nyquist frequency to show up as a 40-Hz signal as illustrated in

Tension Data

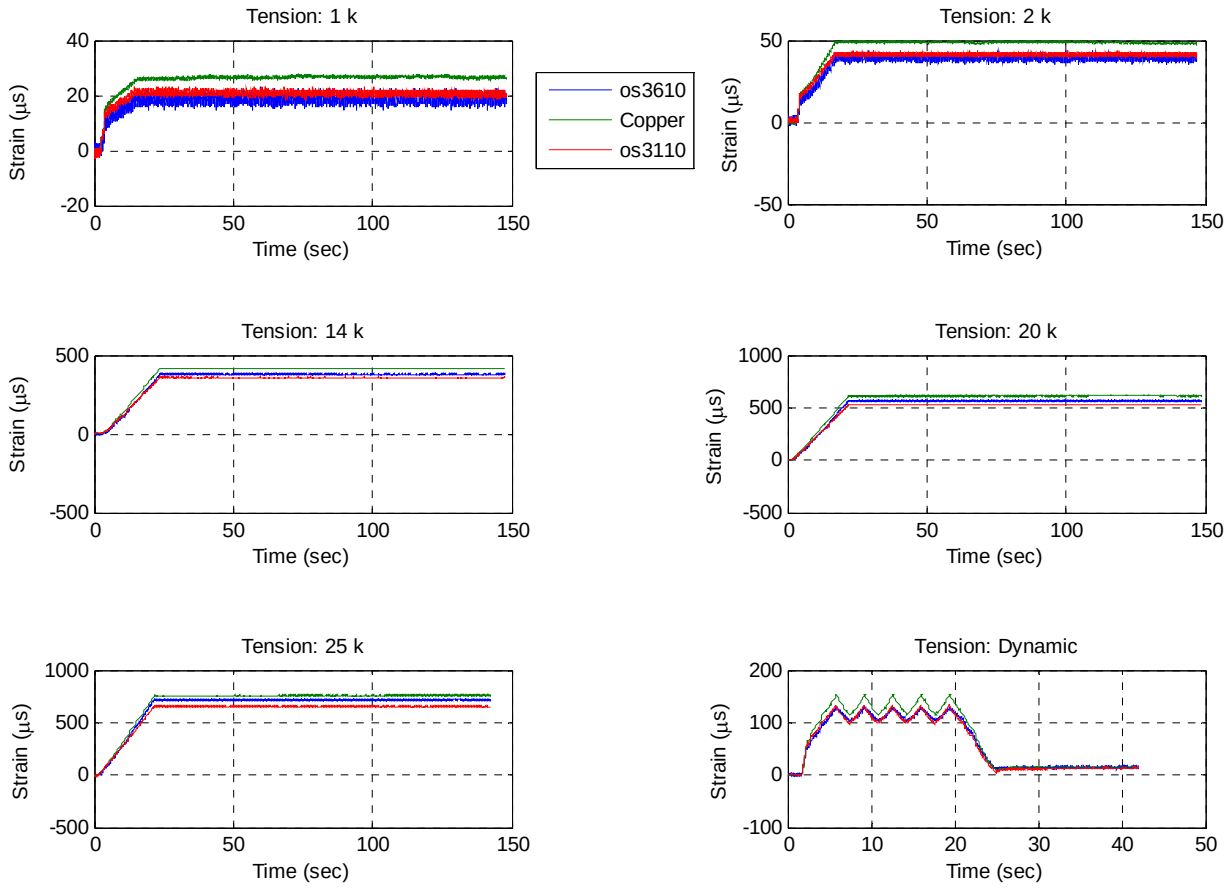

Figure A-2. Tension strain results.

Temperature Data

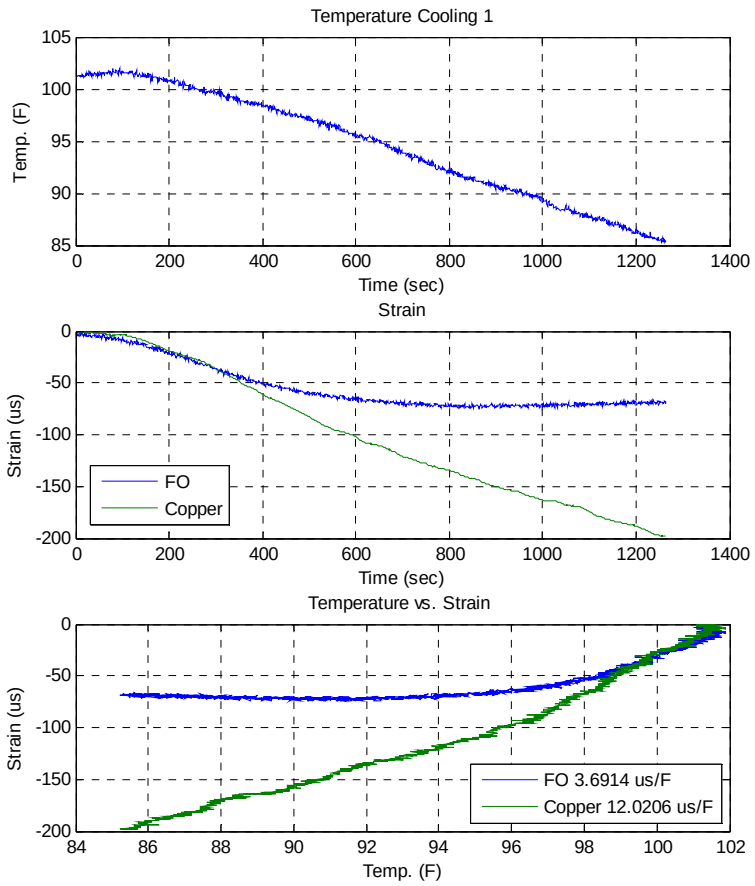

Figure A-3. Cooling strain readings

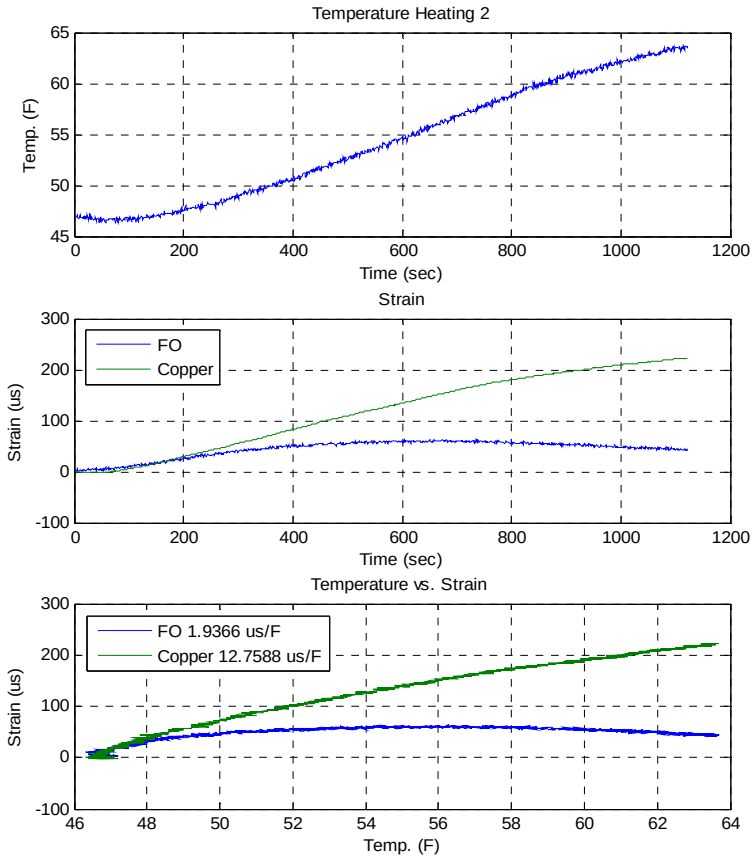

Figure A-4. Heating strain readings

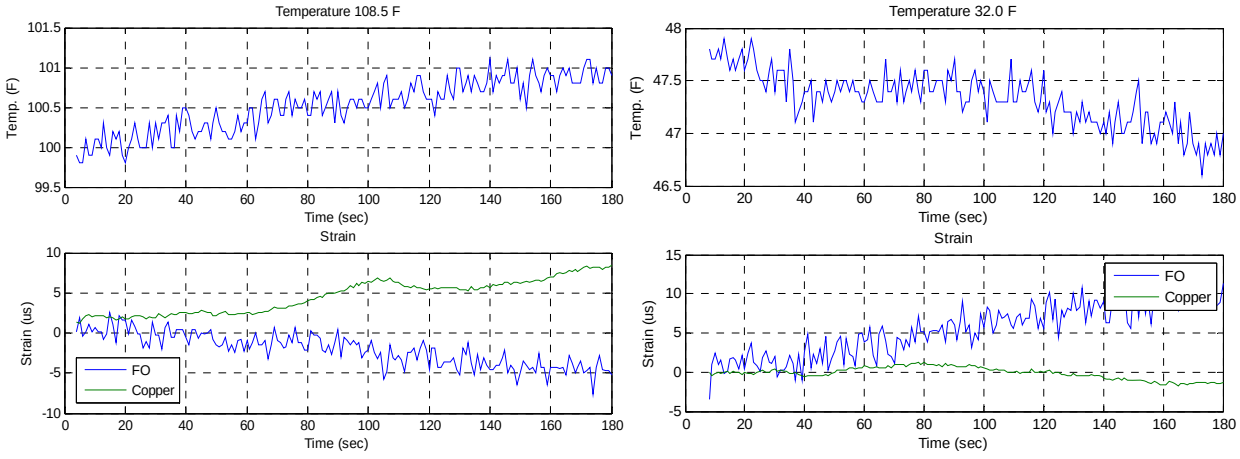

Figure A-5. Hot (left) and cold (right) strain readings.

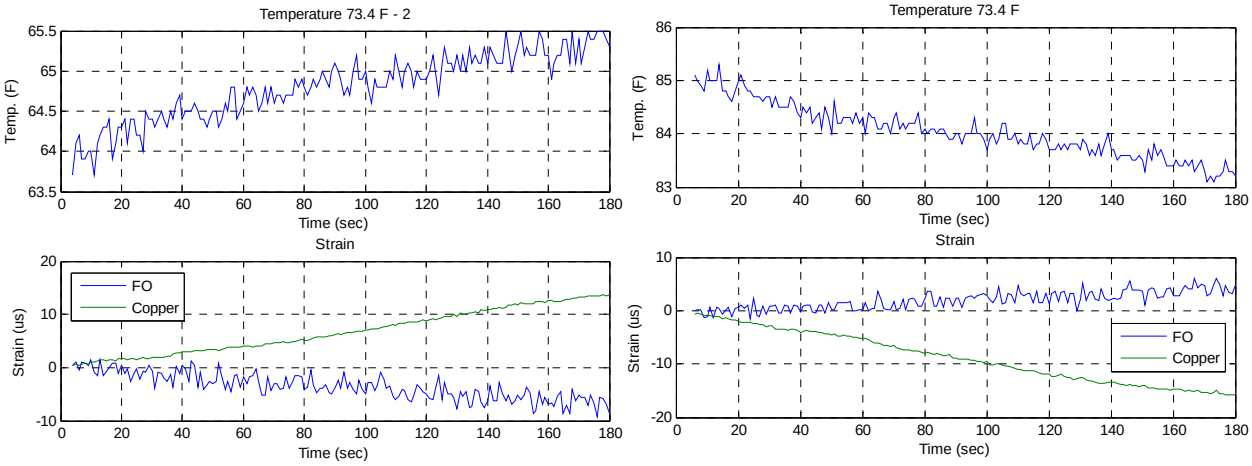

Figure A-6. Room temperature strain readings.

Appendix B: Additional Embedded Dynamic Analysis

Raw Data

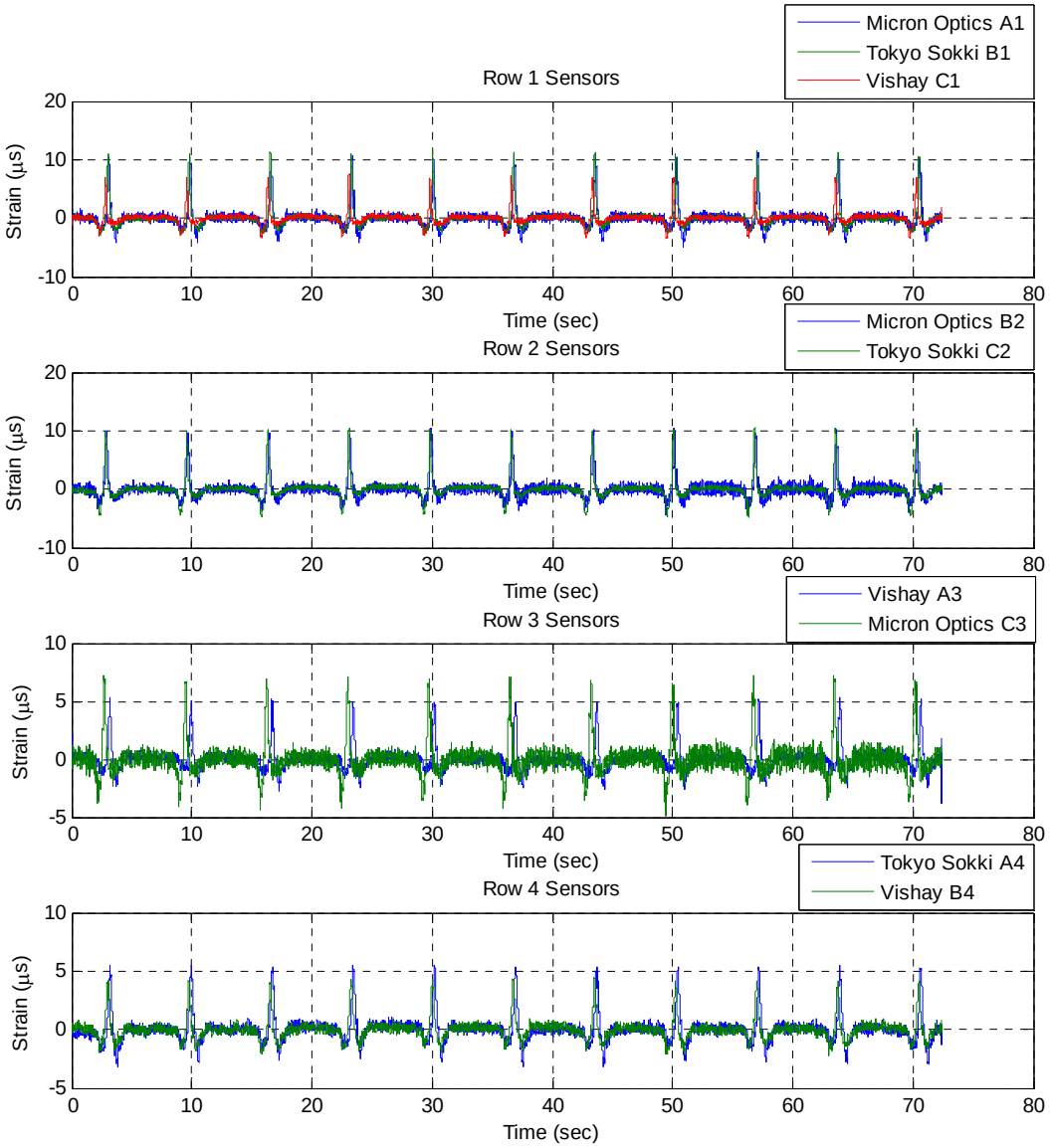

Figure B-1. November 4th 3:00 PM 9-kip dynamic test along row 1, separate plot for each row of sensors.

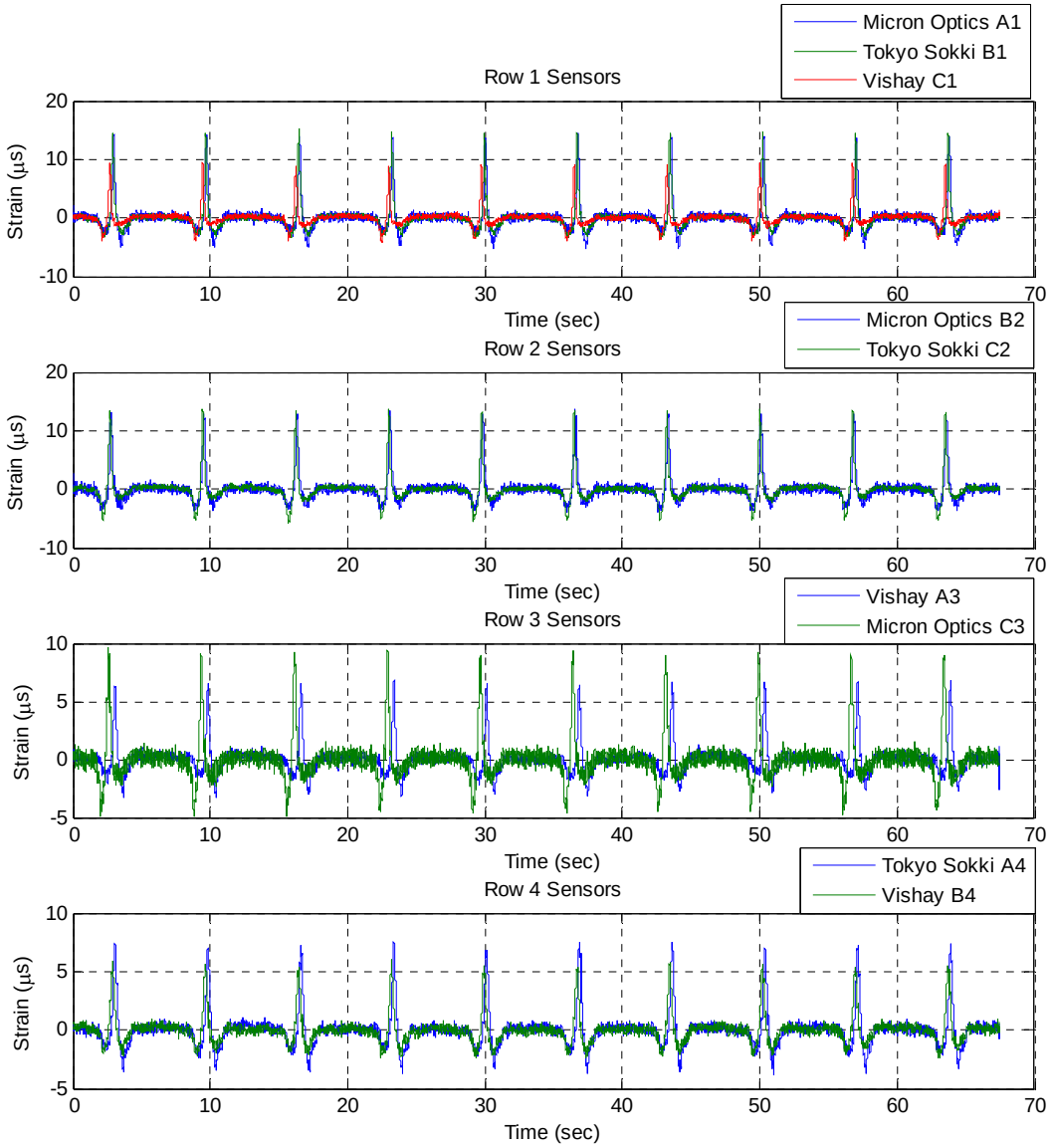

Figure B-2. November 4th 3:00 PM 12-kip dynamic test along row 1, separate plot for each row of sensors.

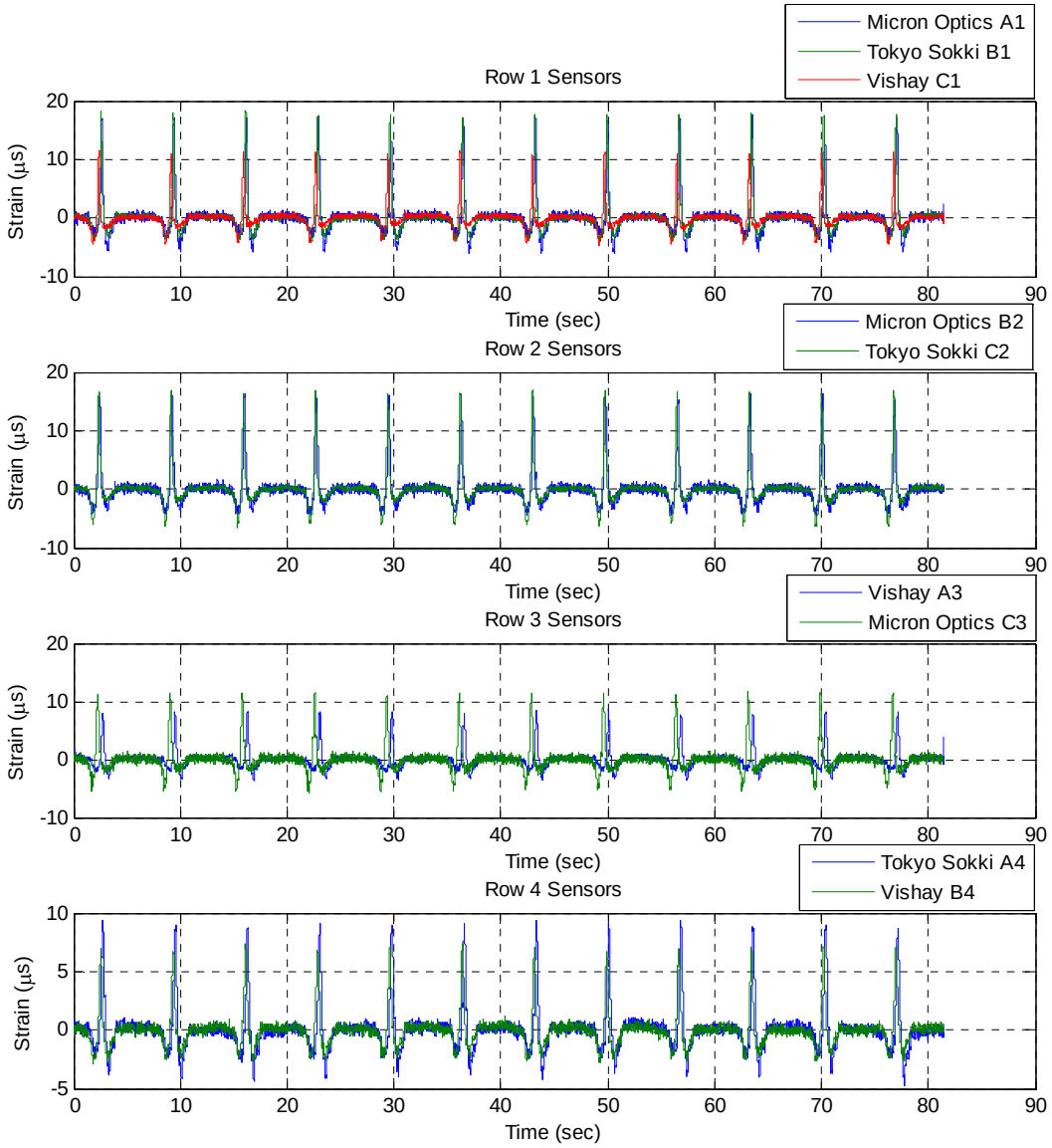

Figure B-3. November 4th 3:00 PM 15-kip dynamic test along row 1, separate plot for each row of sensors.

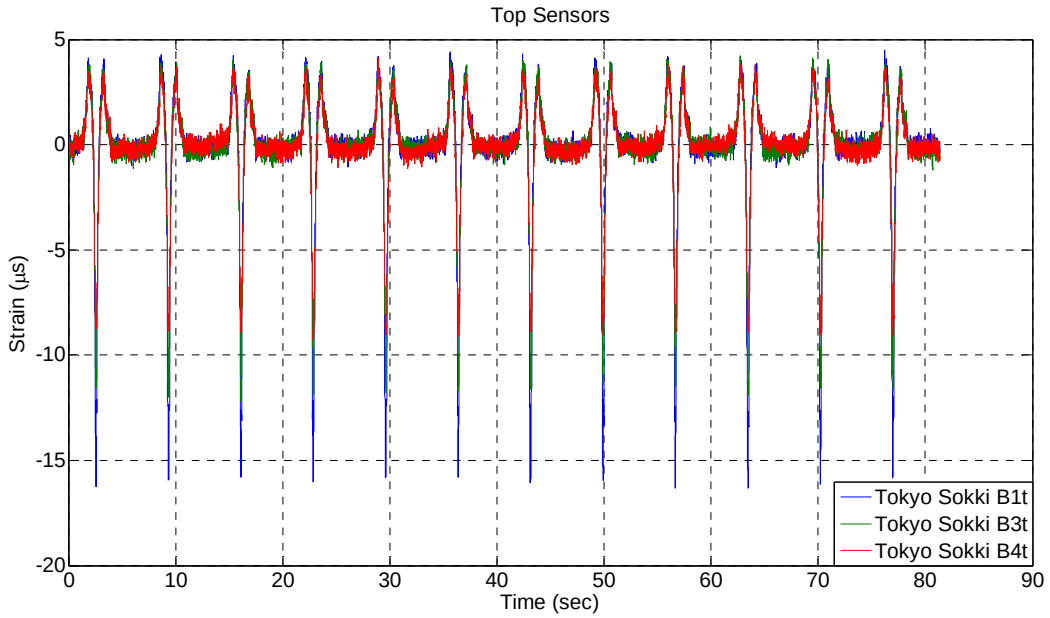

Figure B-4. November 4th 3:00 PM 15-kip dynamic test along row 1, top sensors.

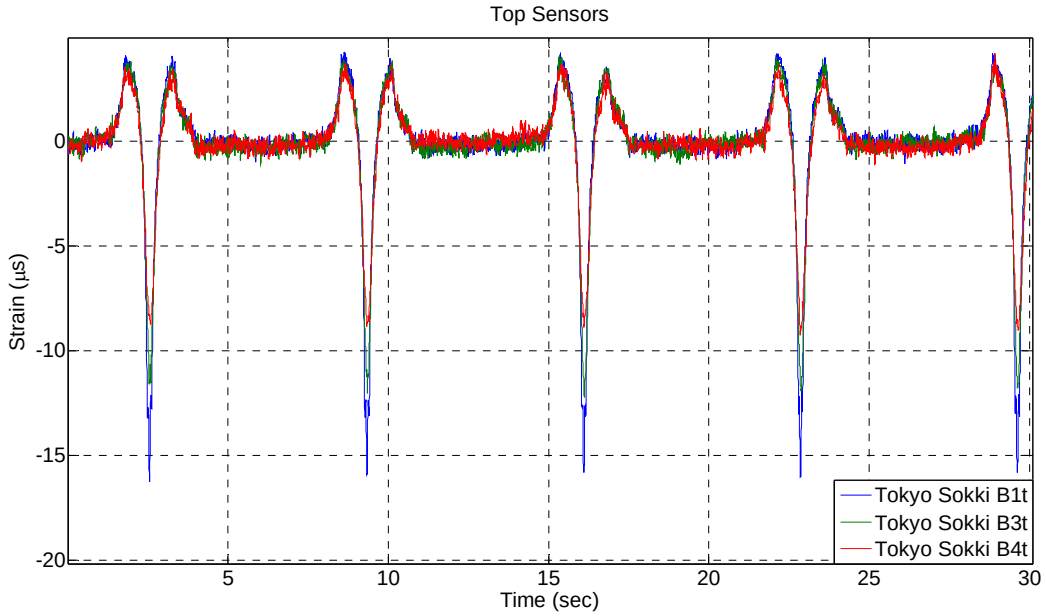

Figure B-5. November 4th 3:00 PM 15-kip dynamic test along row 1, top sensors – zoomed view.

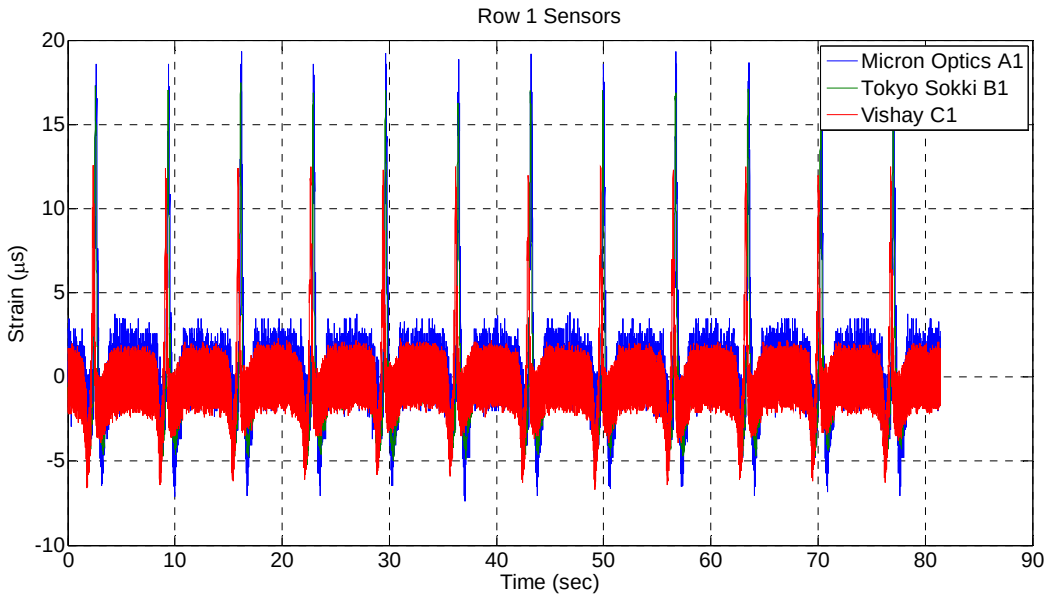

Figure B-6. November 4th 3:00 PM 15-kip dynamic test along row 1, unfiltered data without detrending.

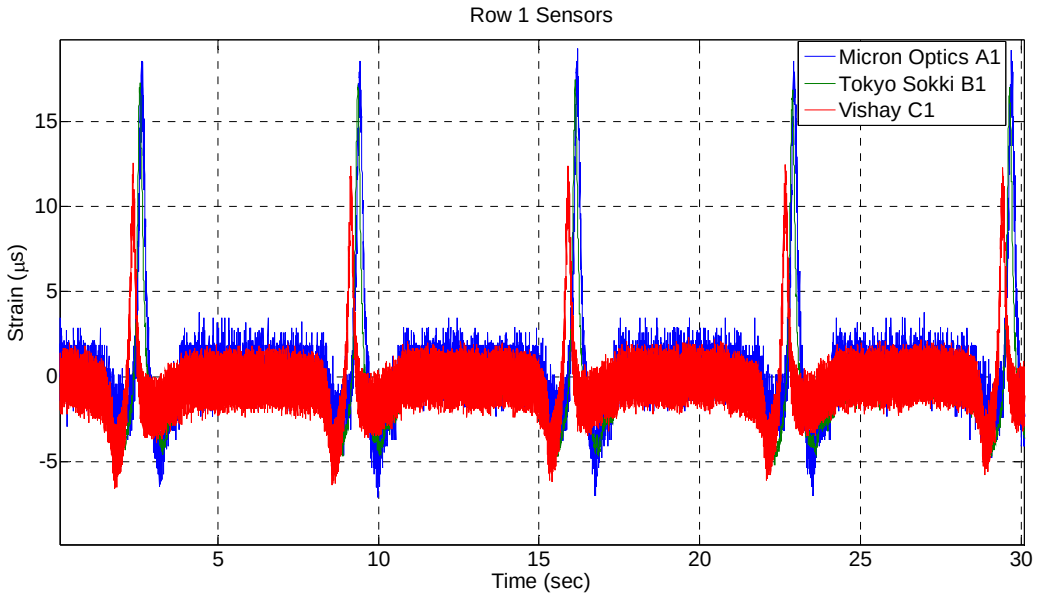

Figure B-7. November 4th 3:00 PM 15-kip dynamic test along row 1, unfiltered data without detrending – zoomed view.

Peak Analysis

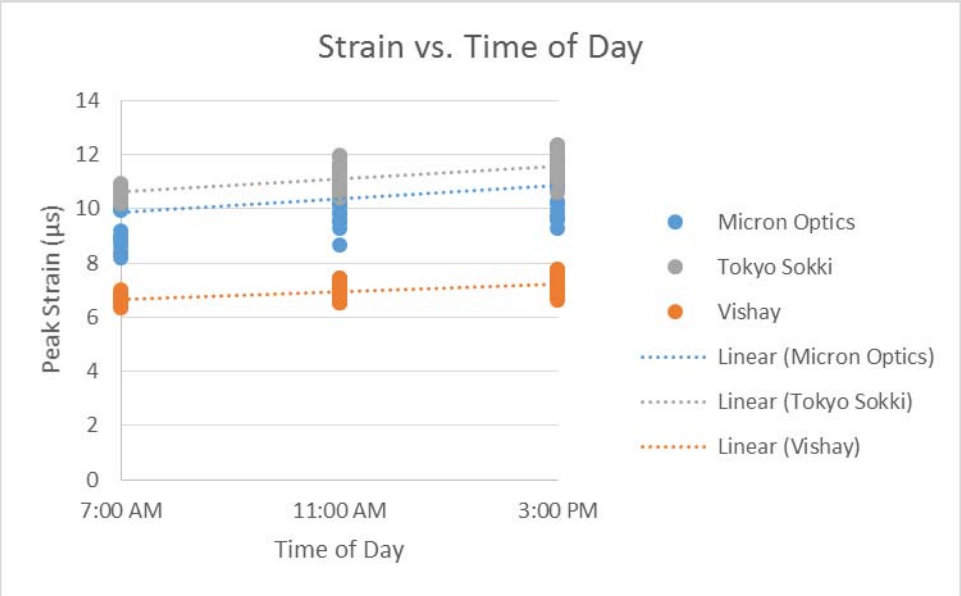

Figure B-8. Strain vs. time of day – 9 kip.

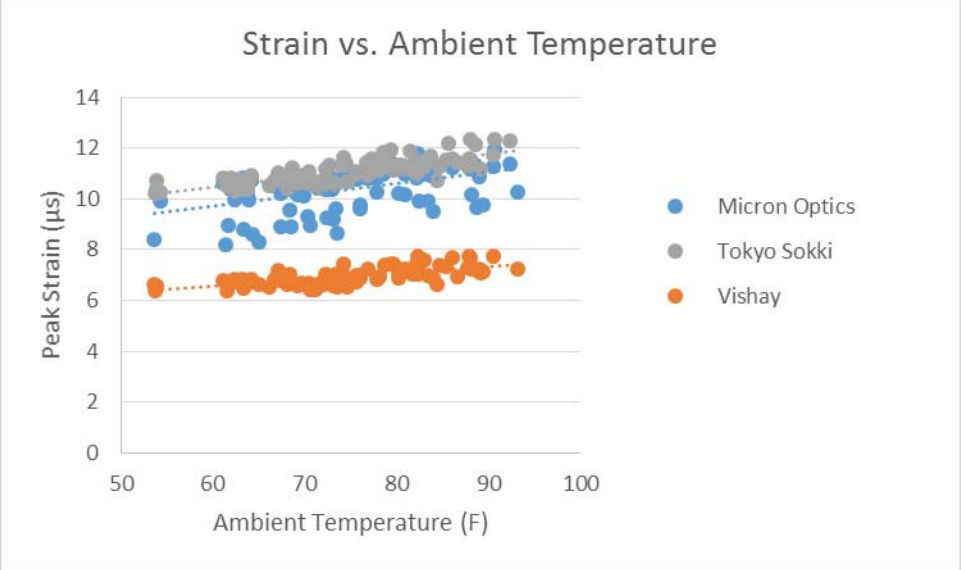

Figure B-9. Strain vs. ambient temperature – 9 kip.

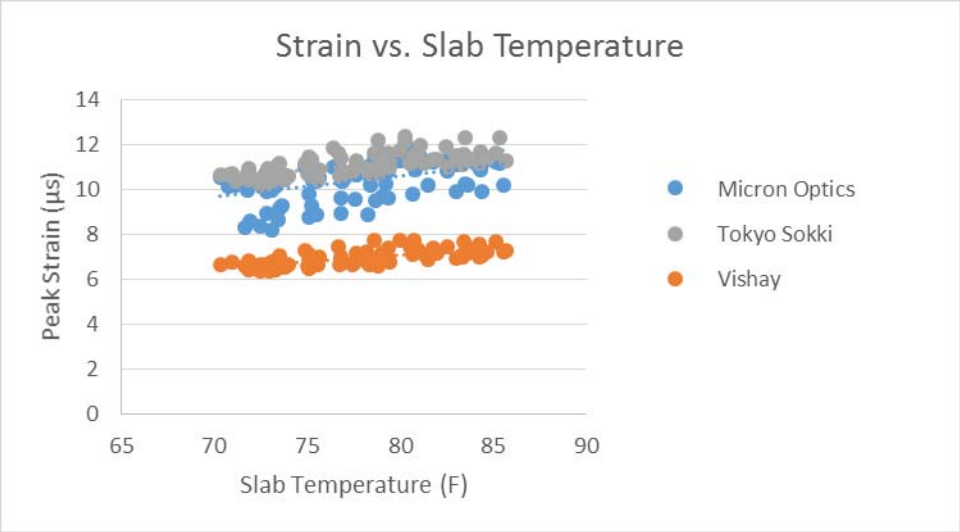

Figure B-10. Strain vs. slab temperature – 9 kip.

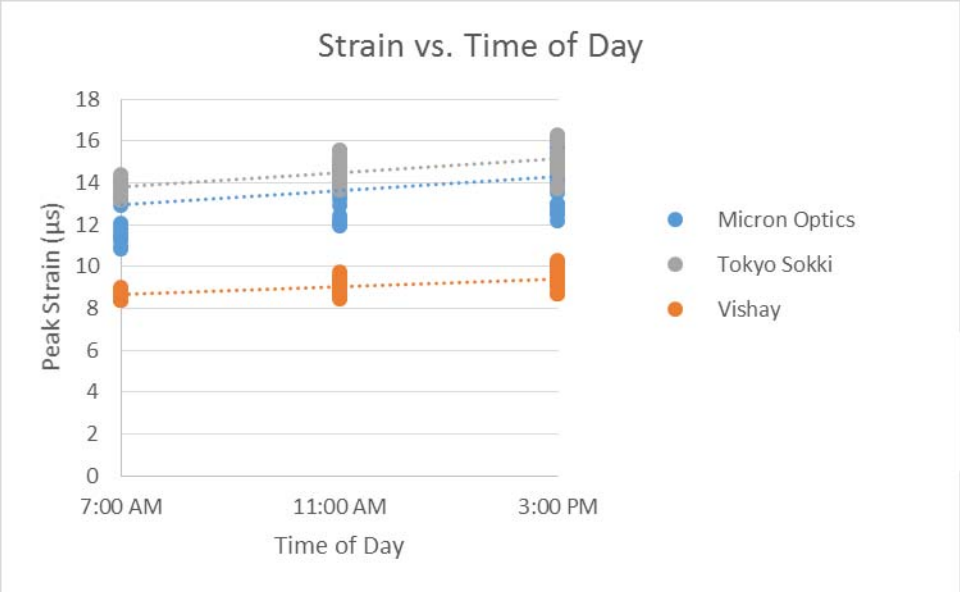

Figure B-11. Strain vs. time of day – 12 kip.

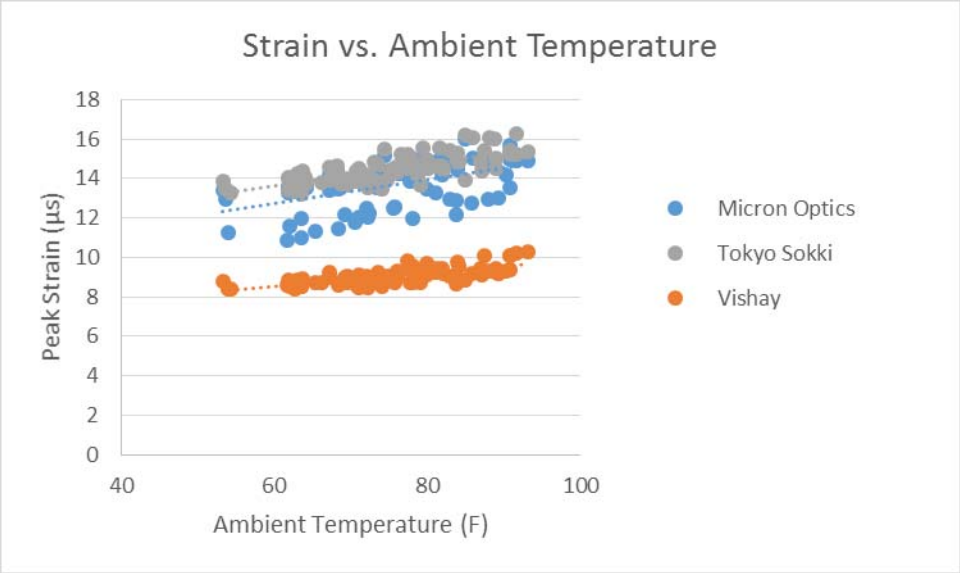

Figure B-12. Strain vs. ambient temperature – 12 kip.

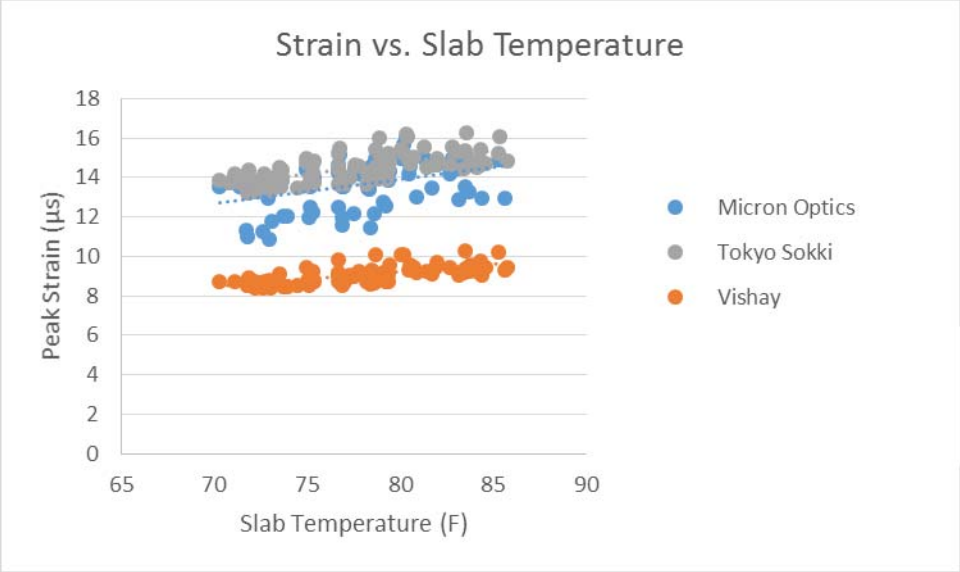

Figure B-13. Strain vs. slab temperature – 12 kip.

Data Repeatability Analysis – Peaks

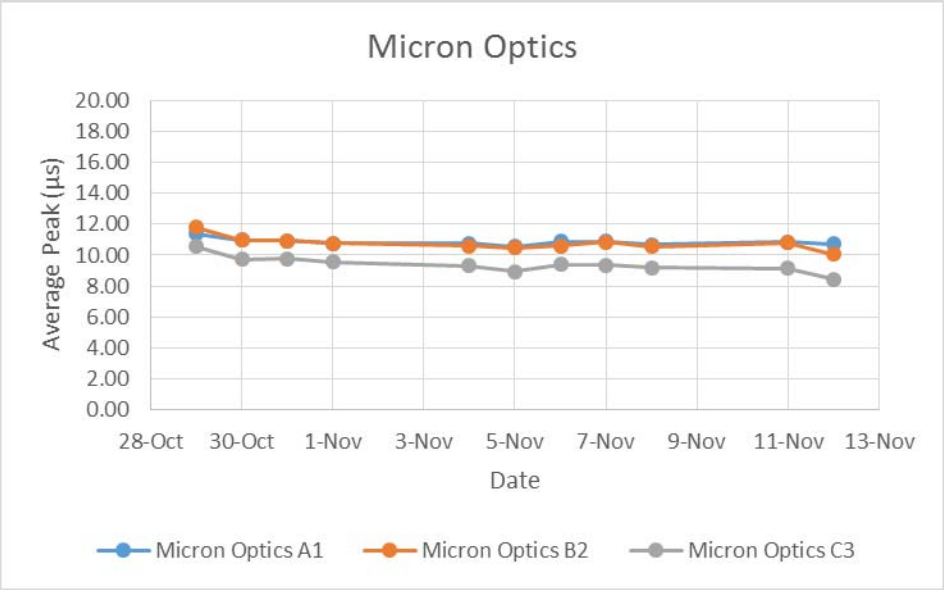

Figure B-14. Micron Optics repeatability plot – 9 kip.

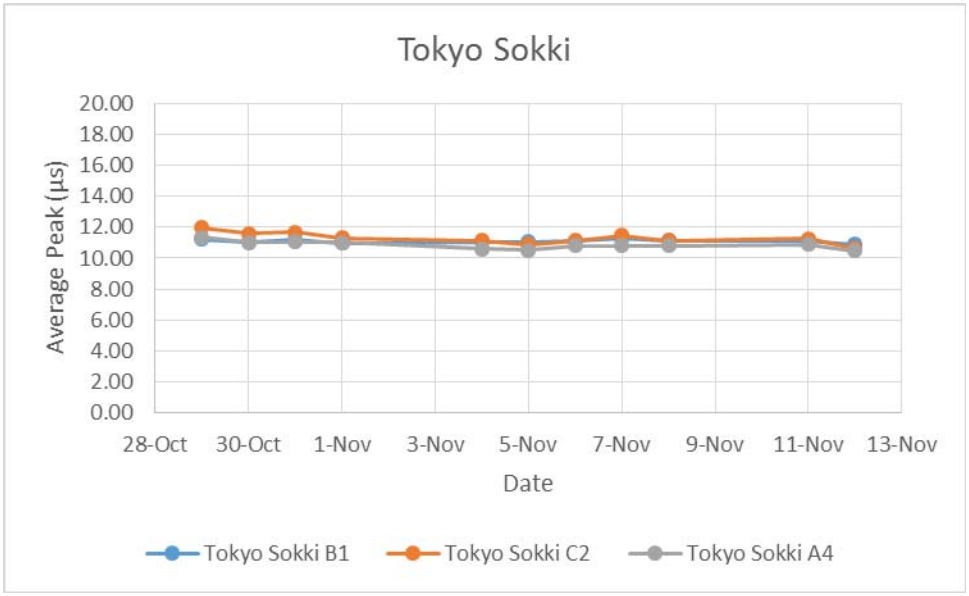

Figure B-15. Tokyo Sokki repeatability plot – 9 kip.

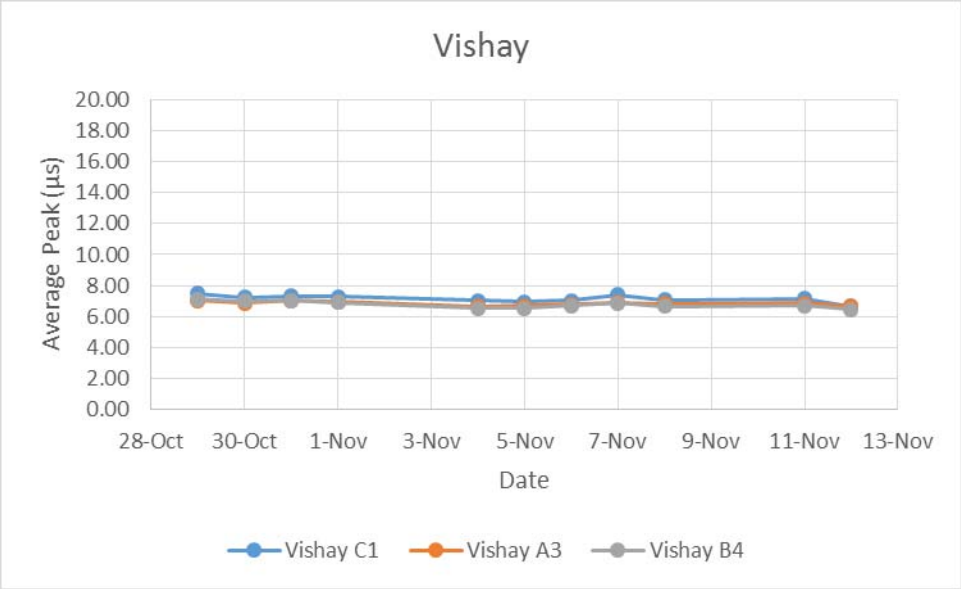

Figure B-16. Vishay repeatability plot – 9 kip.

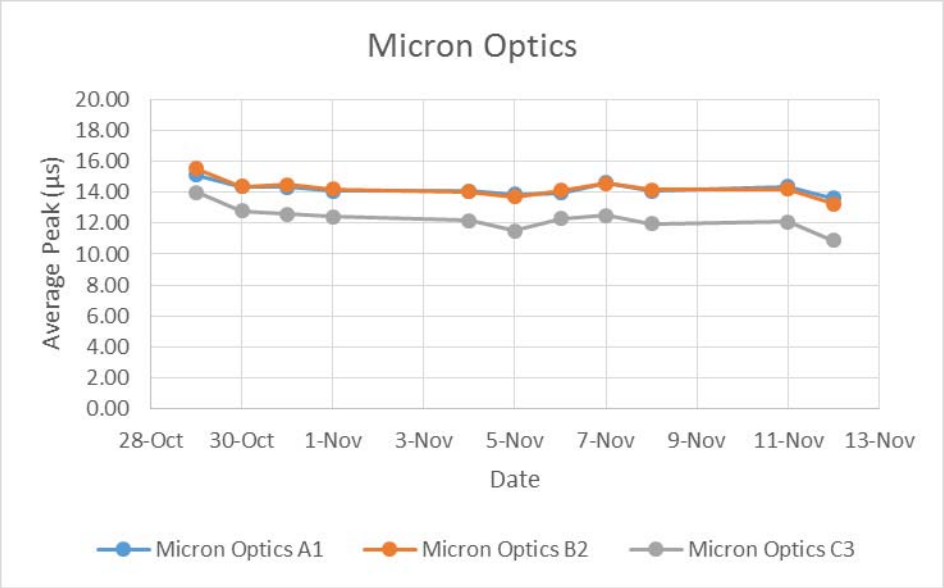

Figure B-17. Micron Optics repeatability plot – 12 kip.

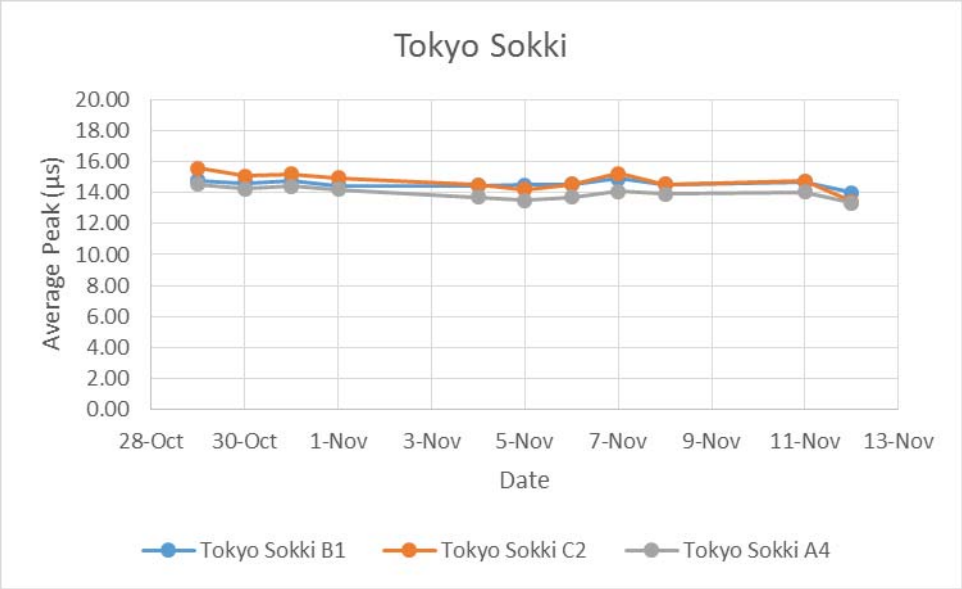

Figure B-18. Tokyo Sokki repeatability plot – 12 kip.

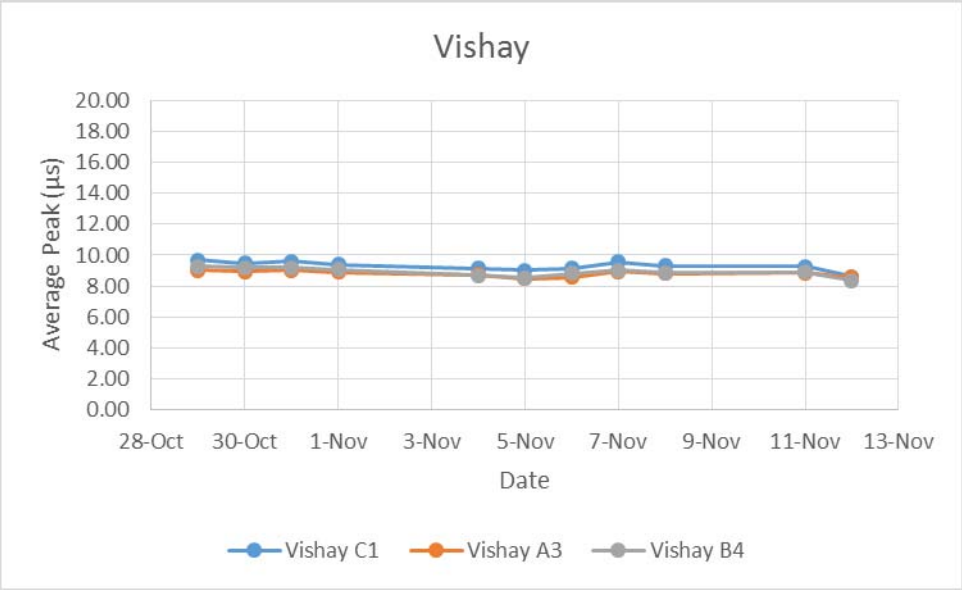

Figure B-19. Vishay repeatability plot – 12 kip.

Strain Distribution

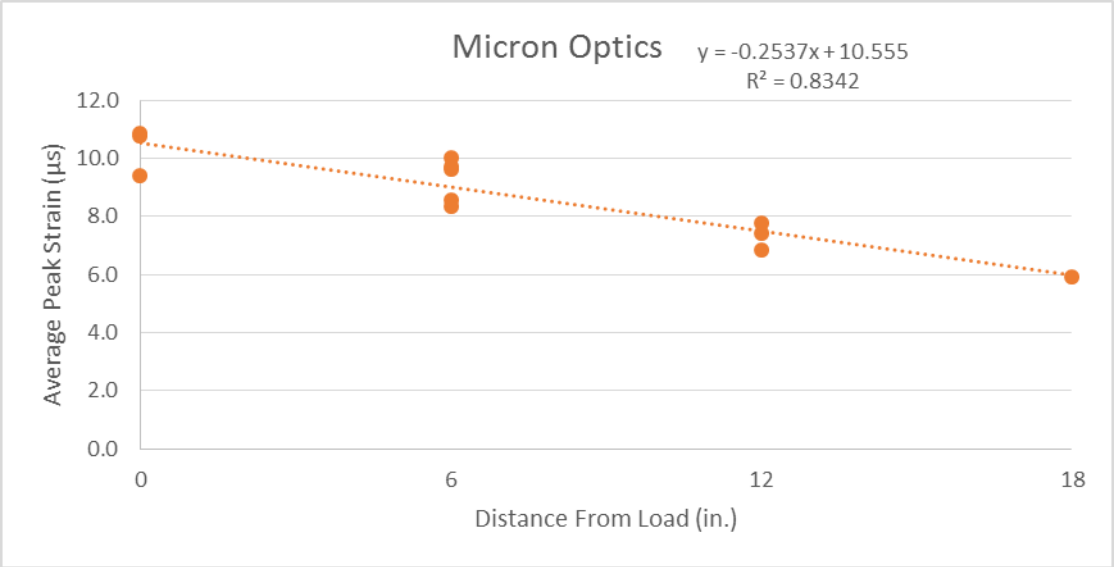

Figure B-20. Micron Optics strain distribution – 9 kip.

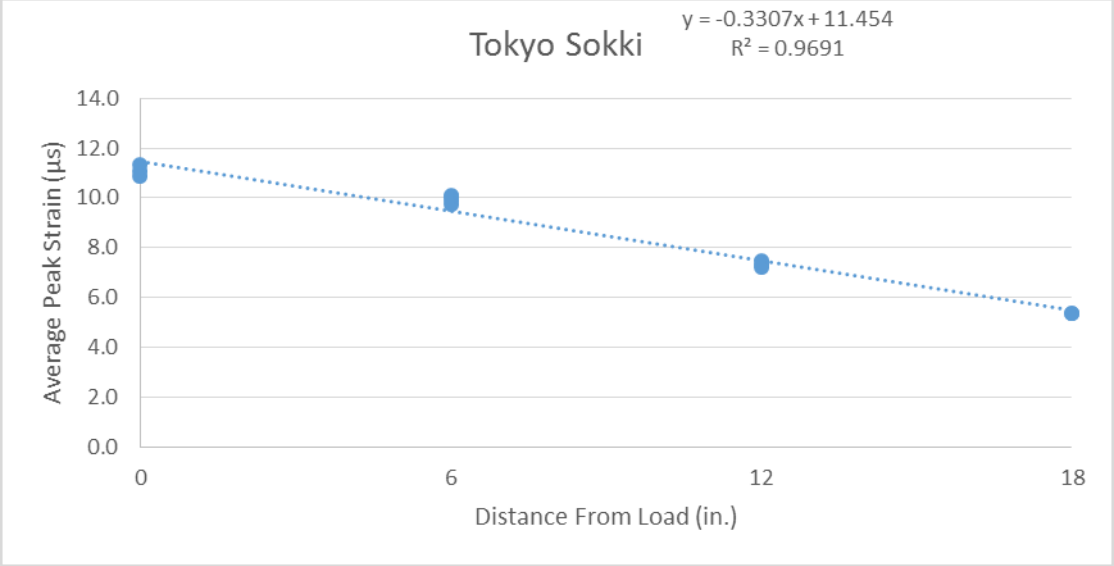

Figure B-21. Tokyo Sokki strain distribution – 9 kip.

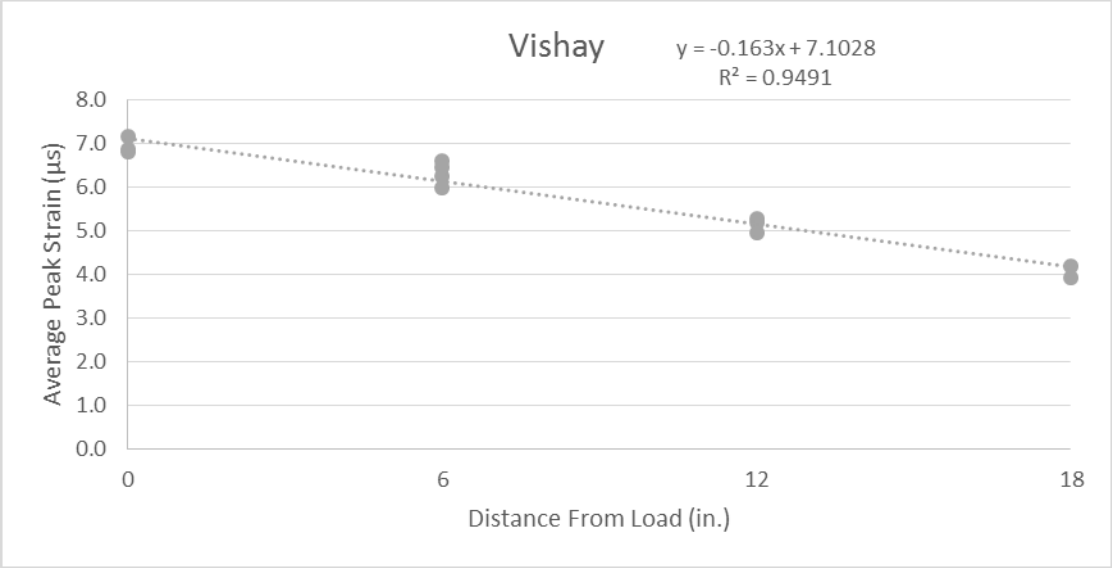

Figure B-22. Vishay strain distribution – 9 kip.

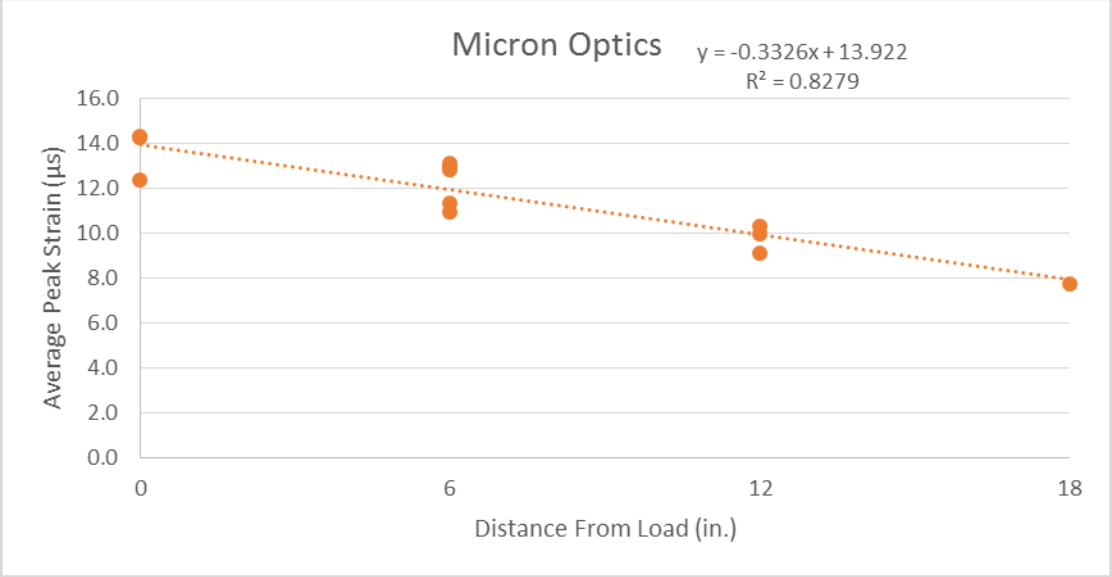

Figure B-23. Micron Optics strain distribution – 12 kip.

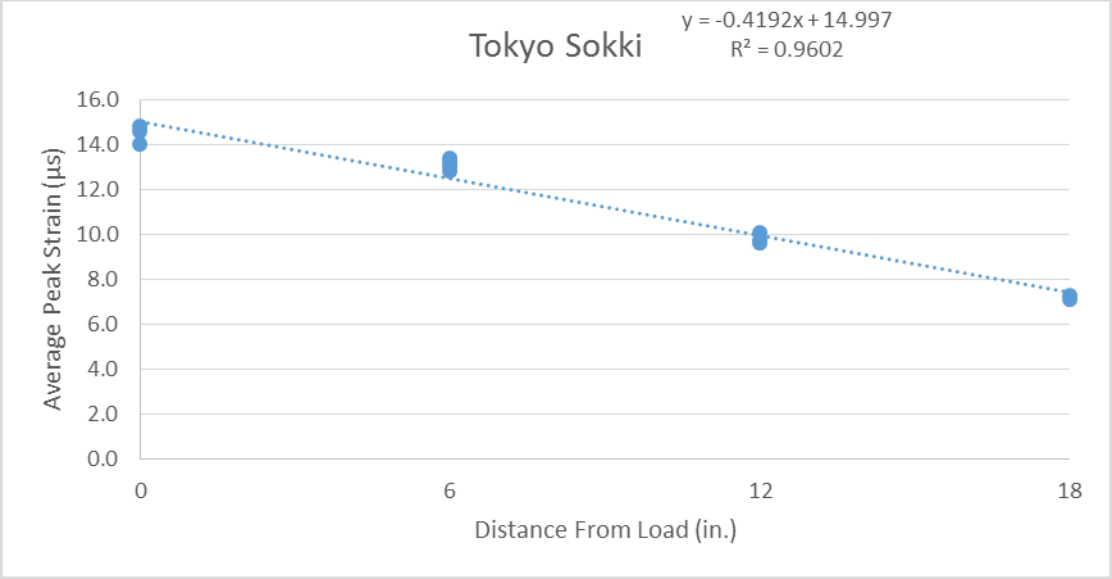

Figure B-24. Tokyo Sokki strain distribution – 12 kip.

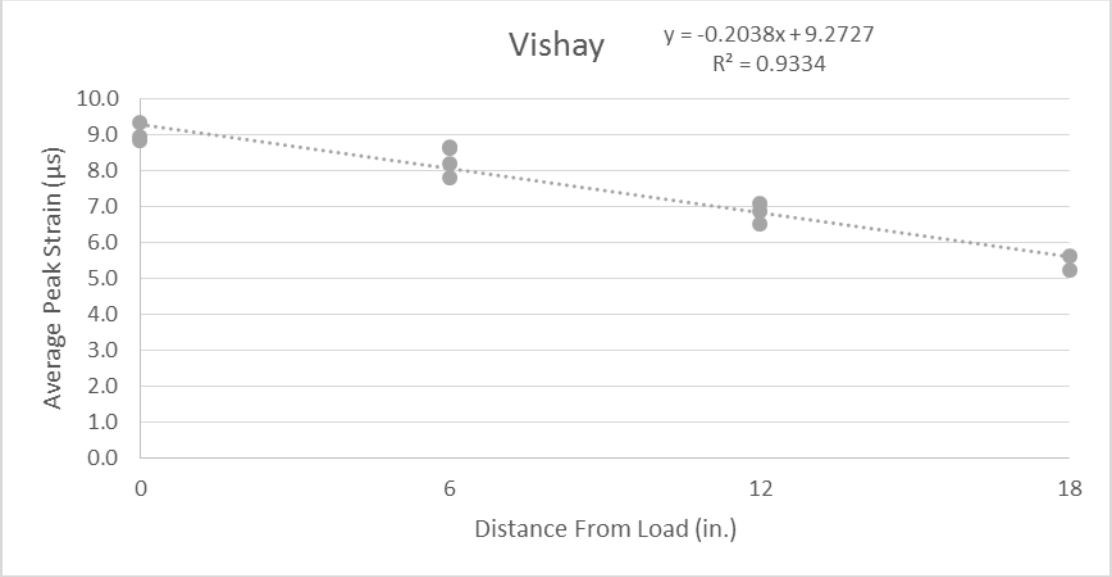

Figure B-25. Vishay strain distribution – 12 kip.. The peaks in the figure represent the energy level at a particular frequency.

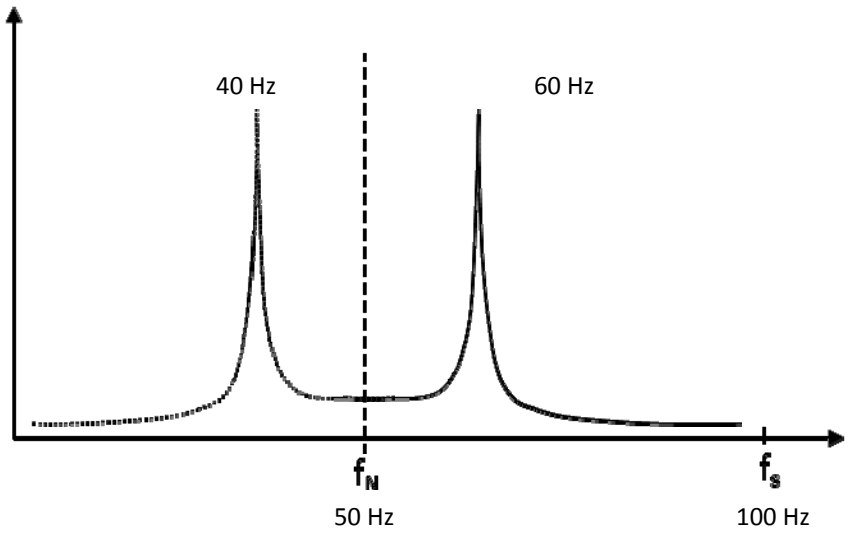

Figure 0-1. Electric hum noise aliased into measured signal.

Figure 0-2 shows one second of an acquired strain signal from of an unloaded, still strain gauge sampled at 100 Hz. A clear harmonic noise is present with a peak-to-peak amplitude of approximately 10 μs. Figure 0-3 shows the frequency content of the same signal with peaks at 40 Hz and 20 Hz, indicating aliased 60 Hz noise.

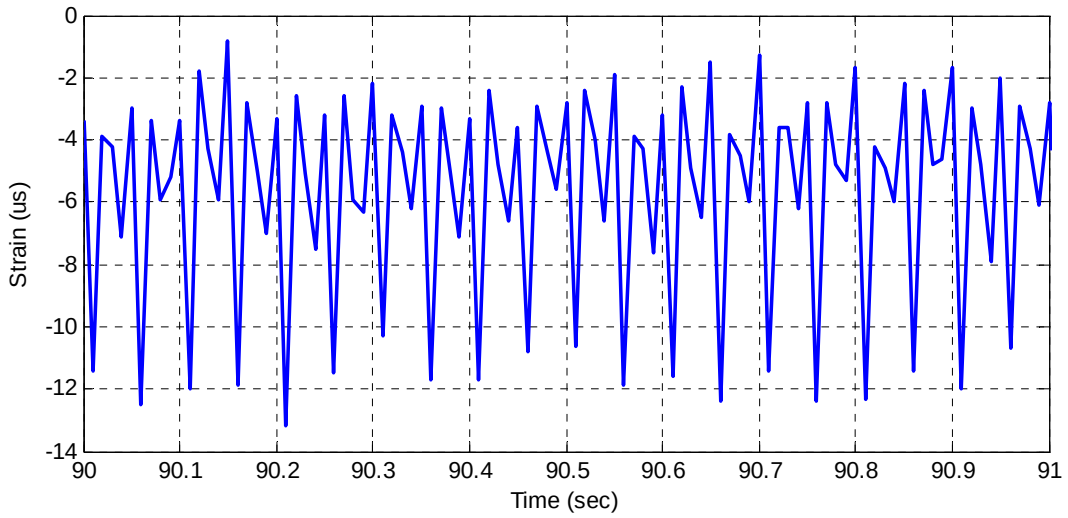

Figure 0-2. Measured electrical hum noise in the time domain using NI Compact DAQ and foil strain gauges.

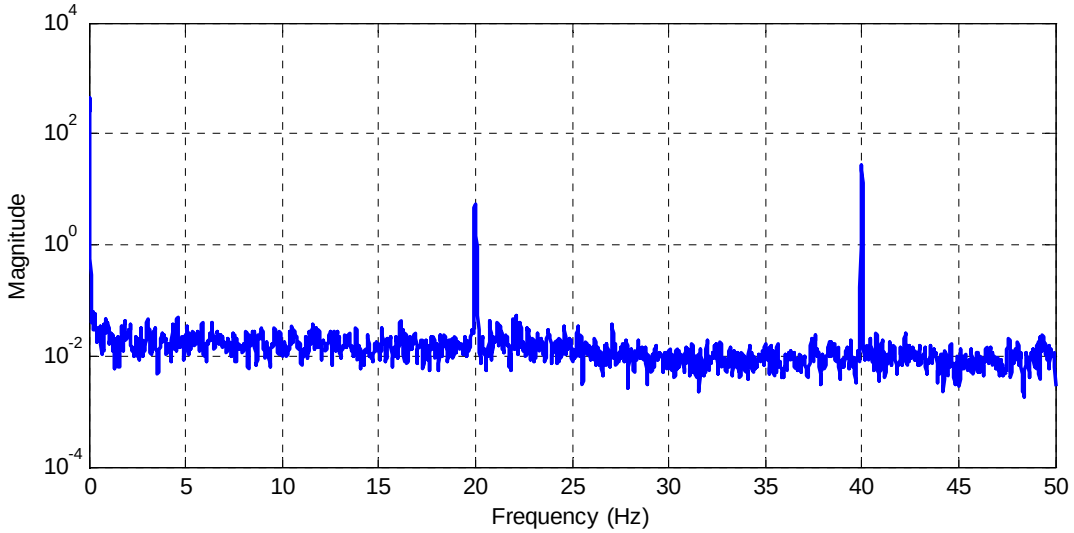

Figure 0-3. Measured electrical hum noise in the frequency domain using NI Compact DAQ and foil strain gauges.

While efforts were made to reduce the 60-Hz noise in the copper strain measurements, it was determined that the best way to minimize the noise would be to implement a digital filter with a cutoff frequency of 40 Hz. Figure 0-4 shows the filter designed and implemented in LabVIEW. The filter is a finite impulse response filter (FIR) with 73 taps. The filter rolls off

between the cutoff frequency, 40 Hz, and about 80 Hz. The result is that some of the 60-Hz energy may be present in the measured signal but at a significantly reduced magnitude. All of the copper-based strain data presented in this section employs this FIR filter. More discussion on post-filter noise levels will be provided in the section describing the noise analysis tests. It should be noted that this 60-Hz noise was not observed in the fiber optic sensors therefore no filtering was applied to their measurement signals.

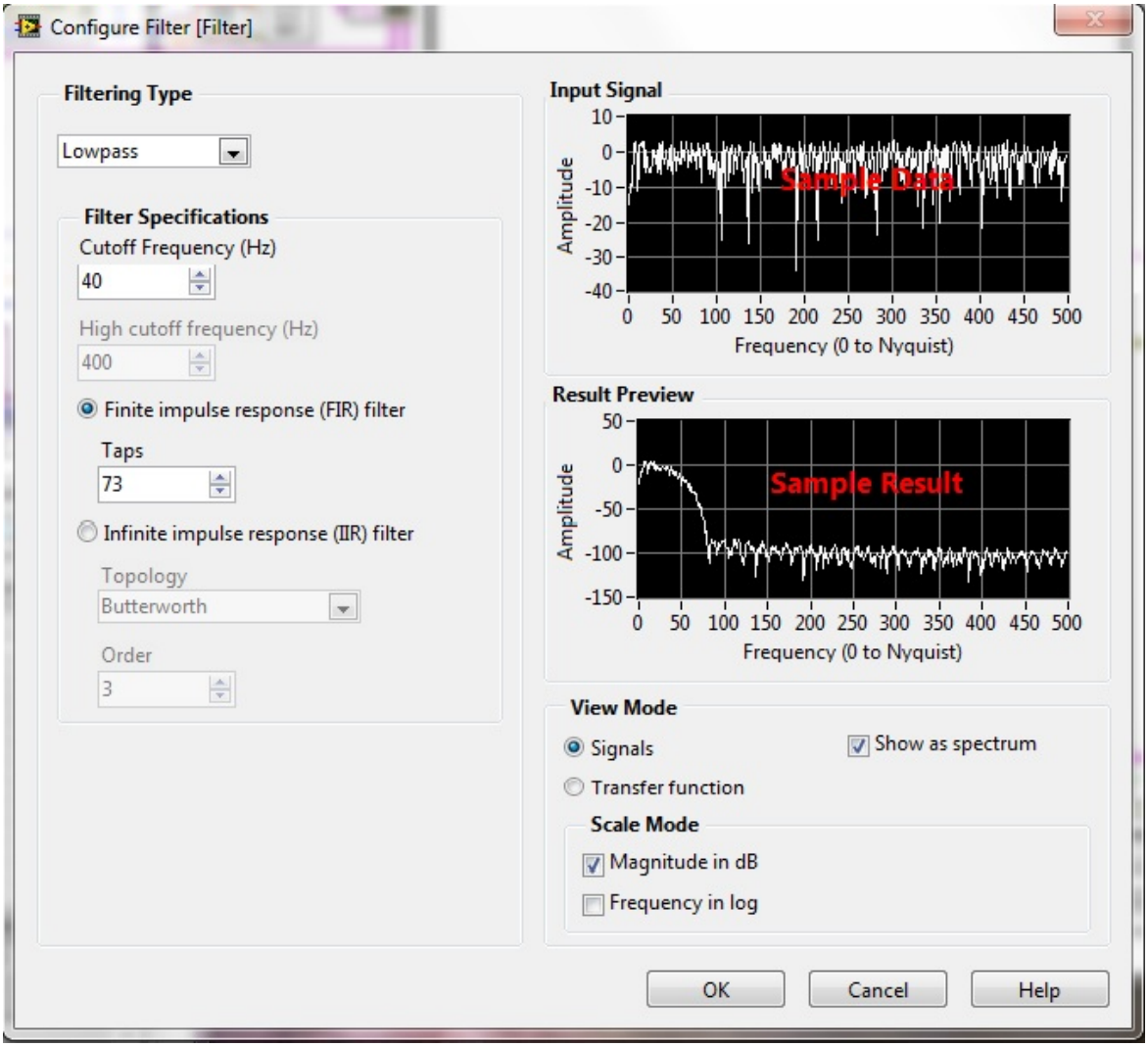

Figure 0-4. FIR filter to reduce 60-Hz noise in strain measurements.

3.2 Compression Test

To assess the performance of the embeddable sensors (both foil and fiber optic) a concrete cylinder was instrumented and tested in uniform compression. This section provides a detailed description of the compression test specimen and its sensor layout. The testing equipment for the compression tests is then outlined and a description of the testing procedures and results are given. Finally, the unique technique for sensor extraction from the cylinder is outlined.

3.2.1 Specimen Description

A concrete cylinder was used to test the sensors in compression and to allow for a comparison of the Micron Optics os3600 embeddable strain sensor to the electronic Vishay EGP-5-120.

The formation of the concrete cylinder was performed using a 36 inch long Sonotube with a 10 inch diameter. This large cylinder size was used to allow for the length of the os3600 sensor, which is one foot in length. A large cylinder was also a necessity to accommodate the large bend radius required for the fiber optic per Micron Optics installation instruction. After the formwork was removed, the cylinder was 26 inches long with a 9.5 inch diameter.

Several precautions were taken in the preparation of the cylinder to facilitate the extraction of the Micron Optics os3600 upon completion of the tests. The os3600 costs approximately $700, and the ability to reuse the sensor after embedment would be advantageous for many future projects. The concrete mix was composed of 30% fly ash to increase its workability, and the concrete only cured for 36 hours before beginning compression tests.

To further facilitate the os3600 removal, the sensors were placed with minimum clear cover (approximately two inches) from the long wall of the cylinder so they would be easier to access upon the extraction cutting. The sensors were suspended from either end of the cylinder using fiberglass rods and then held in place using zip ties. The Micron Optics os3600's Teflon center was wrapped in packaging foam as well as Saran wrap that wrapped almost the entirety of the sensor. The only unwrapped portions of the sensor were the two steel circular plates required to adhere with and displace along with the concrete. Figure 0-5 shows the location of the sensors inside the formwork before the concrete cylinder was cast.

Figure 0-5. Sensor layout for formwork of the concrete cylinder specimen.

After curing for 36 hours, the concrete had a compressive strength of 1,860 psi, modulus of elasticity of 2,500 ksi, and a Poisson ratio of 0.25 (determined by a series of cylinder tests conducted at SMO just prior to the main cylinder test). Figure 0-6 shows the finished concrete cylinder.

Figure 0-6. Finished concrete cylinder specimen.

3.2.2 Testing Equipment

A universal testing machine (UTM) was used for the compression test performed on the concrete cylinder. The UTM, manufactured by Instron, applied forces to the top and bottom of the specimen. The calibration for the machine allows for a loading range of 8 kips to 800 kips in both tension and compression (Instron, 2013). Figure 0-7, is a picture of the concrete cylinder in the UTM before testing.

Figure 0-7. Instron UTM being used for concrete cylinder compression test.

3.2.3 Procedure

The concrete specimen was loaded in compression using the UTM for seven different load cases. The first five load cases were applied statically and held for two minutes each. A dynamic load case cycled between 20 and 25 k compression. The final load case was a stepwise, ramp and hold loading scenario in which data was collected continuously without zeroing. All of the aforementioned load cases are expressed below in Table 0-1. In all cases, the gauges were zeroed at the beginning of each test.

Table 0-1. Compression load cases.

Load Case	Load Type	Load (kip)
1	Static	5
2	Static	10
3	Static	15
4	Static	20
5	Static	50
6	Dynamic	20-25
7	Static ramp and hold	0-25

3.2.4 Results

Plots of all of the data acquired are given in Appendix A. Figure 0-8 and Figure 0-9 show copper and fiber optic (FO) data from the 5 k and 20 k load cases, respectively. The top plots show the strain measurements taken from each gauge type as the load was steadily applied and then held at the prescribed level. The bottom plot shows the difference between the two signals during the hold portion (last 100 seconds) of the test. The percent variation is also indicated in the difference plot.

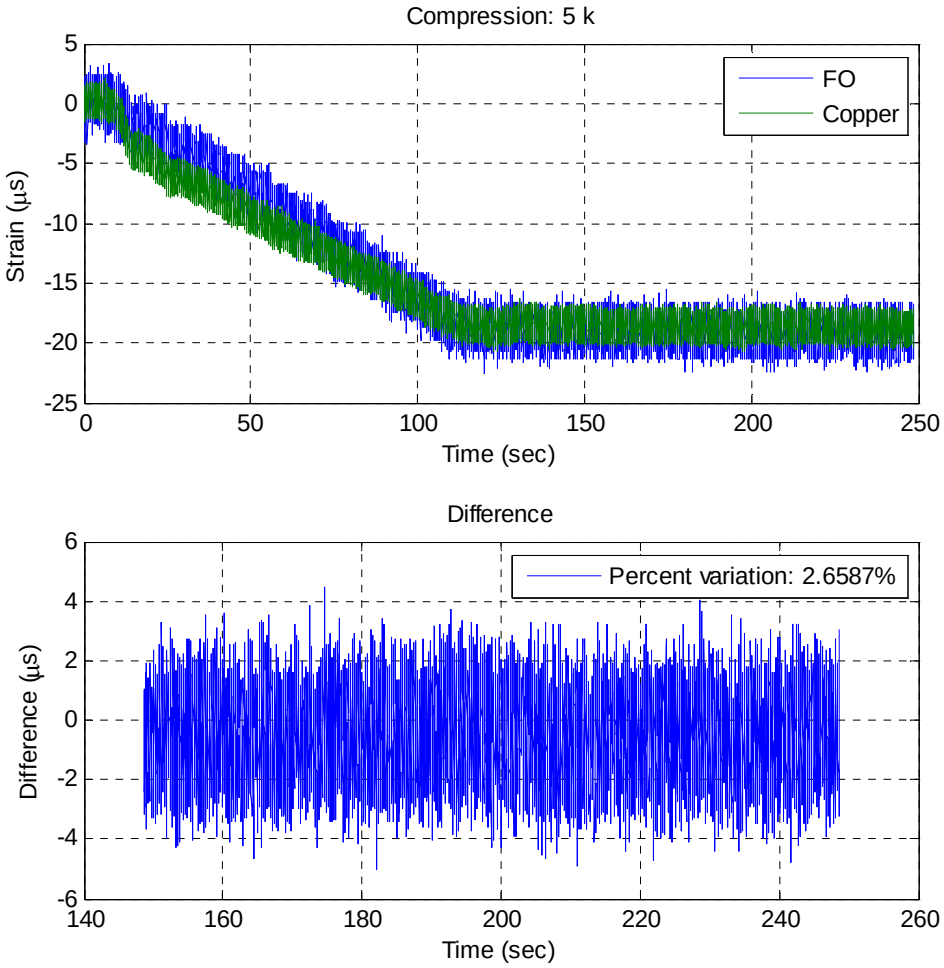

Figure 0-8. 5 k compression strain measurements and sensor measurement difference.

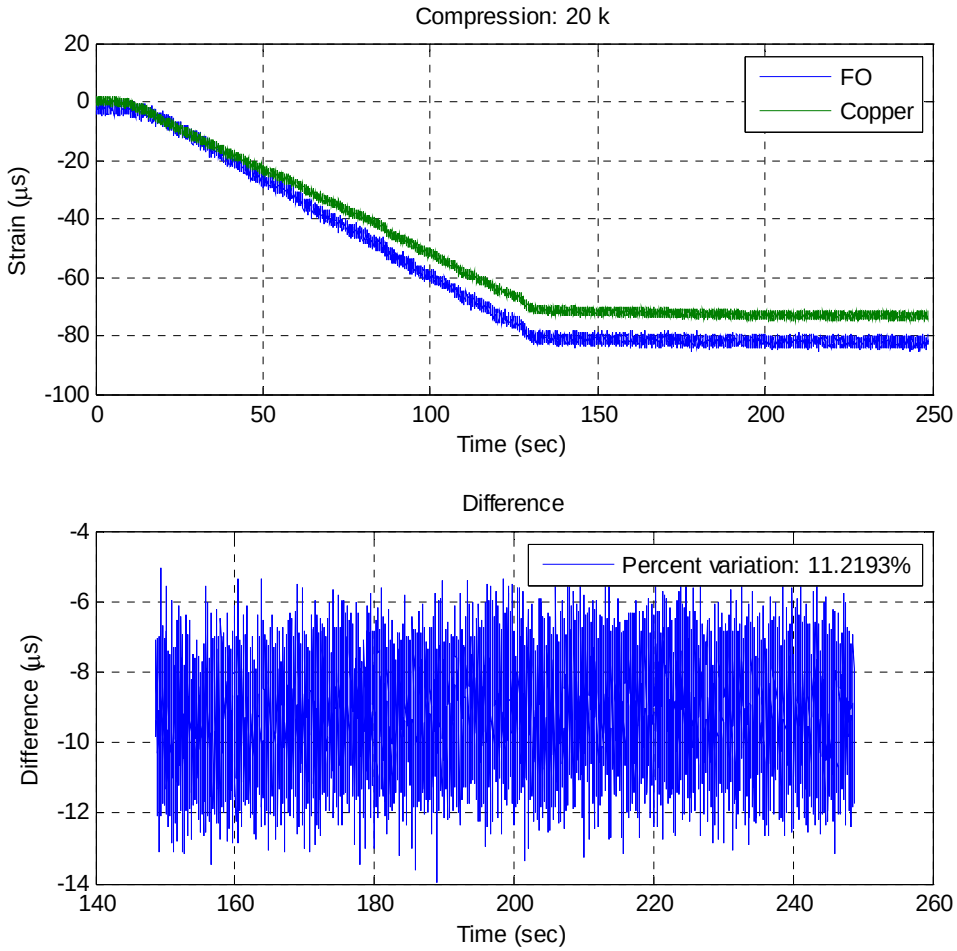

Figure 0-9. 20 k compression strain measurements and sensor measurement difference.

Table 0-2 summarizes the results of the static load tests with the average strain from both gauges and both the absolute difference and percent difference given for each load case. It can be seen that the differences (both absolute and percent) increase with increasing strain values. This phenomenon is further illustrated in the results from the ramp and hold test, as shown in Figure 0-10. Table 0-2 also presents the noise level (given as the RMS values of the strain during the last 100 seconds of the test data) for both gauges, with consistent values of approximately 1 μs.

Table 0-2. Static hold compression load results.

Load Case	Load (kip)	Average Strain (μs)	Mean Difference (μs)	Percent Difference (%)	RMS Noise FOS (μs)	RMS Noise Copper (μs)
1	5	-18.89	0.51	2.66	1.07	0.96
2	10	-37.14	2.55	6.64	1.03	0.96
3	15	-56.74	4.46	7.57	1.04	1.02
4	20	-77.30	9.19	11.22	1.05	1.06
5	50	-206.61	49.40	21.36	1.02	1.01

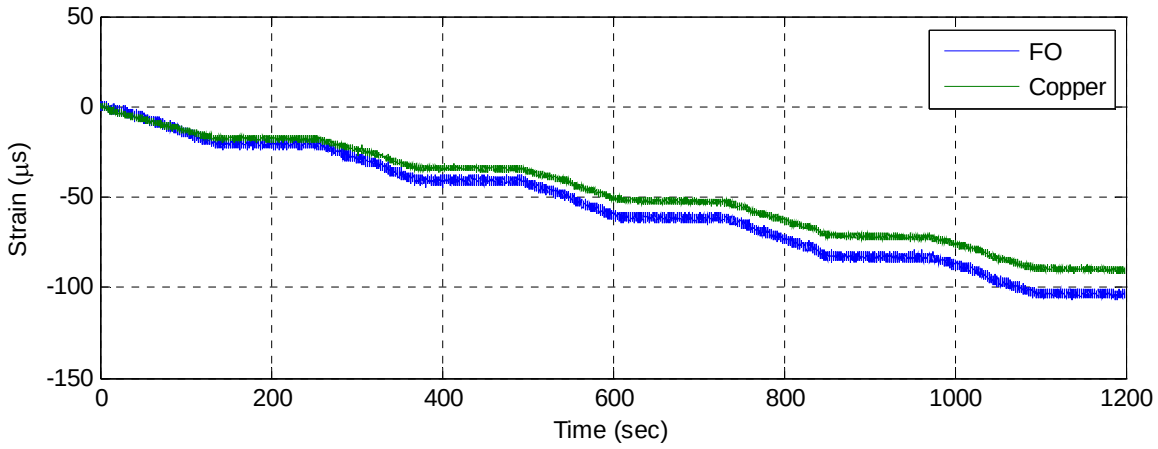

Figure 0-10. Ramp and hold compression strain measurements.

Figure 0-11 shows the strain measurements during the load cycling portion (between 20 and 25 k) of the dynamic compression test. Both gauges were responsive to the dynamic load and showed a consistent difference of approximately 10 μs.

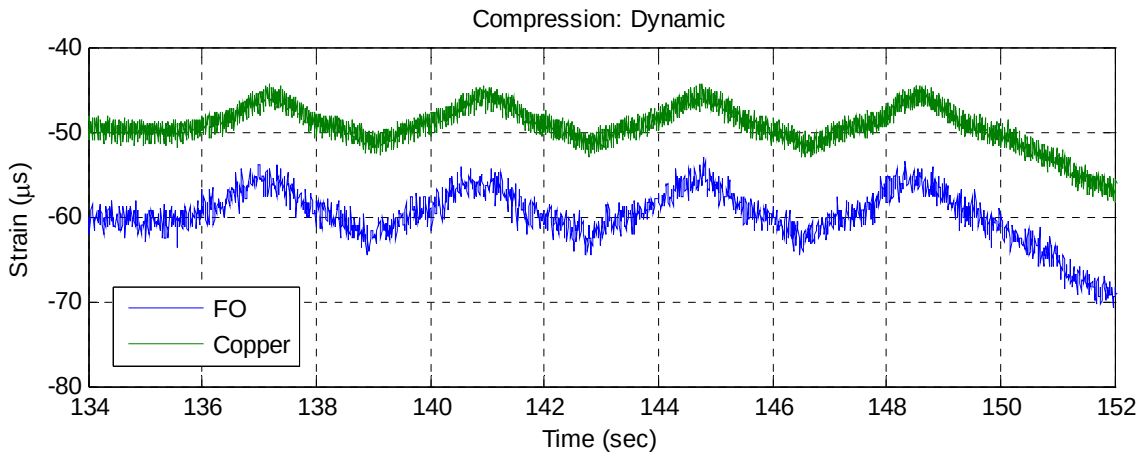

Figure 0-11. Dynamic compression strain measurements.

The non-homogenous nature of concrete made an assessment of the relative accuracy of each sensor type embedded in the concrete challenging; however, the results of the compression tests indicated that the gauges output similar strain values at the same loads with percent differences ranging from 2.6 to 21.4 percent. The differences were consistent during each test with the fiber optic gauge reading slightly higher than the foil gauge in each test. Each gauge output a steady array of strain output during the static load holds. It can be concluded that both gauges offer reasonable and consistent strain measurement capabilities for embedded concrete testing.

3.3 Sensor Extraction

After the compression test was conducted using the UTM, the sensor extraction process took place. A circular saw was used to cut approximately four inches off the top and the bottom of the cylinder. Then a longitudinal cut was made along the length of the cylinder (through the Vishay EGP-5-120) to allow for a prying technique to split the cylinder open and expose the Micron Optics sensor. The sensor was successfully extracted from the cylinder, and it maintained its ability to read strain. Figure 0-12 through Figure 0-15 show the sensor extraction process.

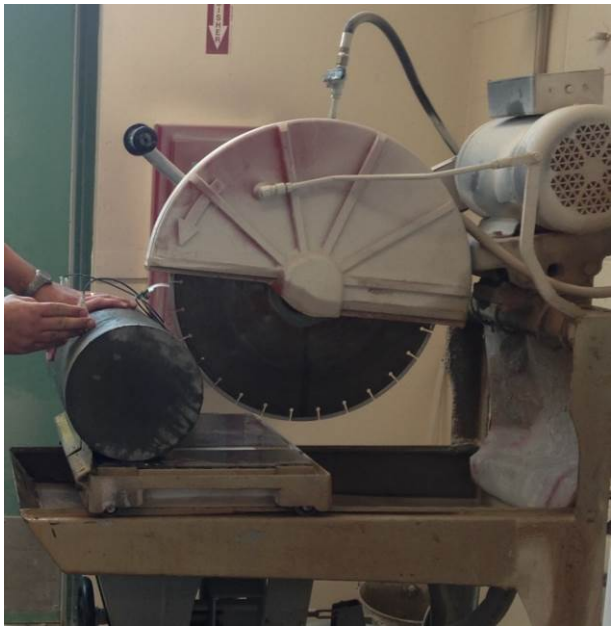

Figure 0-12. Transverse cut along top and bottom.

Figure 0-13. Longitudinal cut.

Figure 0-14. Prying technique used for sensor removal.

Figure 0-15. Micron Optics os3600 after extraction.

3.4 Tension Test

3.4.1 Specimen Description and Sensor Layout

A 24”x4”x1/2” steel specimen was used to mount the sensors evaluated in the tension tests. The steel plate is a 1018 low-carbon steel tight tolerance bar made to ASTM A36 standards (McMaster-Carr, 2013a). ASTM 36 standards for material characteristics yield a thermal coefficient of expansion of 7.06 x 10^{-6} in/ºF, tensile strength of 58-80 ksi, elongation of 18-23%, and a yield strength of 36,000 ksi (McMaster-Carr, 2013b). The material characteristics and

dimensions allowed for 1241 μs before yielding (which would cause permanent deformations) and 746 μs before buckling (which only occurs in compression).

Both copper-based and fiber optic sensors were adhered mid-length across both sides of the four-inch width of the specimen, with identical sensor types on each side. The strain sensors tested on the specimen were the Micron Optics os3110 optical strain gauge designed for mounting via spot welding (Micron Optics, 2010c), the os3610 surface mountable strain gauge, and Tokyo Sokki's PFL-30-11-5L surface mount foil gauge (Tokyo Sokki, 2013c). The foil strain gauge is the most commonly used strain gauge for this type of specimen. The os3110 was used because it resembles the foil gauge in that it is also applied directly to the surface and they share a similar gauge length. The os3610 was used because the sensing technology is the same as the os3600 which is used for concrete embedment.

Temperatures were recorded using the Micron Optics os4100 temperature compensation sensor (Micron Optics, 2009b) and the Omega TT-K-24-100 thermocouple wire. The thermocouple wire is often used in SMO testing applications, and the os4100 was expected to experience similar effects and provide comparable results to that of the thermocouple. The os4100, os3110, and foil gauges are small enough that they were placed between the steel plate and the mountable os3610. Figure 4-1 illustrates the sensor layout for the steel specimen where three sensors were epoxied to the steel plate beneath the os3610 which was mounted above them. Figure 0-17 and Figure 0-18 show the steel specimen before and after the installation of the os3610.

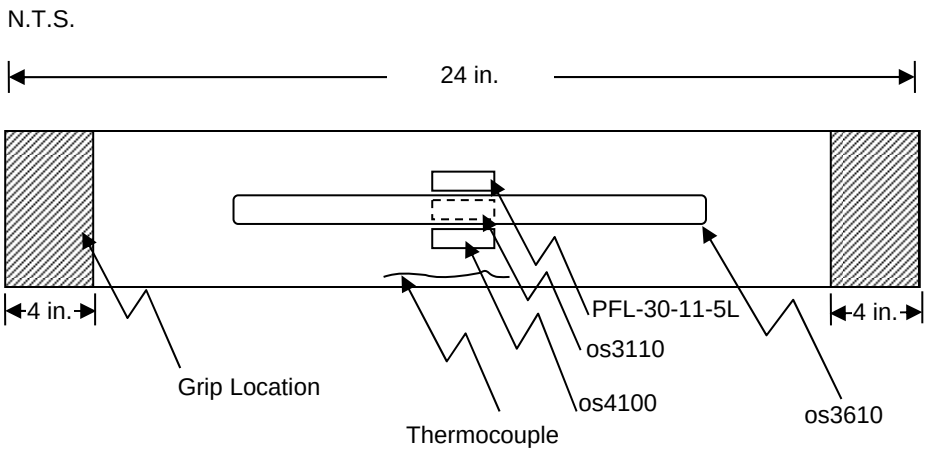

Figure 0-16 Steel plate sensor layout.

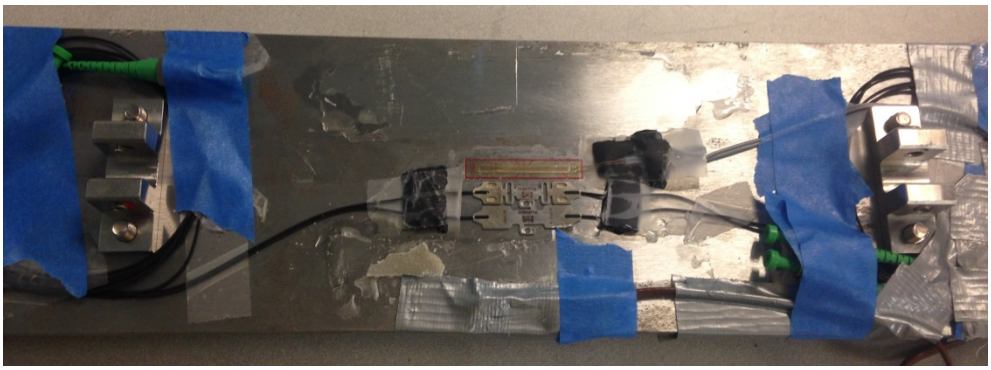

Figure 0-17. Sensor layout before installation of os3610.

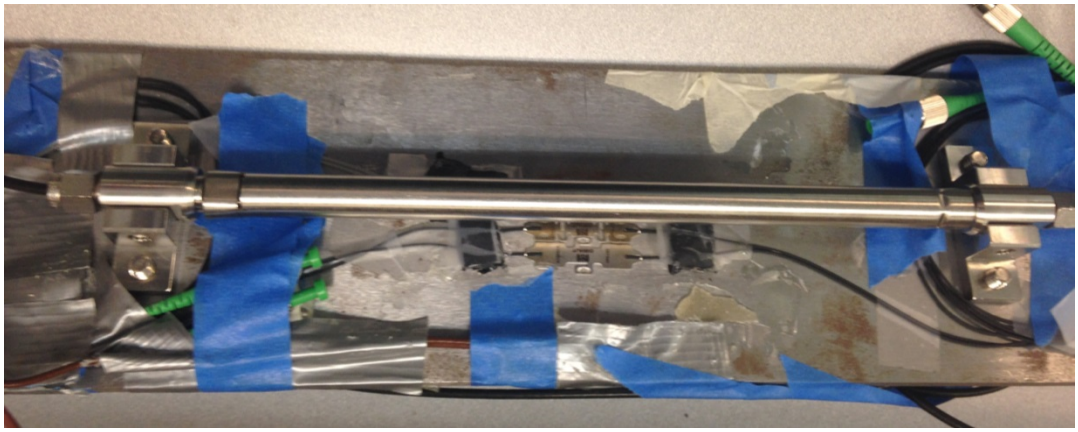

Figure 0-18. Sensor layout after installation of os3610.

3.4.2 Testing Equipment

The UTM that was used for the compression tests (detailed in Section 3.2) was also used to apply tension to the steel plate. The upper limit of the loading capacity of the machine was not required during the tensile tests since the yield strength of the specimen controlled at 1241 μs or 36 kips. The UTM used five inch grips on either end of the plate. Misalignment of the machine's grips can cause the specimen to experience improper loading conditions. The loads could also potentially cause the specimen to bend, which would affect the results of the strain measurements. If the grips are misaligned, the axis of the specimen would not be completely vertical which would cause the sensors to read inaccurately. Figure 0-19 shows the UTM loaded with the steel specimen.

Figure 0-19. Instron UTM being used for steel plate tension test.

3.4.3 Procedure

The UTM was used to induce both static and dynamic tensile loads. For static tests, seven different tensile loads were applied. Upon full application of the load, the sensors recorded two minutes of strain measurements. Table 0-3 shows the anticipated strains and plate elongations in response to these loadings, as well as the applied loads for the various load cases. The final row of the table shows the yield limitations for the steel plate. The yield threshold was to not be exceeded during testing.

Table 0-3 Static tensile load cases.

Load Case	Load (kips)	Expected Strain (μs)	Elongation (in)
1	1	34.5	1.4E-06
2	2	69.0	2.9E-06
3	14	482.8	2.0E-05
4	20	689.7	2.9E-05
5	25	862.1	3.6E-05
Maximum Upper Limit for Tension	36	1241.4	5.2E-05

For the dynamic test, the tensile load oscillated between 4.5 kips and 5.5 kips at a rate of 1 Hz. These loads produce expected calculated strains of 155.2 and 189.7 μs, respectively.

3.4.4 Results

Representative data from the 2 k and 20 k load cases are shown in Figure 0-20 and Figure 0-21, respectively. Similar to the plots for the compression test, the top plots show the strain measurements taken from each gauge type as the load was steadily applied and then held at the prescribed level. The second plots show the difference between the os3610 and the foil gauge signals during part of the hold portion (last 100 seconds) of the test. Then, the third plots show a similar analysis of the difference between the os3110 measurements and the measurements of the foil gauge. Finally, the fourth plots show the variance between the two fiber optic gauges. The percent variation of each comparison is indicated in the legend of the particular difference plot. Plots of all of the data acquired during the tension tests can be found in Appendix A.

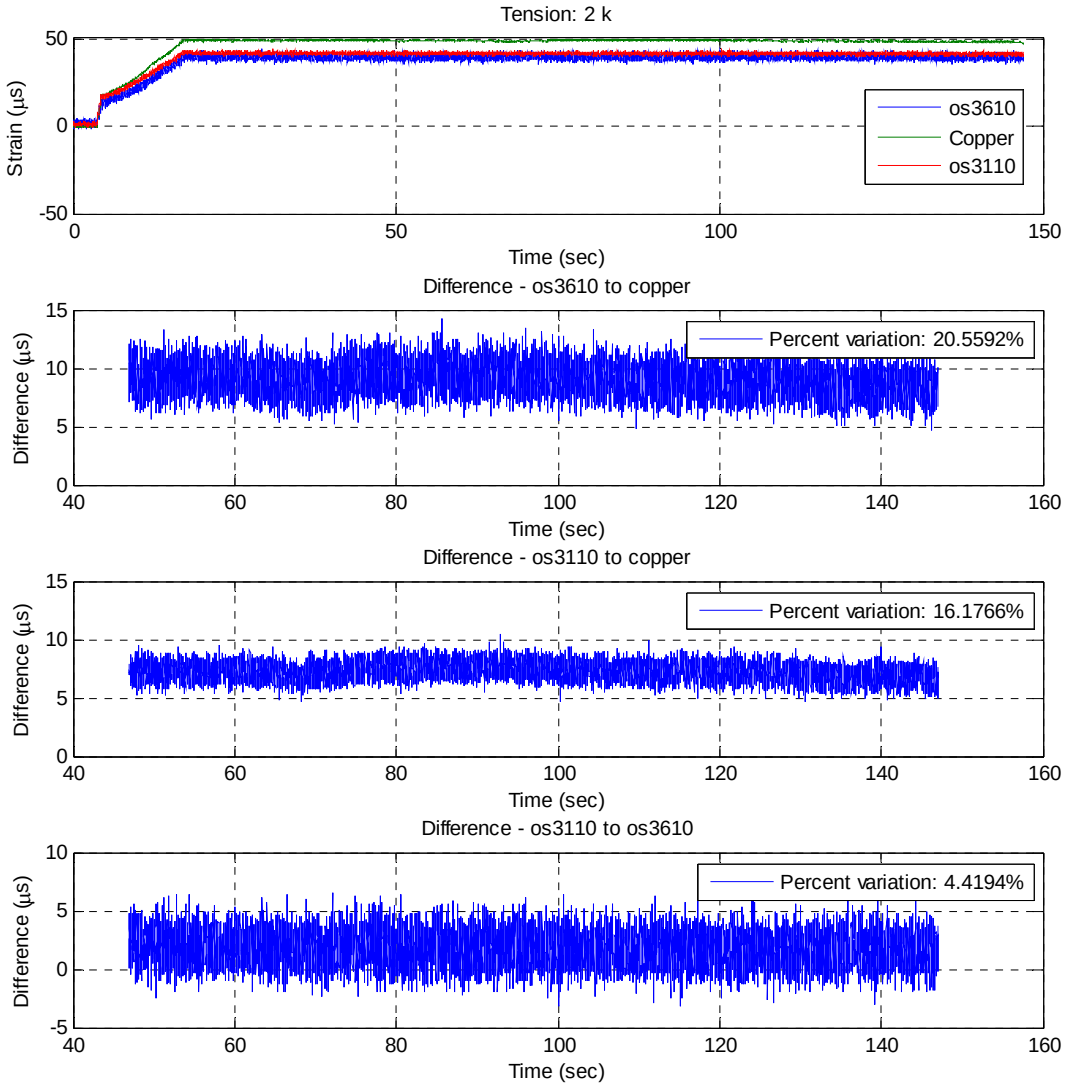

Figure 0-20. 2 k tension strain measurements and sensor measurement differences.

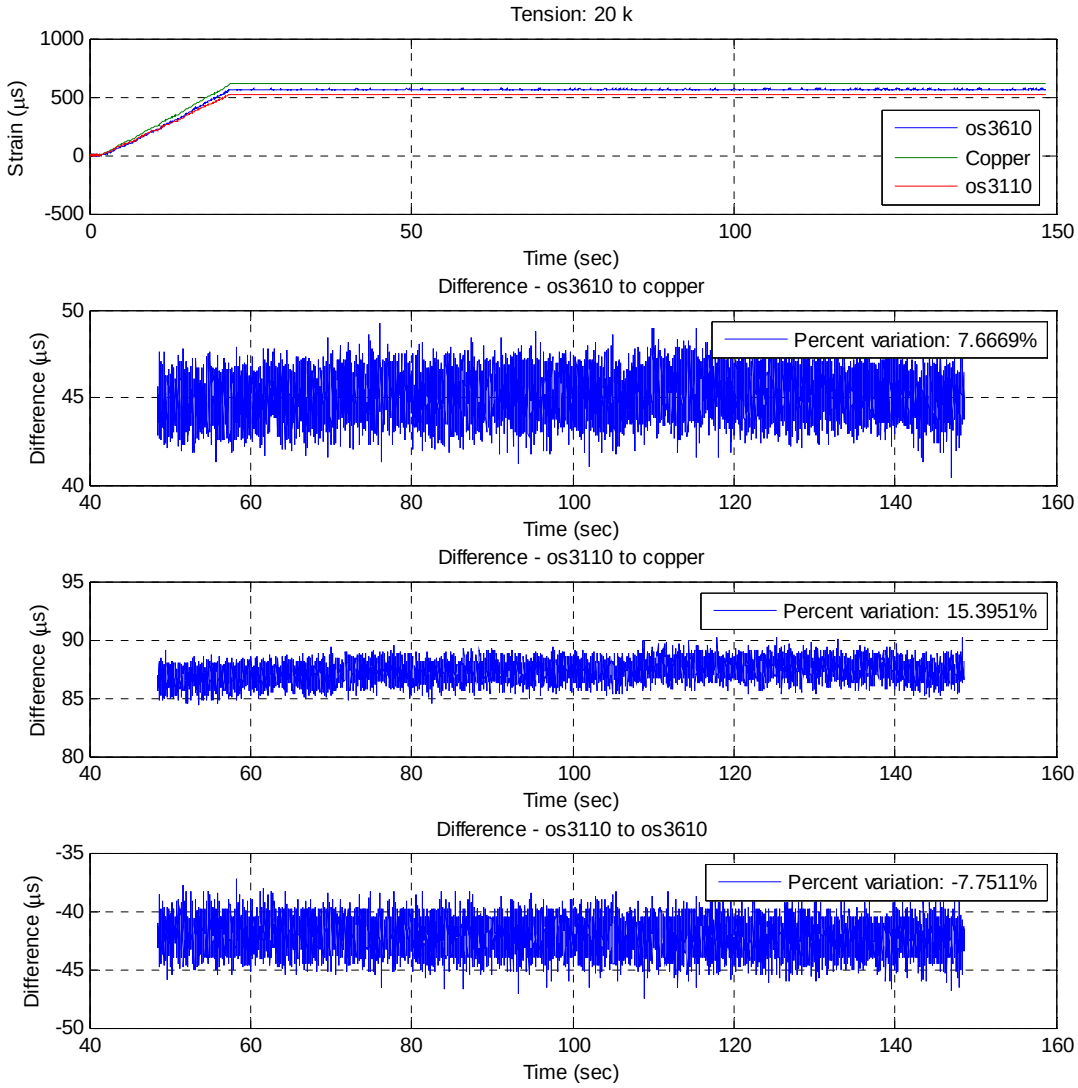

Figure 0-21. 20 k tension strain measurements and sensor measurement differences.

Figure 0-20 and Figure 0-21 show that the two Micron Optics models compared favorably with one another (< 10% variation). The difference between the two fiber optic gauges was smaller at the beginning of the tests during the load increase. While the fiber optic gauges had reasonable agreement with one another, they both read lower strain levels than the copper gauge (up to ~ 20% lower).

Table 0-4, Table 0-5, and

Table 0-6 summarize the results of the static load tests. The average strain for the various loads is given for each sensor, and both the absolute difference and percent difference given for each load case.

Table 0-4 details the os3610 data in comparison to the foil gauge data. Table 0-5 details the data from the os3110 in comparison to that of the foil gauge. Finally, Table 0-6 details the data from the os3610 in comparson to the data from the os3110, which shows the small percent difference between the two FOS gauges and how the larger average strain value came from a different FOS depending on the load case.

Table 0-4. Static hold tension load results for os3610 compared to the foil strain gauge.

Load Case	Load (kip)	Foil Gage Average Strain (µs)	os3610 Average Strain (µs)	Mean Difference (µs)	Percent Difference (%)
1	1	26.66	18.83	7.83	34.43
2	2	48.60	39.54	9.06	20.56
3	14	417.72	378.20	39.52	9.93
4	20	610.43	565.36	45.07	7.67
5	25	759.69	716.20	43.49	5.89

Table 0-5. Static hold tension load results for os3110 compared to the foil strain gauge.

Load Case	Load (kip)	Foil Gage Average Strain (µs)	os3110 Average Strain (µs)	Mean Difference (µs)	Percent Difference (%)
1	1	26.66	20.73	5.93	25.01
2	2	48.60	41.32	7.27	16.18
3	14	417.72	358.68	59.04	15.21
4	20	610.43	523.17	87.26	15.40
5	25	759.69	653.74	105.95	14.99

Table 0-6. Static hold tension load results for os3610 compared to the os3110.

Load Case	Load (kip)	os3610 Average Strain (με)	os3110 Average Strain (με)	Mean Difference (με)	Percent Difference (%)
1	1	18.83	20.73	1.90	9.63
2	2	39.54	41.32	1.79	4.42
3	14	378.20	358.68	-19.52	-5.30
4	20	565.36	523.17	-42.19	-7.75
5	25	716.20	653.74	-62.46	-9.12

The signal variation for the various load cases is detailed in Table 0-7. Similar to the noise values in the compression test, the values in this table are given as the RMS values of the strain during the last 100 seconds of the test data.

Table 0-7. Noise during tension test.

Load Case	Load (kip)	Foil Gage RMS Noise	os3110 RMS Noise (με)	os3610 RMS Noise (με)
1	1	0.313	0.718	1.29
2	2	0.427	0.708	1.31
3	14	0.402	0.687	1.11
4	20	0.391	0.709	1.18
5	25	0.402	0.703	1.02

In this data, large percent differences between the foil gauges and both fiber optic sensors were observed in the first load case. Likewise, the second load case for the os3610 shows a large percent difference. The percent difference at lower strain levels is somewhat misleading due to the small levels of strain measured (23 – 45 με); in all three cases, the absolute strain difference is reasonable for the intended application, at less than 10 με.

The os3110 data proved very consistent in its variation from the foil gauge. Both of these gauges were attached directly to the surface of the specimen, which allows for similar strains to be experienced, resulting in a consistent percent strain difference with the foil gauge at approximately 16.5%. The os3610, which was mounted to the surface using brackets, showed inconsistent percent differences in comparison to the foil gauge readings; for the higher load cases (14 – 25k) the percent strain difference between the os3610 and the foil gauge ranged between 6 and 10%. The mounting mechanism may have contributed to the inconsistent measurements.

Similar strain differences between the fiber optic gauges and the foil gauge were observed during the load cycling portion (between 4.5 and 5.5 k) of the dynamic tension test, as shown in Figure 0-22. All three sensors were responsive to the dynamic load. Table 0-8 summarizes the dynamic tension data.

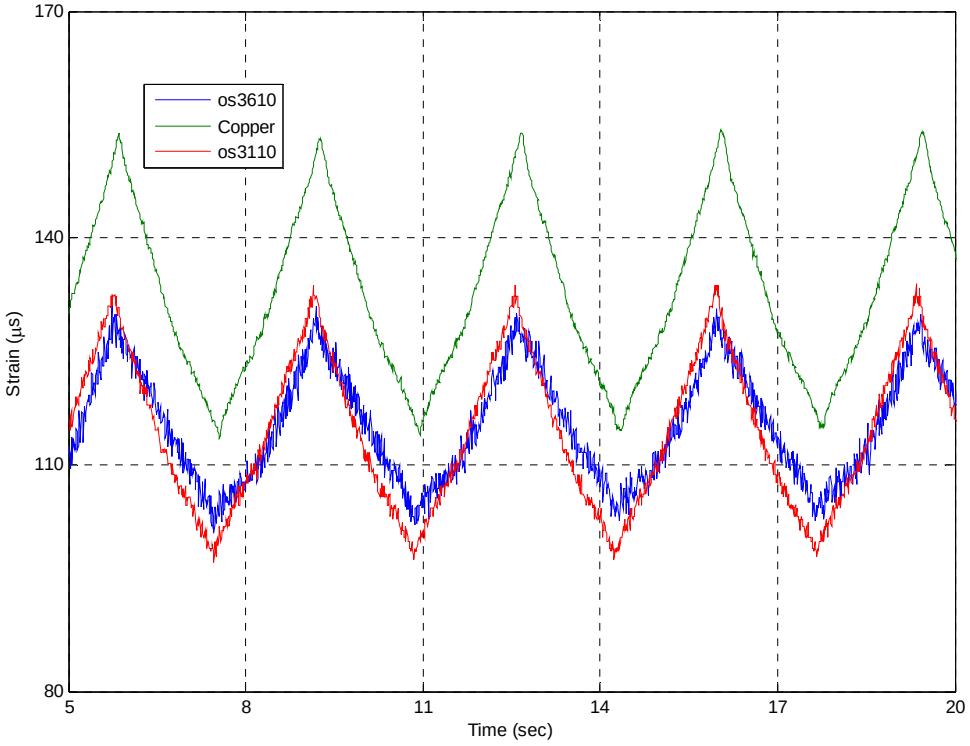

Figure 0-22. Dynamic compression strain measurements.

Table 0-8. Dynamic tension test results compared to the foil gauge readings.

Sensor	Average Strain (με)	Mean Difference (με)	Percent Difference (%)
os3610	67.99	9.32	14.66
os3110	67.22	10.50	16.93

The fiber optic sensors output strain levels that were consistently lower than the foil strain gauge readings. It is challenging to determine the exact strain experienced by the specimen, resulting in the use of comparative analysis as the primary tool for the assessment of the sensors. The consistency between the fiber optic sensors is promising, as is the stable and responsive behavior of all sensor types. While the source of the different strain levels of the copper and fiber optic gauges cannot be definitively determined, the tensile tests are not representative of the way the sensors will be applied in the test pavement. The results of the compression tests provide a better representation of the anticipated sensor measurement environment.

3.5 Temperature Test

Both copper-based and fiber optic strain sensors are susceptible to temperature variations. The properties of the sensors can vary with changing temperatures making their output a function of both the strain they measure and the temperature changes they experience. The change in the strain measurements usually varies linearly with temperature changes. A range of approaches can be taken to correct for sensor readings impacted by temperature ranges. The Micron Optics os3600, to be used in the embedded slab tests, has built-in temperature sensor used for temperature compensation in the ENLIGHT (or other selected DAQ) software. The copper-based strain gauge, however, did not have any automatic compensation in place.

It is expected that embedded gauges in the test pavement will experience a wide range of temperatures during their measurement lifetime, both due to the environmental variations and during the concrete curing process. Thus, a precise understanding of temperature effects on each sensor type is essential. This portion of the testing was focused on quantifying the temperature

sensitivity of a copper strain gauge and a temperature-compensated fiber optic gauge. Temperature effects will also be evaluated in the embedded testing section.

3.5.1 Specimen Description

The steel specimen (detailed in Section 4.1) was also used for the temperature tests. The os3610 has a temperature sensitivity of 22 pm/°C. The PFL-30-11-5L foil gauge has an operational temperature of -20°C to +80°C and a temperature compensation range of +10°C to +80°C; a specific sensitivity is not given in the data sheet.

3.5.2 Testing Equipment

Temperature tests were conducted using the Blue M Steady State/Stability Test Chamber, model number CEO9xx-4. The temperatures for this machine can range from 0°C to +99 °C (Blue M, 2011). Figure 0-23 shows the environmental chamber used in temperature tests.

Figure 0-23. Blue M CEO9xx-4 test chamber.

The specimen was simply supported in order to allow separation between the sensors and the plate inside the chamber. See Figure 0-24 for an image of the specimen inside the environmental chamber.

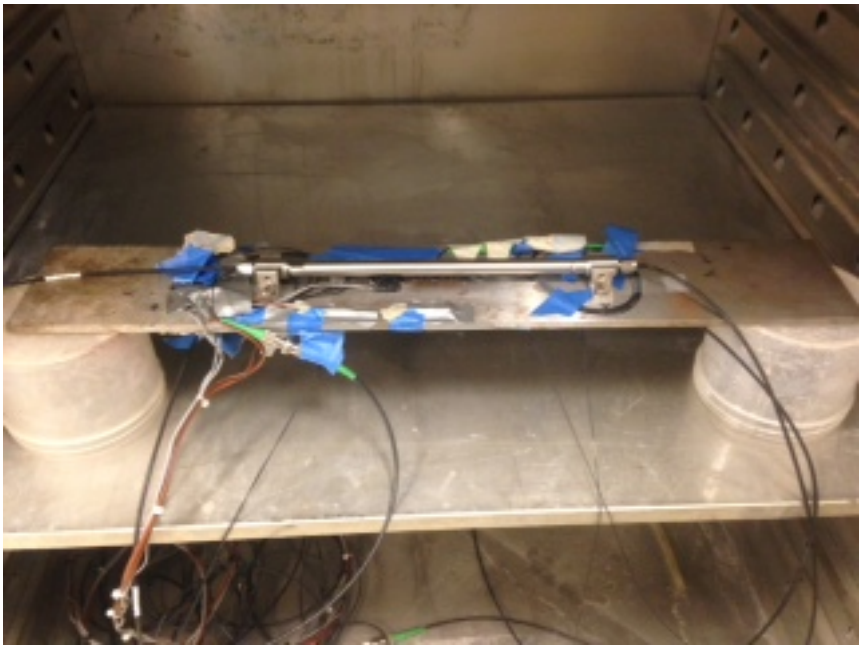

Figure 0-24. Temperature test setup inside environmental chamber.

3.5.3 Procedure

The specimen was inserted into the chamber at 73.5°F. Strains due to temperature change were measured at 1 Hz over a three-minute period. Strain and temperature data was recorded as the chamber heated from 73.5°F to 108.5°F. Upon reaching 108.5°F, the strains were again measured for a three-minute period. The chamber temperature was then decreased back to 73.5°F as another set of data was recorded. Once again, the data was recorded for three minutes at the 73.5°F temperature. The data logging process was then repeated as the chamber cooled to 32°F before finally heating back to the original 73.5°F. A log of the various temperatures and duration of the data sets is displayed below in Table 0-9.

Table 0-9. Various temperatures tested.

Test	Temperature (°F)	Duration (min)
Constant Room Temp 1	73.5	3
Heating 1	73.5 – 108.5	30
Constant Hot	108.5	3
Cooling 1	108.5 – 73.5	20
Constant Room Temp 2	73.5	3
Cooling 2	73.5 - 32	40
Constant Cold	32	3
Heating 2	32 – 73.5	20
Constant Room Temp 3	73.5	3

3.5.4 Results

The complete test results are given in Appendix A while the results of the one heating and one cooling test are presented here in Figure 0-25 and Figure 0-26, respectively. In the figure, the top plot shows the temperature measured by the thermocouple, the middle plot shows the corresponding strain readings from each gauge type, and the bottom plot shows the strain plotted vs. temperature for each gauge type. The bottom plot illustrates the relationship between the strain measurement and the temperature and the slope of the line (determined using linear regression to provide an estimate of the temperature sensitivity) is given in the legend of the plot.

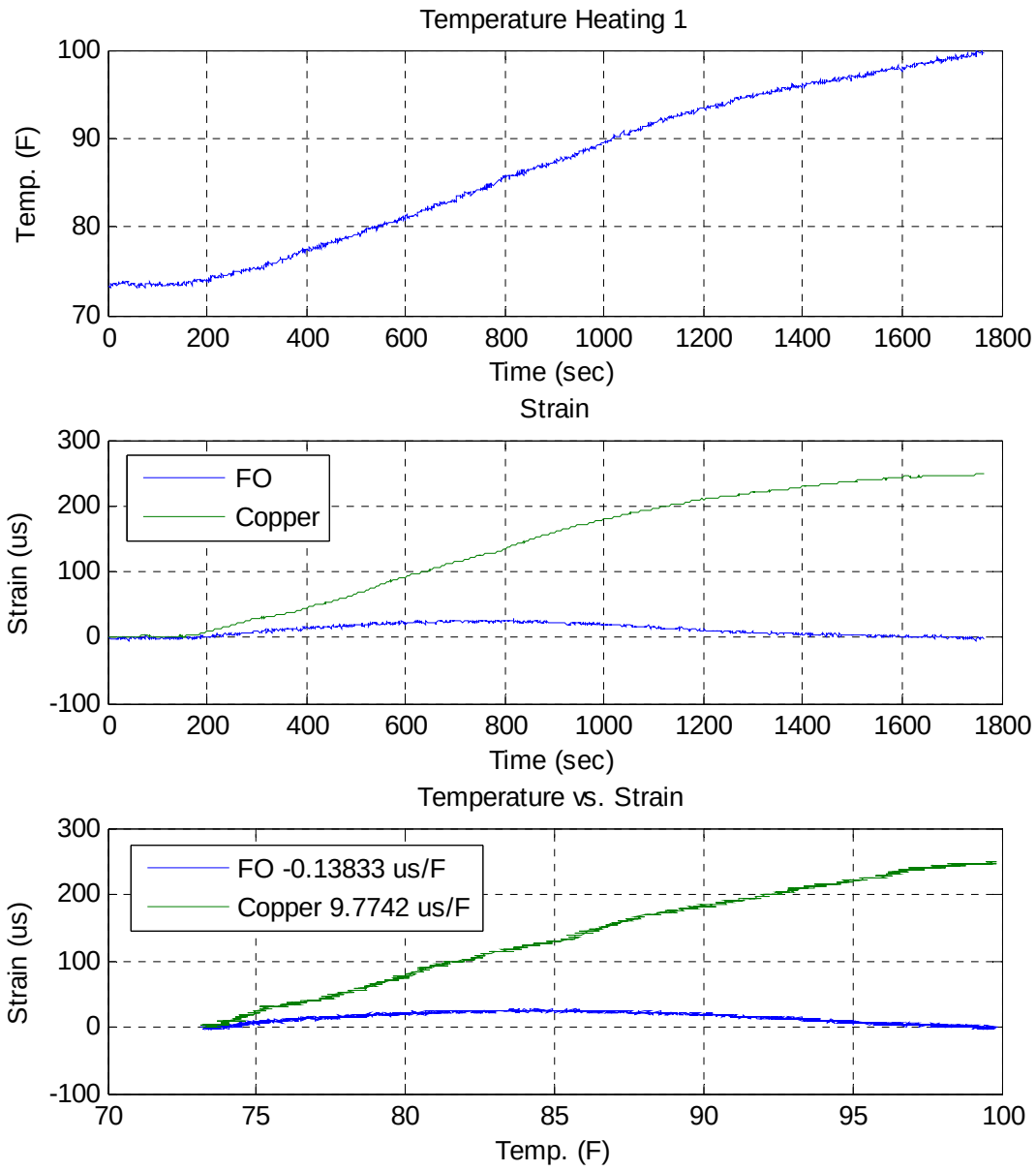

Figure 0-25. Strain readings during heating: temperature (top), strain (middle) and strain vs. temperature (bottom).

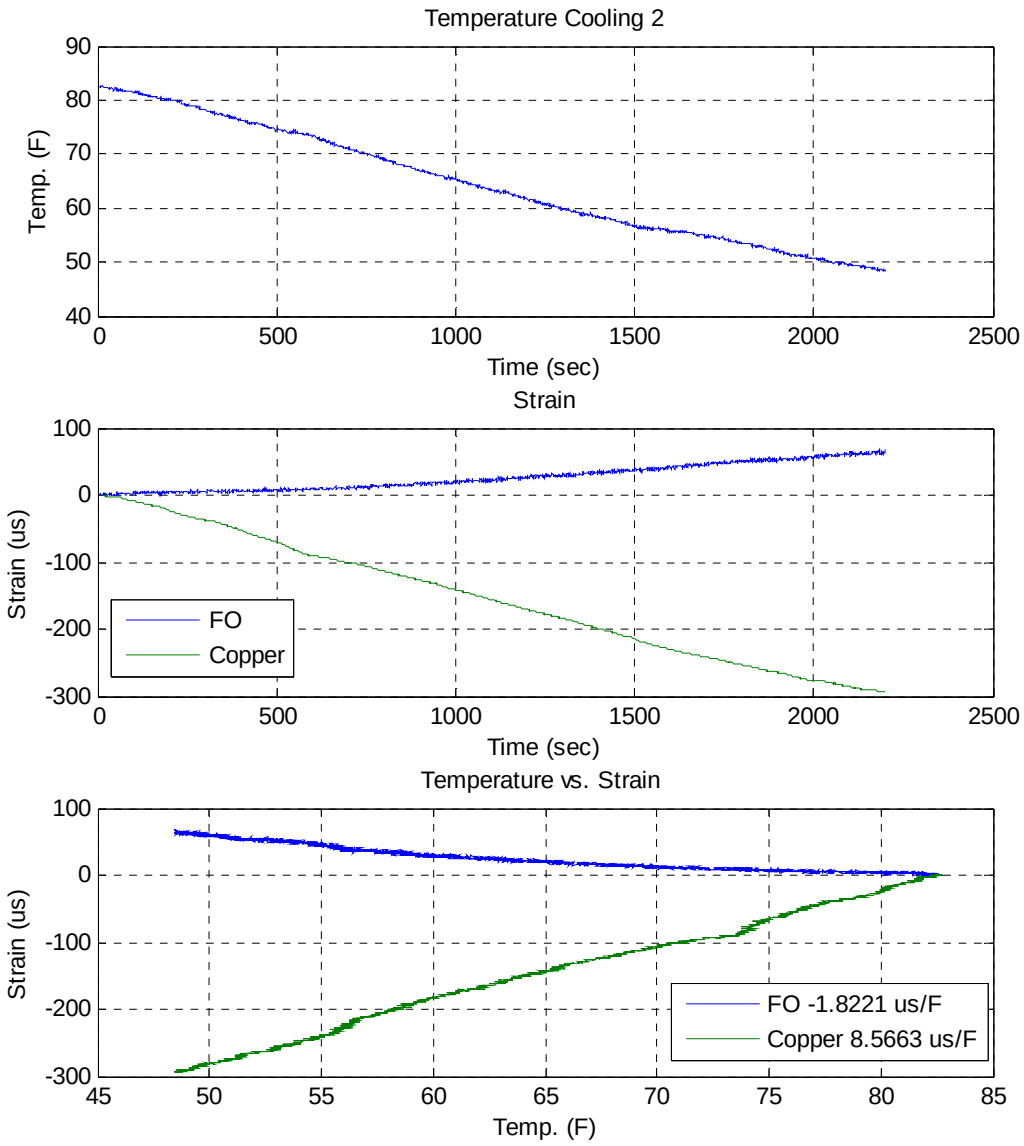

Figure 0-26. Strain readings during cooling: temperature (top), strain (middle) and strain vs. temperature (bottom).

It is clear that the foil gauge is highly susceptible to temperature changes. The temperature sensitivity for the foil gauge ranged from 8.6 to 12.8 μs/°F during the heating and cooling tests, with an average sensitivity of 10.8 μs/°F.

As expected, the copper gauge response is fairly linear with temperature change while the temperature compensated fiber optic sensor exhibits strain changes that are not linear with

change in temperature (with an estimated sensitivity of 0.9 μs/°F). Temperature compensation embedded in the ENLIGHT software attempts to remove any effects of temperature; however it is clear that this correction is imperfect and results in a non-linear response the sensor to temperature changes. This response may be due to a difference in the temperature changes experienced by the steel specimen and the sensor. Secondary effects of the steel specimen lengthening/shortening could be a factor to consider as well (i.e.,, the measurement contains actual strain in addition to temperature effects).

3.6 Noise Test

One of the critical challenges in the proposed test pavement instrumentation is the susceptibility of the sensor leads to noise interference (electromagnetic interference, EMI). As the sensor leads increase in length, the noise amplitudes also increase, compromising the measured signal and potentially masking important results. Since the US-301 test road requires lead distances exceeding 130 feet, there is great potential for noise to impact data. While fiber optic sensor technology is not subject to EMI interference, all sensing technology is subject to a range of noise sources. The purpose of this phase of testing is to quantify the inherent noise levels present in each of the sensor types.

3.6.1 Specimen Description

The steel specimen (detailed in Section 3.4) was also used for the noise tests. The cable lead distance was 277 inches, 187 inches, and 429 inches for the os3610, foil gauge, and thermocouple, respectively.

3.6.2 Testing Equipment

Noise analysis tests were conducted by wrapping the sensors in foam and setting the sensor on an empty, still table. The purpose of the foam was to isolate the test specimen from any real dynamic vibrations present in the building. No additional test equipment was employed as the purpose was to test the sensors in the absence of any loading or vibration. Both copper strain, fiber optic strain and thermocouple data was collected for each test.

3.6.3 Procedure

Noise tests were conducted at three different effective sampling rates: 1 Hz, 100 Hz, and 500 Hz. Three minutes of data were collected for the 1 Hz test, and 30 seconds of data were collected for the 100 and 500 Hz tests. It is important to note that the copper strain gauge data was filtered using the FIR filter discussed in Section 2. This filter will not only reduce the 60-Hz noise, but will suppress any noise with frequencies above 40 Hz. No filtering was used on the fiber optic strain data.

3.6.4 Results

The time history measurements recorded for each sensor are presented in Figure 0-27, Figure 0-28, and Figure 0-29. The RMS levels of strain measured for each strain sensor were determined for each test and are presented in Table 6-1. In addition to time domain quantification of the noise levels, the data were also examined in the frequency domain. Figure 0-30 shows the frequency responses for both gauge types sampled at 500 Hz. The higher the amplitude of frequency response plot, the higher the noise is in the signal, as measured in dB. For the plots shown in Figure 0-30, the fiber optic gauge has a noise floor of approximately -50 dB while the filtered copper gauge has a noise floor of -100 dB. The noise floor of the copper gauge is consistent with the filter illustrated in Figure 0-4. The roll off of the frequency response in the copper gauge is also consistent with the applied filter. Note, however, that the 60-Hz noise is still present in the signal.

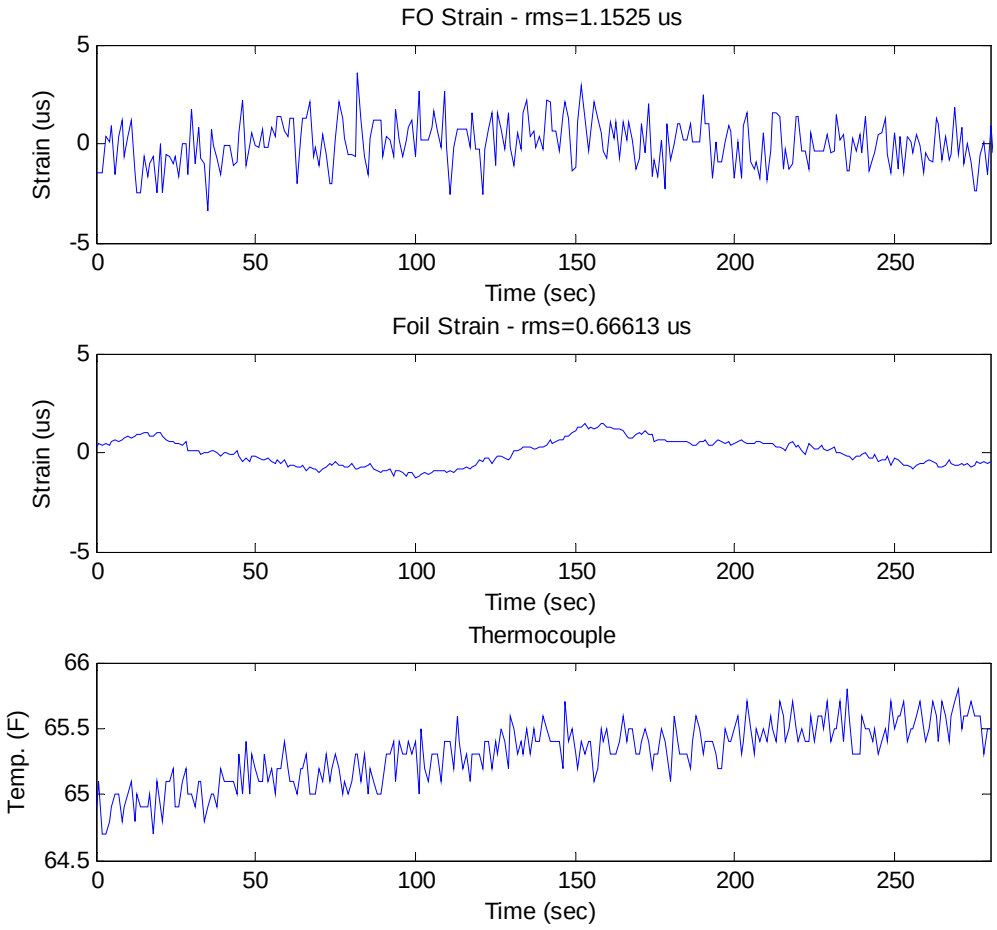

Figure 0-27. 1 Hz noise tests: Fiber optic (top), foil gauge (middle), and thermocouple (bottom).

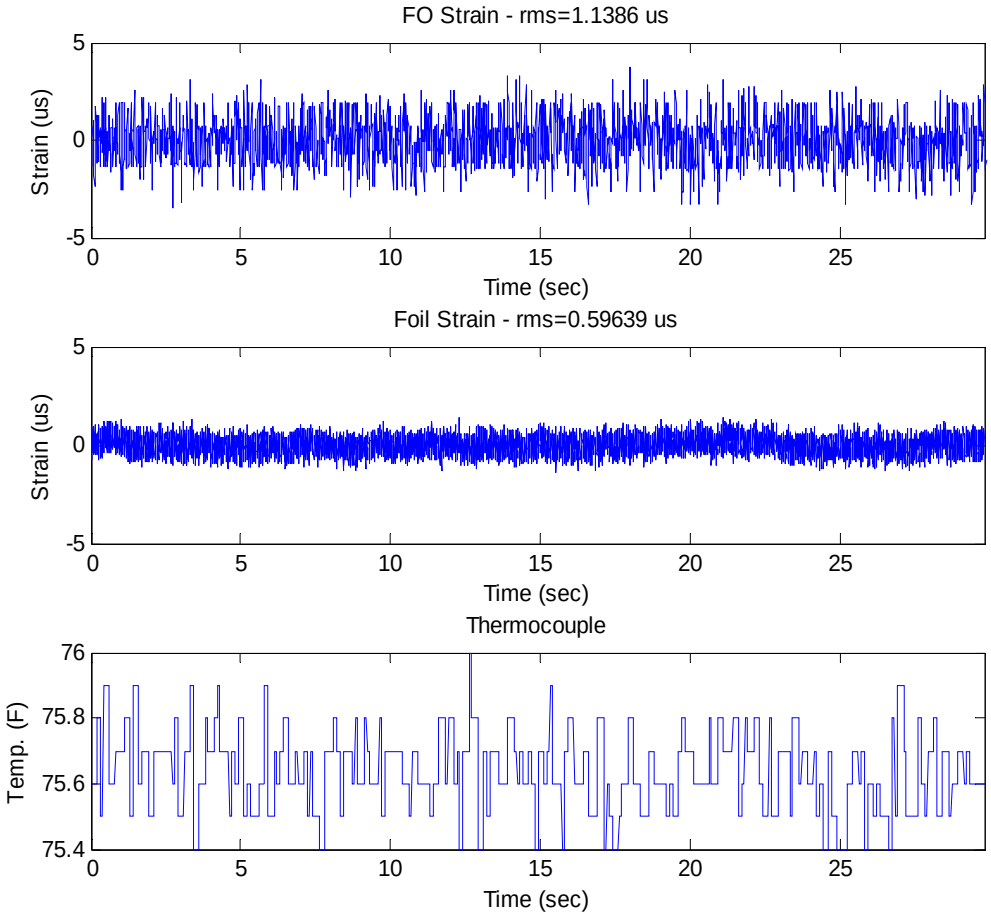

Figure 0-28. 100 Hz noise tests: Fiber optic (top), foil gauge (middle), and thermocouple (bottom).

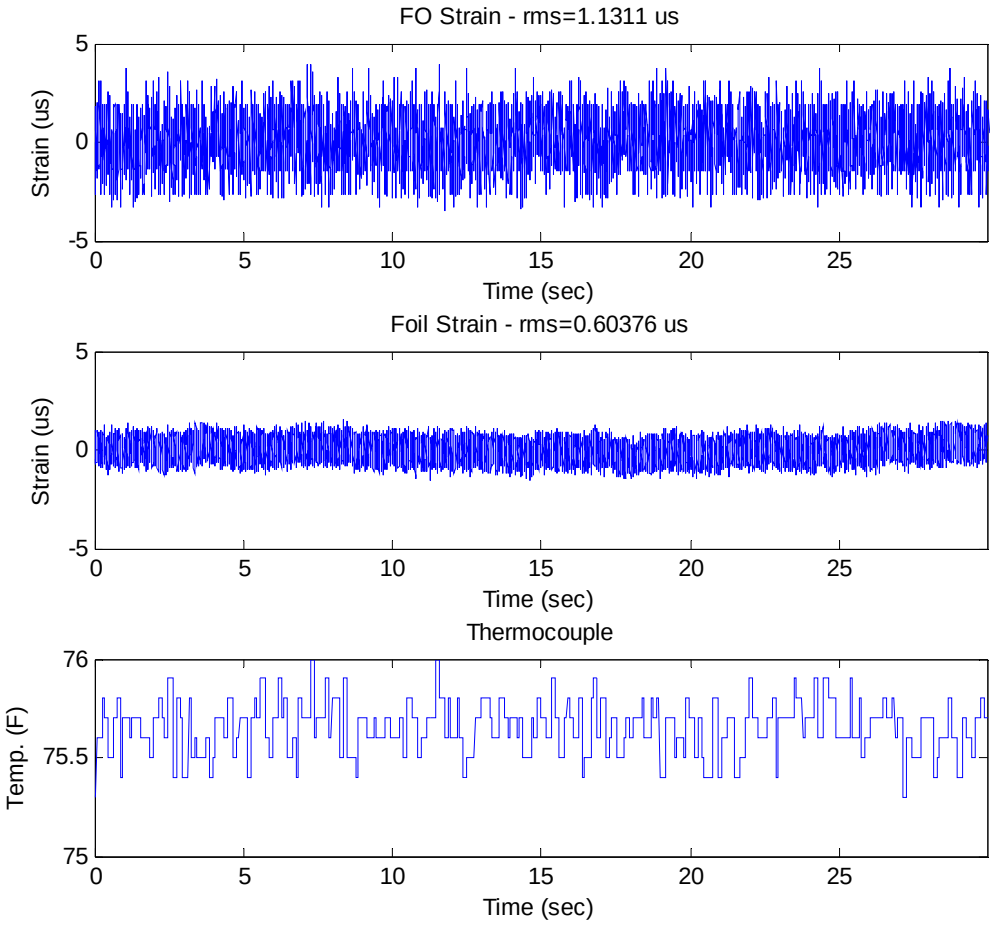

Figure 0-29. 500 Hz noise tests: Fiber optic (top), foil gauge (middle), and thermocouple (bottom).

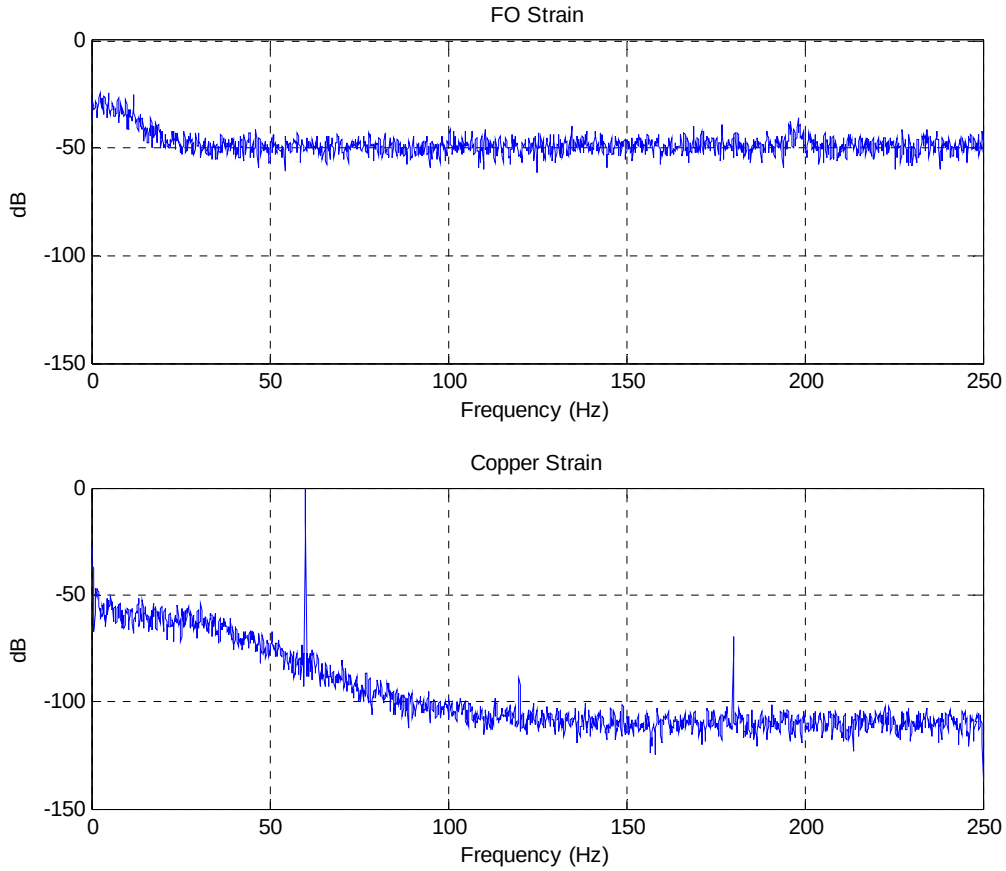

Figure 0-30. 500 Hz noise analysis frequency responses.

Table 0-10. Noise analysis results.

Sampling Rate (Hz)	**RMS Noise (μs)**		**Noise Floor (dB)**	
	Filtered Copper	Fiber Optic	Filtered Copper	Fiber Optic
1	0.67	1.15	5	-35
100	0.60	1.14	-35	-60
500	0.60	1.13	-50	-110

The noise results indicate that the noise present in the signals of both sensor types is minimal and does not change significantly due to the sampling rate. The filter applied to the copper gauge suppresses both electric hum and other high frequency sources of noise and is

recommended for future testing. It is expected that the noise in the copper sensors will increase significantly when longer leads are employed in future tests.

3.7 Initial Testing Conclusion

This portion of the report presents the results of four sets of experimental tests conducted in the initial testing and evaluation period of this research. The four tests evaluated the sensors' accuracy and reliability under compression and tension as well as temperature sensitivity and susceptibility to noise effects. The performance of the fiber optic sensors was compared to the performance of the copper-based.

The results from the four sets of experimental tests performed for out of pavement testing demonstrate that the fiber optic sensors manufactured by Micron Optics, Inc. provided consistent measurements during the various loading scenarios in comparison to the data from traditional electronic sensors. While some differences between the copper-based and the fiber optic sensors were observed, the percent differences in most cases did not exceed 20% and when multiple fiber optic gauges were used, they agreed well with one another. Sensor noise analysis showed low noise levels for both sensor types. Temperature tests demonstrated a linear response to temperature changes in the foil gauges and small, but nonlinear response of the temperature-compensated fiber optic gauge.

In addition to the sensor output evaluation, the tests presented in this section also enabled assessment of the data acquisition software and ease-of-use of each sensor type. The Micron Optics sensors were easy to install and the ENLIGHT software was fairly user-friendly, with appropriate training. It should be noted that the configuration files that were required for all testing with the fiber optic sensors were provided by Micron Optics support staff based on the parameters of the tests and the sensors to be used. It is suggested that FDOT/UF researchers work to acquire the ability to create these files independently. The challenges related to aligning data from two different data acquisition systems may not be present in future tests where the systems are integrated; however, the issue of data alignment should be kept in mind when designing a test plan with a hybrid sensor system.

The performance of the Micron Optics sensors will be further evaluated in the next section based on embedded slab testing; however, the results of this initial testing phase indicate

that the Micron Optics gauges are a viable alternative to traditional electronic sensors. Furthermore, the ease of use of the Micron Optics sensors, both during installation and testing, was comparable to the traditional electronic sensors.

4 Embedded Testing

4.1 Introduction

The goal of the tests presented in this section is to characterize and assess the performance of the candidate sensors (Vishay and Tokyo Sokki strain gauges, Geokon vibrating wire, thermocouples, and Micron Optics fiber optic strain and temperature sensors). In contrast to the numerous test setups and specimens reported in the previous section, the testing reported in this section consists of a single test specimen (a full-scale concrete slab) and sensor layout, with two distinct data acquisition scenarios. The first measurement scenario utilized a low sample rate and long duration data record to measure the strain and temperature responses over the entire curing period of the slab (approximately four days). The second measurement scenario, described herein as the dynamic tests, encompassed a series of short-term, higher sampling rate tests that recorded strain and temperature while the slab was subjected to dynamic wheel loads. While there was only a single slab utilized in this phase of testing, much more data was recorded relative to the out of pavement tests, and the measurement results from each sensor type were analyzed and compared across a number of metrics and test conditions. The amount of recorded raw data enabled statistical evaluation of the response of the sensors and clear data trends could be observed.

While the embedded test environment is a good representation of pavement full-scale pavement, it is not ideal for direct comparison of sensor performance. The concrete's nonhomogeneous nature, coupled with non-uniform loading and boundary conditions result in inconsistency in the pavement's behavior over its volume. Therefore, the sensors may experience different strains and temperatures once embedded in the heterogeneous material – even when they are installed close to one another. In addition, it is imperative that all installation and data acquisition procedures are assessed prior to embedding these expensive sensors in order to prevent errors and increase efficiency.

Section 4.2 of this report discusses the various components pertinent to the setup of the specimen for testing. These components include a description of the slab's material and section properties, followed by a commentary on the sensor layout and installation concerns. Then, a summary of both the hardware and software for the data acquisition (DAQ) is provided. Finally,

the testing apparatus for this phase, the Heavy Vehicle Simulator (HVS), is detailed in Section 4.2.5. Section 4.3 specifies the purpose, analysis techniques, and results of the two test types conducted on the test slab, Curing and Dynamic as well as the testing performed while using the NI-PXI set up. Finally, the contents of this section are concluded in Section 4.4. There are also additional plots found in the Appendix at the end of the report.

4.2 Test Setup

4.2.1 Slab Description

The slab used for the embedded testing was designed to be 12 feet wide, span 13 feet, and have a depth of 9 inches. Since the fiber optic interrogator was rented for a one month period, it was determined that high-early strength concrete would be used to minimize time waiting for the slab to cure and gain adequate strength for accelerated loading. Therefore, a concrete mix design was used to meet Section 353 of the FDOT Standard Specifications for Road and Bridge Construction. Section 353 concrete specifies a six-hour compressive strength of 2200 psi and a 24-hour compressive strength of 3000 psi.

Two additional cubic yards from the same mixture as the slab were provided at the time of delivery to create and test companion specimens to determine the actual material properties of the slab. Testing of the companion specimens showed the material properties of the slab did not meet the specifications of the contract. The six-hour compressive strength was determined to be 900 psi, and the 24-hour compressive strength was determined to be 4200 psi. Though the material properties did not meet the specifications outlined in the contract with the consultant, the slab was deemed adequate for the purpose of the evaluations of the sensors in this experiment.

4.2.2 Sensor Layout

The slab was instrumented with five different strain gauge types and two different temperature gauge types. The temperature gauges used were the Omega TT-K-24-100 thermocouple wire and the Micron Optics os4350 temperature gauge. The strain gauges used were the Micron Optics os3600, Vishay EGP-5-120, Geokon 4200A-2, and Tokyo Sokki's PML-60-2L and KM-100BT models. Table 4-1 summarizes the sensors in the slab.

Table 4-1. Slab sensors.

Measurement Type	Manufacturer	Model
Temperature	Micron Optics	os4350
Temperature	Omega	TT-K-24-100
Strain	Micron Optics	os3600
Strain	Vishay	EGP-5-120
Strain	Tokyo Sokki	PML-60-2L
Strain	Tokyo Sokki	KM-100BT
Strain	Geokon	4200A-2

The Omega thermocouples were assembled into a thermocouple tree which had thermocouple locations at depths of 1”, 2”, 3”, 4.5”, 5”, 6”, 7”, and 8” from the surface of the slab. Micron Optics temperature gauges were then placed on the same tree at depths of 1.5” and 7.5”. Figure 4-1 shows the wooden rod fully assembled into a thermocouple tree and a schematic of the sensor layout embedded in the slab.

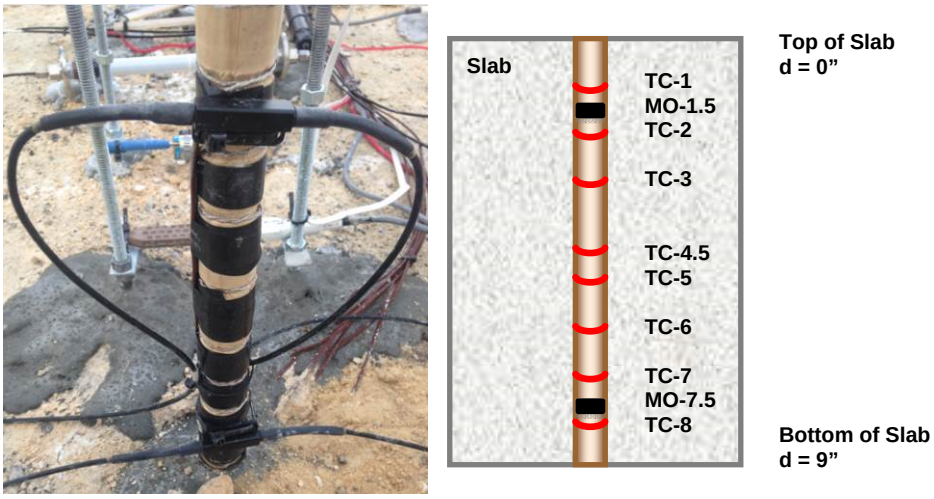

Figure 4-1. Thermocouple tree.

The strain gauge array used for testing was centered in the middle of the slab with the majority of the placed at the bottom of the slab at a depth of 6.5 inches (2.5 inches from the

bottom of the slab). A few additional strain gauges were placed closer to the top surface of the slab at a depth of 2.5 inches. The number and layout of the sensors was selected to provide adequate comparison between each sensor type. These different sensor locations allow each sensor type to effectively capture the strain distribution throughout the width and span of the slab.

Figure 4-2 and Figure 4-3 show the sensor layout for both the bottom and top depths of the slab, respectively. For convenience, the two Tokyo Sokki models are both shown in red for these figures since the sensor technology is similar. The difference in the two models is the exterior casing and aggregate texture used for bonding to the concrete. Additionally, Micron Optics is shown in blue, Vishay is yellow, and Geokon is green. The thermocouple tree is located at the east end of column B. The columns of sensors run south to north along the 13 foot span length and are labeled A – C with 18 inch center-to-center spacing. The rows, which run west to east along the 12 foot slab width, are labeled 1 – 4 with 6 inch spacing. In column B there is an upper layer of strain gauges placed on a strain gauge tree to compare the strains experienced at the top and bottom of the slab. A sample of a strain gauge tree, using Vishay gauges, is shown in Figure 4-4. During the dynamic tests, to be described in more detail in a later section, the load path of the wheel runs north to south along the rows of sensors. The wheel is shifted to run across each row for the various dynamic tests. Finally, Figure 4-5 shows the full sensor layout of the slab before the concrete was placed.

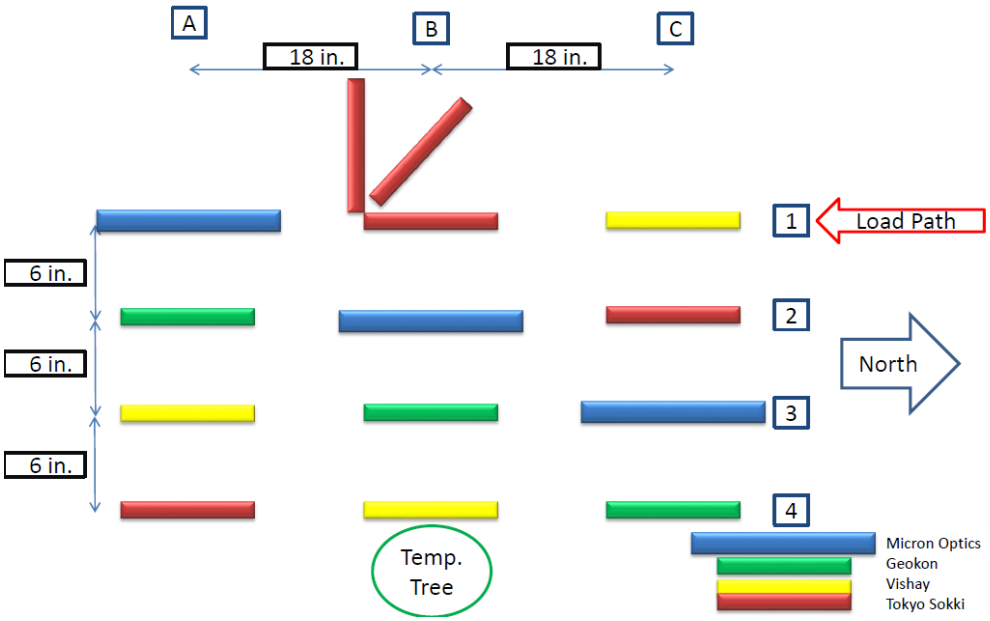

Figure 4-2. Sensor layout – bottom.

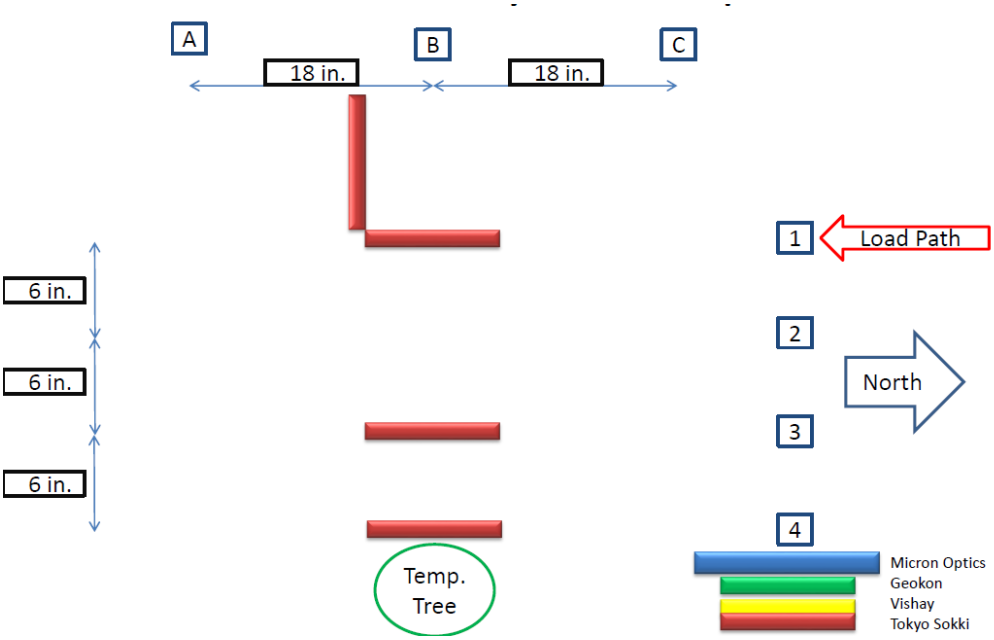

Figure 4-3. Sensor layout – top.

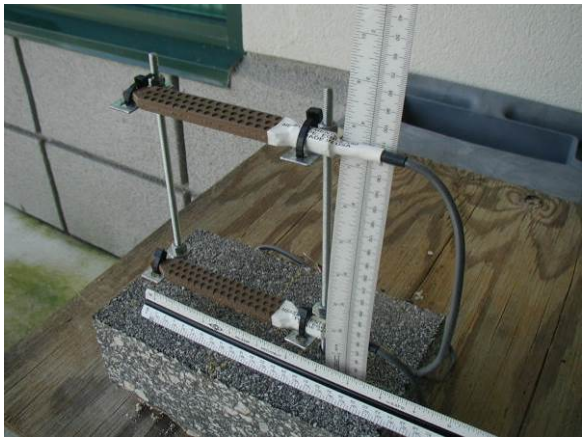

Figure 4-4. Strain gauge tree.

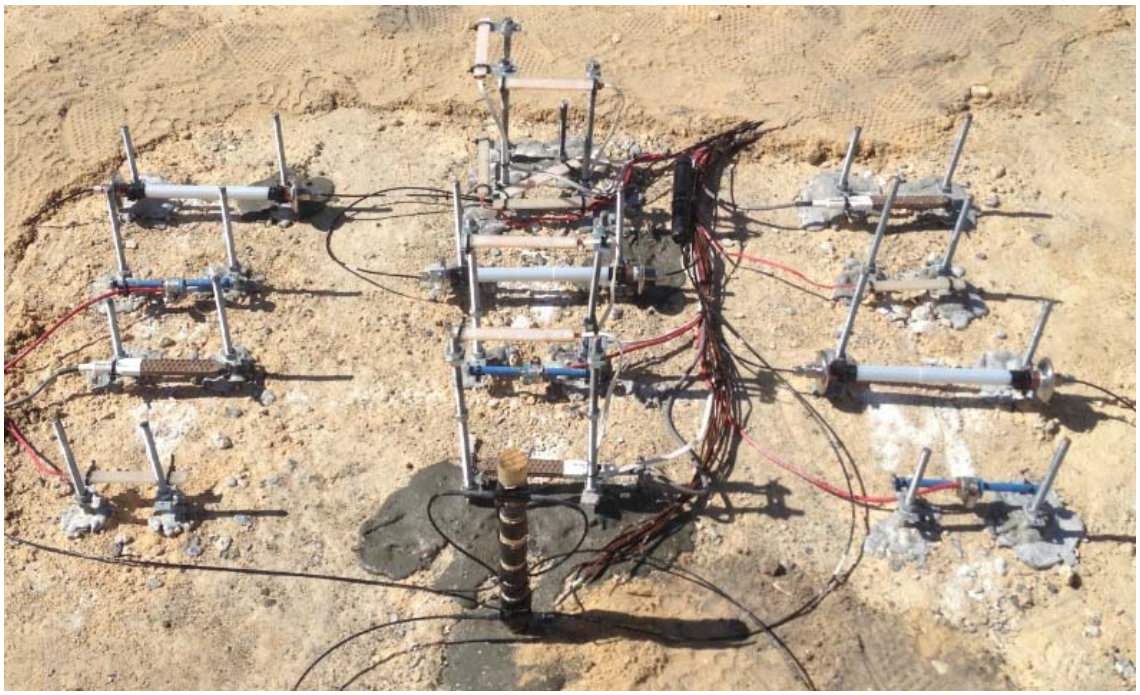

Figure 4-5. Sensor layout – full.

4.2.3 Installation Considerations

To install the sensors while ensuring accurate preservation of the layout plan, holes were drilled into the limerock subgrade and the surrounding space in the opening was filled with grout to stabilize stainless steel rods. The sensors were then placed on the angle connections and leveled. Once each sensor was adequately placed, it was secured by zip ties at the both ends of the gauge. This was a tedious process, and in the future, it is recommended that pre-

manufactured cages be used for their ease of use and faster installation. The cables were then buried in a trench leading to the DAQ modules in the weather-resistant DAQ cabinet, which was used throughout the embedded tests.

During the installation of the sensors for this slab, three different sensor cables required extension in order to reach the DAQ cabinet: the Vishay gauge at A3; the Tokyo Sokki gauge at C2; and the thermocouple at 4.5 inches. The extension of the copper-based sensors required a soldered connection to an additional length of cable to reach the DAQ cabinet. This technique takes time and precision to ensure an effective connection. As an alternative to soldering, unsoldered cable splicing is a quick, cheap, and easy way to resolve a short cable, but may result in added noise or water infiltration. The cables used for the Micron Optics sensors can be extended much more easily than the copper-based cables. Special female-to-female couplers are used to connect the Micron Optics cables and extend the cable length. The coupler is designed to create a weatherproof connection and is very easy to use. Although the extension of the Micron Optics cables is easily achieved and does not degrade the signal, the additional cable lengths and couplers must be purchased in advance and cost more than standard copper cabling.

The Micron Optics sensors are much easier to connect to the interrogator than the electronic sensors are to connect to the DAQ modules. The Micron Optics sensors only require a single connection whereas the electronic sensors connect three wires from each cable. Also the Micron Optics connection itself is easier to achieve than any single wire connection from the electronic cables.

Upon connecting the sensor cables to the DAQ modules, the DAQ software was run to verify that each sensor was connected correctly to the DAQ system and the output was as expected. To conduct this initial check, the sensors were simply pressed on manually while simultaneously using the DAQ software to observe proper response to the applied force.

4.2.4 Data Acquisition

This section describes the basic data logging applications for the copper sensors, which were developed in LabVIEW and the fiber optic Micron Optic's interrogator and ENLIGHT software, which is a combination configuration and data-logging application.

Hardware

There are several components to the DAQ hardware. The DAQ hardware used for the slab measurements consisted of National Instruments compact-DAQ (cDAQ) equipment including a cDAQ 9188 chassis, 9235 modules to collect data from the 120 ohm strain gauges, and 9213 modules to collect data from the type-K thermocouples. All Micron Optics data collection was performed by the four-channel sm130-500 interrogator. The specific sensor types are detailed earlier in this report in Section 4.2.2.

Software

The data collection software was set up in a similar fashion to that described in Section 3.1. The DAQ software was developed based on the experience from the out of pavement testing, with the data acquisition for the copper sensors and fiber optic sensors utilizing separate software. The data from the copper-based sensors was acquired with a LabVIEW interface. The signals from all of the copper strain gauges were filtered with a 60-Hz lowpass filter during data collection to eliminate higher frequency noise Additional filtering was applied to all collected strain data (copper and fiber optic) during data post processing, as described in Section 3.2. For the embedded tests, two sampling rates were used: 500 samples per second for dynamic tests and 1 sample per minute for the curing data acquisition.

The data logging functions of the LabVIEW software verified the sensor readings, selected a data file name and storage location, collected data through the I/O hardware, assembled data into a row and column format with a time stamp, and placed the data into a file with column headers.

The ENLIGHT software performed similar tasks for the Micron Optics data acquisition, but utilized a configuration file to detail the test conditions, rather than developing an application as done in LabVIEW for the copper sensors. Once the configuration file is created, the user interface is the same for all testing.

LabVIEW has the capability of directly integrating ENLIGHT output to instantaneously join the fiber optic data with the other data collected in LabVIEW; however, the time constraints of the interrogator rental for this project did not allow time for development of software to utilize this feature. As a result, each experimental test had two separate data files, one for copper

sensors and one for fiber optic sensors. Thus, a separate LabVIEW application was developed to assemble the two separate file types and align the data sets for each test. To facilitate analysis, this "join" application joined and saved the data as a single file, using the time stamp on each data collection point to ensure time synchronization. This application was not trivial to develop, and provided a means for potential error. Therefore, it is recommended that future experiments utilize the LabVIEW integration capability of ENLIGHT.

4.2.5 Heavy Vehicle Simulator

To assess behavior of the sensor measurements under dynamic loading and simulate many cycles of vehicle loading, the slab was placed under accelerated loading by the SMO's HVS, Mark IV model. The HVS is capable of wheel loads between 7 and 45 kips along a maximum span of 30 feet. Up to 24,000 passes per day can be applied in bidirectional mode and 14,000 in unidirectional mode (Greene & Choubane, 2012).

For this slab testing, the HVS induced unidirectional loading during the dynamic tests. The HVS was placed in a bidirectional mode between the dynamic test times. Data was not recorded while the slab experienced bidirectional loading. Throughout the duration of the tests that were conducted on this slab, there were 286,832 total repetitions of the HVS tire, with 204,052 passes using a 12-kip load under bidirectional mode and 82,780 passes in unidirectional mode with 9, 12, and 15 kips while collecting dynamic strain data.

The exterior of the HVS is shown in Figure 4-6. Figure 4-7 gives an interior view of the HVS which shows the wheel that applies the accelerated loading.

Figure 4-6. HVS exterior.

Figure 4-7. HVS interior.

4.3 Tests

Two primary test and data acquisition approaches were utilized to evaluate the performance of the strain gauges and assess the behavior of the instrumented slab under various load and environmental conditions. Lower sampling rate data was collected from the unloaded slab over several days during curing and higher sampling rate data was acquired during HVS loading several times a day over a few weeks. Details on the goals of these tests, the data acquisition and analysis techniques, as well as results are outlined in this section.

4.3.1 Curing Tests

There were two primary goals for measuring strain and temperature data during the curing process. The first was to gain an understanding of the strains induced during the high temperature cure process of the slab and the second was to monitor the strain responses due to daily temperature fluctuations. During curing, data was gathered at an effective sampling rate of 0.0167 Hz (or one sample per minute) for the first four days from the time the concrete was placed. During this time, the slab temperatures experienced an initial heating due to the exothermic process of concrete hydration in the first eight hours, followed by an overall drop in temperature during the next three days. In addition to the temperatures experienced as a result of curing, the slab also experienced diurnal temperature fluctuations with the ambient temperature during the day.

Unloaded strain and temperature data provided readings during two distinct conditions: (1) In the first eight hours, prior to the hardening of the concrete, when the sensor response is

almost entirely due to temperature, and (2) after the maximum temperature has been reached and the concrete has hardened when the sensors measure the strains induced in the slab due to the temperature gradient induced by varying ambient temperatures and sunlight exposure.

Figure 4-8 shows the temperatures of the Omega thermocouples at the various depth locations of the thermocouple tree. The ambient temperature is also shown in green. The curing data began at 8:32 AM on October 24, 2013. The resulting temperature variations thought the depth of the slab will be presented in the results.

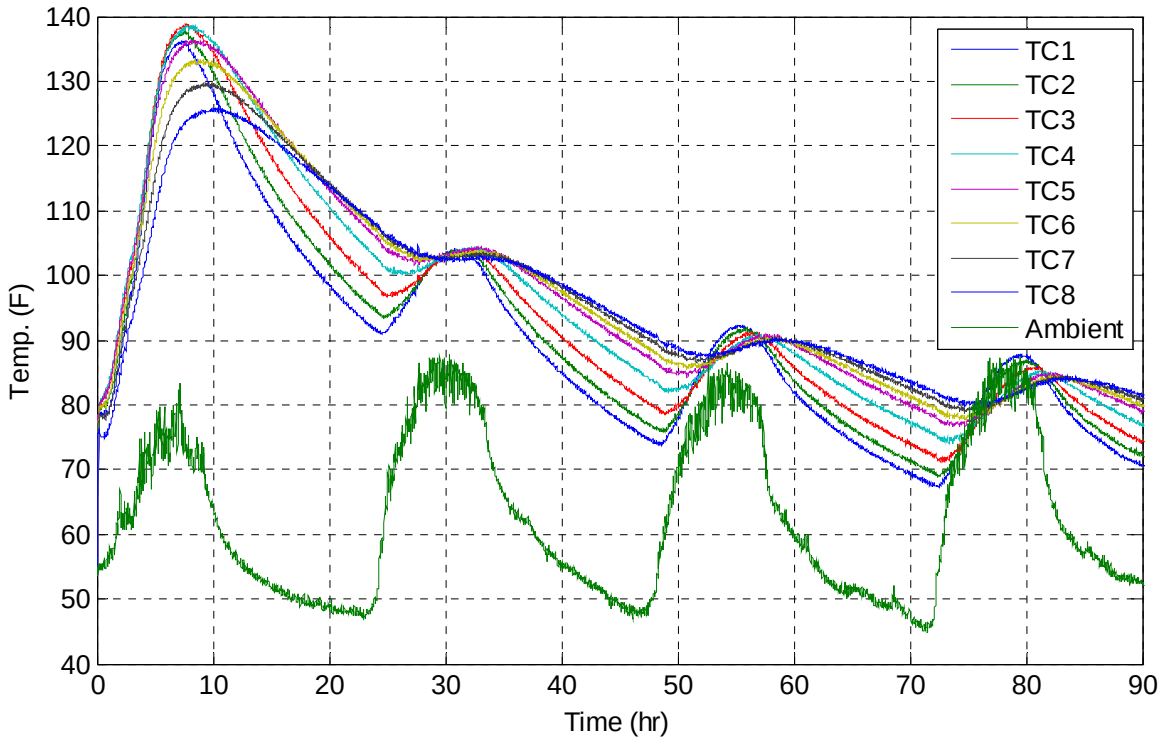

Figure 4-8. Slab and ambient temperatures during and after curing.

Variation in Strain Due to Temperature

To compare the strain measurement at different temperatures, the data sets measured from each strain sensor type were combined into an ensemble average to provide an average of the strain values from each sensor type at each point in time. The result was a single time history data stream per sensor type over the four day test period. For example, the Micron Optics os3600

is located at three locations: A1, B2, and C3. For each time sample, the ensemble average of Micron Optics averages the strain reading across the three sensor locations.

Figure 4-9 shows the temperature vs. strain response of the different strain gauge types during the curing test, including the period prior to concrete hardening. The data prior to hardening indicates the direct temperature sensitivity of the sensor since no strain is induced from stressed developed in the concrete, and is indicated in blue. The Micron Optics gauges show the least temperature sensitivity, resulting from their built-in temperature compensation. Based on the spread of strain along the vertical axes in this figure, the Tokyo Sokki gauges are more susceptible to temperature effects than Vishay gauges. All of the gauges experienced a cyclic strain reading after reaching the maximum temperature and hardening of the concrete due to the curing process, resembling a hysteresis effect, and indicated in green.

It is important to understand the temperature sensitivity and behavior of the embedded sensors so the strain readings can be interpreted appropriately. The reading from a sensor with higher temperature sensitivity will contain strain response from the material being measured and the strain response of the sensor due to temperature change, making the true strain response of the material being measured difficult to extract. The results presented here indicate that the temperature compensation of the Micron Optics gauges, while not perfect, will ensure that the majority of the measured response can be isolated to slab strain.

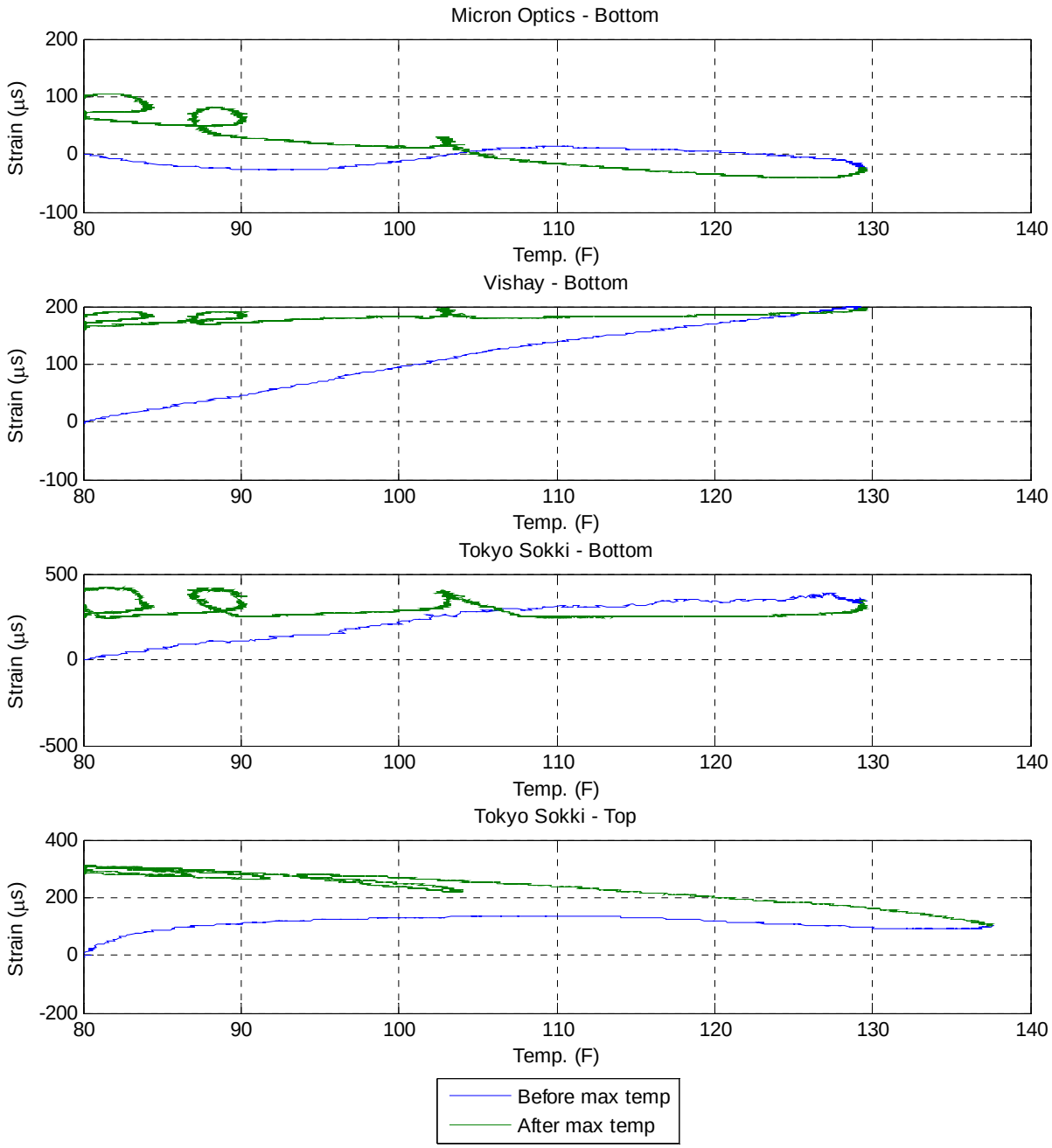

Figure 4-9. Temperature vs. strain response.

Temperature Gradients

The temperature gradient in the slab at any given time is calculated by taking the difference in measured temperature between the top (d = 1 inch) and bottom (d = 8 inch) of the

slab. A higher temperature gradient is expected to result in higher slab stresses due to the differential in thermal expansion between the top and bottom of the slab. It is useful to understand when the maximum and minimum temperature gradients occur during each day and to evaluate the corresponding strains measured in the slab. To establish thoroughly cured concrete behavior, the minimum and maximum temperature gradients were only considered after the first four days, when the concrete temperatures follow the ambient temperature as seen in Figure 4-8.

Plots of the average, minimum, and maximum recorded temperature gradients are shown in Figure 4-10. Figure 4-11 and Figure 4-12 depict the ensemble strain values of the Tokyo Sokki gauges at the top and bottom of the slab. The findings are summarized in Table 4-2. The strain gradient, defined as the difference between the top and bottom strains in the slab, was 41.8 με when the temperature gradient was zero. The strain gradient was 550.2 με when the temperature gradient was at its maximum, 18.2 °F, with a resulting change in strain per change in temperature of 30.2 με/°F. For reference, the ensemble average of Micron Optics readings at the bottom of the slab for the minimum temperature gradient was 55.4 με while the ensemble average was 618.2 με for the maximum temperature gradient. The ambient temperatures were 65.1 °F and 54.1 °F for the minimum and maximum gradients, respectively. The slab reference temperature is the zero line on the x-axis of the simplified temperature gradient plots.

In general, the maximum temperature gradients observed over the testing period occurred at approximately 8:30 am and the minimum gradients occurred at approximately 3:00 pm.

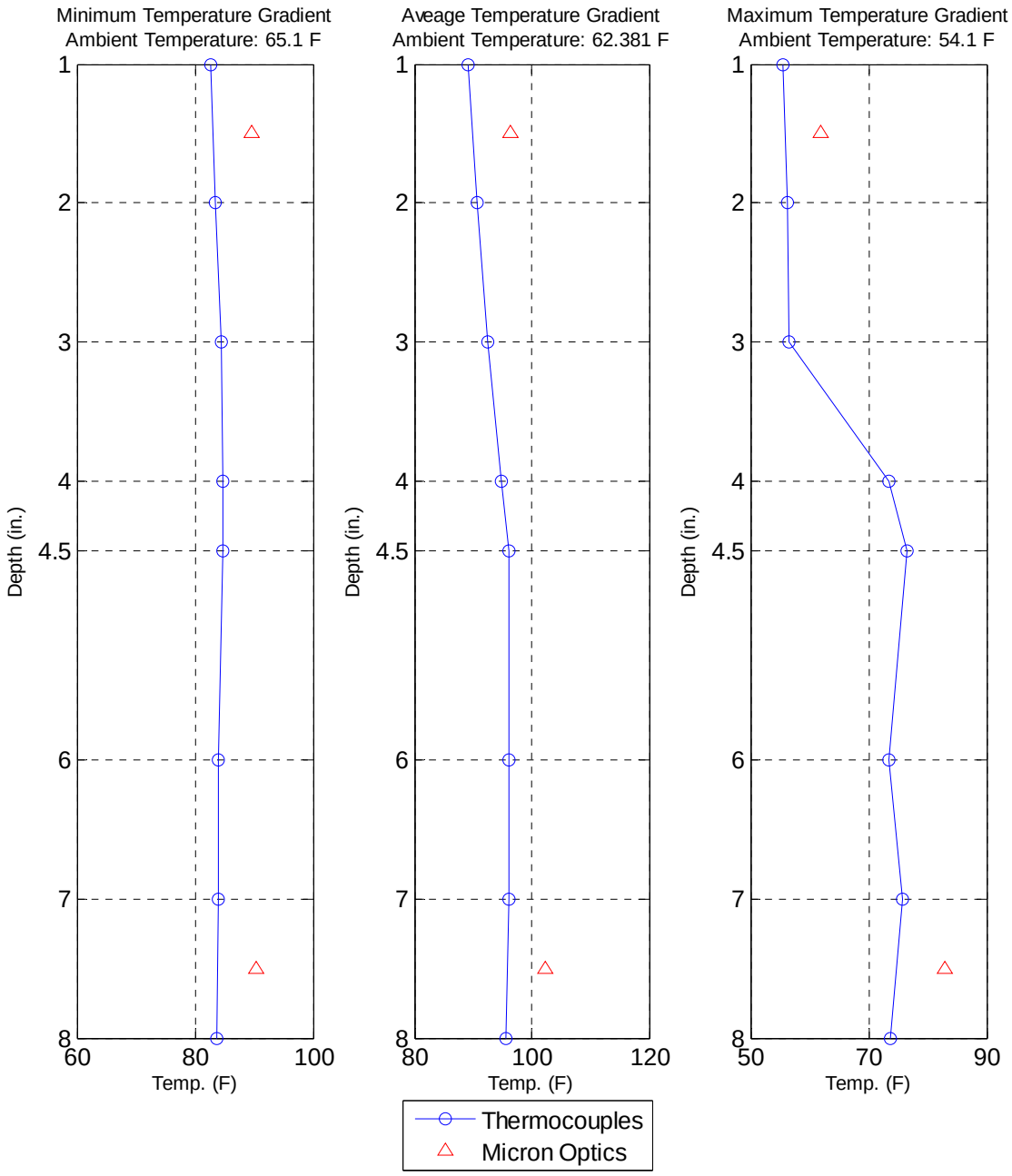

Figure 4-10. Slab temperatures corresponding to the minimum measured temperature gradient (left), the average ambient temperature (middle), and the maximum measured temperature gradient (right).

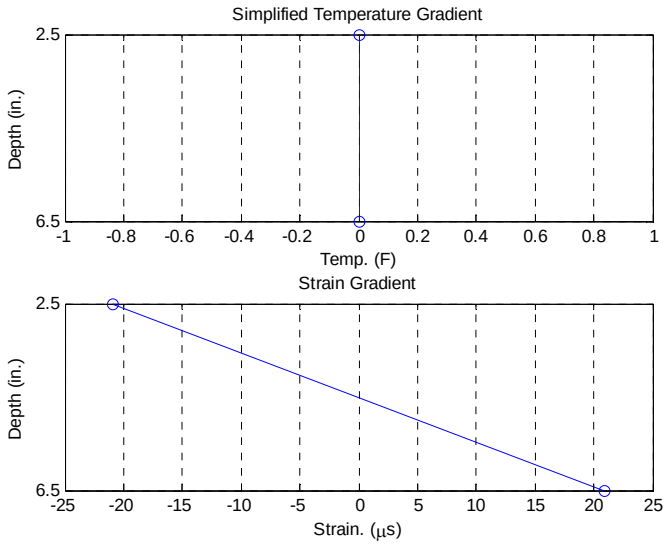

Figure 4-11. Minimum simplified temperature and strain gradients.

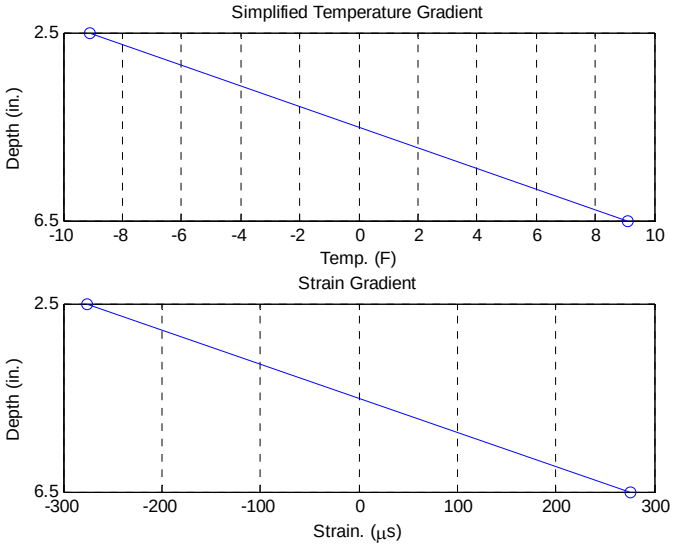

Figure 4-12. Maximum simplified temperature and strain gradients.

Table 4-2. Temperature and strain gradient summary table.

	Minimum Gradient	Maximum Gradient
Ambient Temp (°F)	65.1	54.1
Slab Ref Temp (°F)	84.0	65.5
ΔT	0	18.2
Δμs	41.8	550.2
μs/°F	-----	30.2

4.3.2 Dynamic Tests

To gain an understanding of the strains induced during dynamic loading of the slab, strain data were collected from the sensors at an effective sampling rate of 500 Hz. The HVS was placed in unidirectional mode for the dynamic tests and bidirectional mode between tests.

The different HVS wheel load magnitudes used were 9, 12, and 15 kips. For each load, the wheel ran north to south along a row approximately 10 times to establish a sample set of peak strains as the load was applied directly above the sensors. The wheel was then repositioned to run along the next row. Upon completion of tests for all four rows, the magnitude of the load was set to the next value and all four tests were repeated.

The testing produced 12 files for each testing period, with data points for each of the strain gauges as well as the temperature sensors. In total, 352 tests files were generated during from the dynamic load tests.

Preprocessing of the data prior to in-depth analysis ensured that the effects of noise and any drift in the mean value were minimized to allow meaningful comparison between the sensors. While very little observable drift was noted, each of the strain data sets was detrended to eliminate any slope of the mean values. The noise in each sensor varied and was estimated during the dynamic test prior to the application of the first wheel pass (i.e., during an initial period of no loading). For peak comparisons, all strain data (copper and fiber optic) were filtered with a 40-Hz lowpass filter to remove high frequency noise. The large amount of detrended and filtered data for each sensor was then analyzed to determine the peak strains corresponding to each pass of the wheel load.

A representative plot of the filtered and detrended dynamic data is shown below in Figure 4-13. This data is from the test along row 1 with a 15 kip load that took place on November 4th at approximately 3:00 PM. A zoomed in view of the first 30 seconds of the same test is shown in Figure 4-14. Clear peaks are observed corresponding with each wheel load pass with each sensor type exhibiting similar strain measurements.

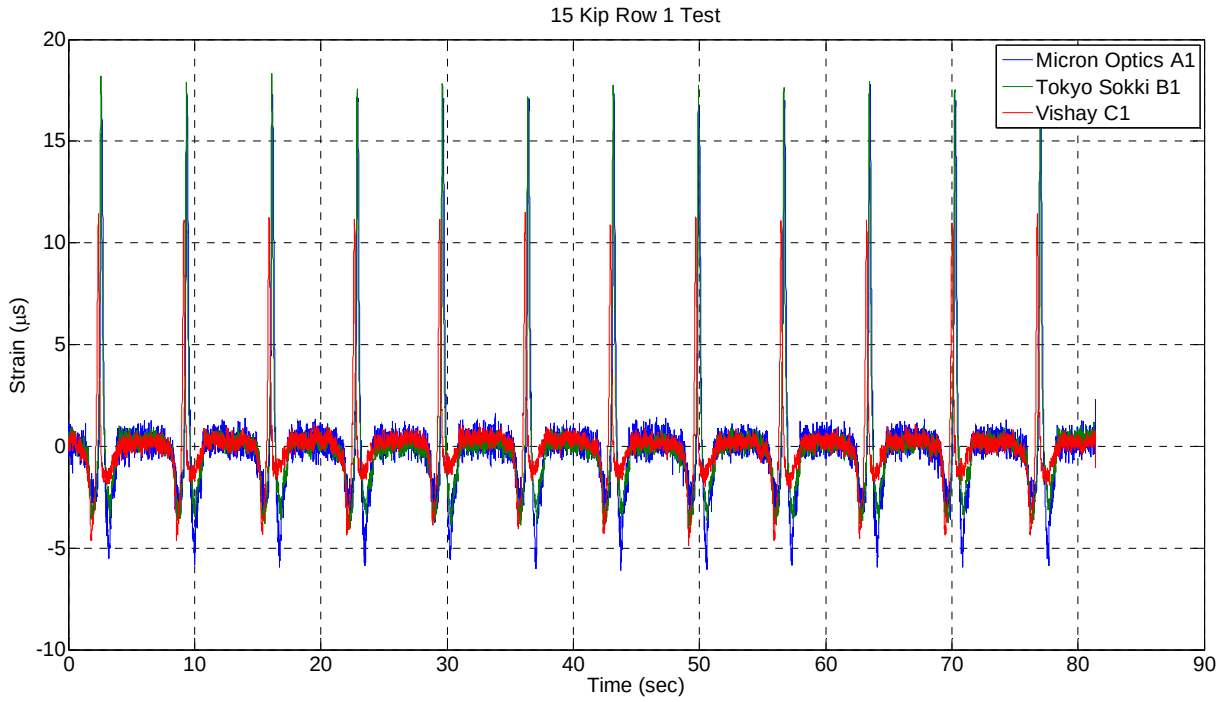

Figure 4-13. Representative dynamic plot.

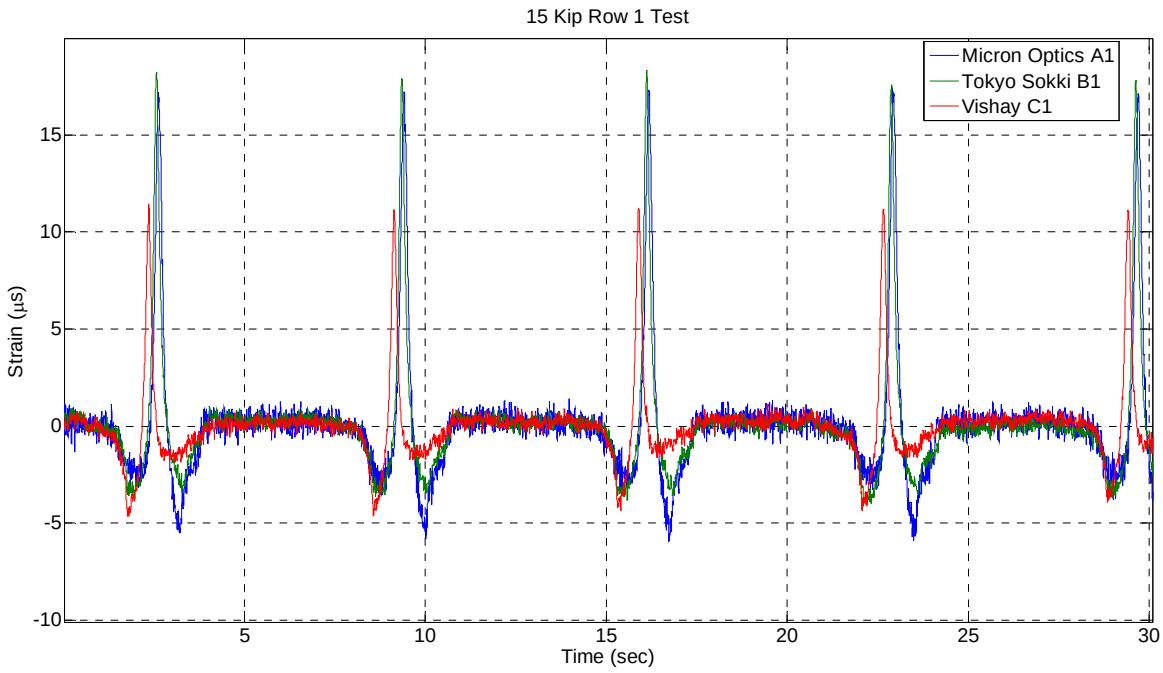

Figure 4-14. Representative dynamic plot – zoomed view.

Peak Analysis

One metric used to compare the output and consistency of each sensor type was their average peak measurement for each load level. To create a general summary of the peak strain values of the sensors, an ensemble average of the peak values for each sensor type along the longitudinal base of the slab was created. The analysis, summarized in this section, shows that the values of the ensemble averages were stable throughout the duration of the testing. The Vishay strain gauges read consistently lower than the Tokyo Sokki and Micron Optics gauges. Although, the percent standard deviation of the average peak values was consistent for both the Tokyo Sokki and Vishay gauges. The Micron Optics standard deviations were larger than the electronic gauges by a factor of almost two.

Figure 4-15 and Table 4-3 show the analysis of the ensemble average peak values for the three sensor types. In Figure 4-15 the error bar represents the percent standard deviation, which corresponds to the last row of values in Table 4-3.

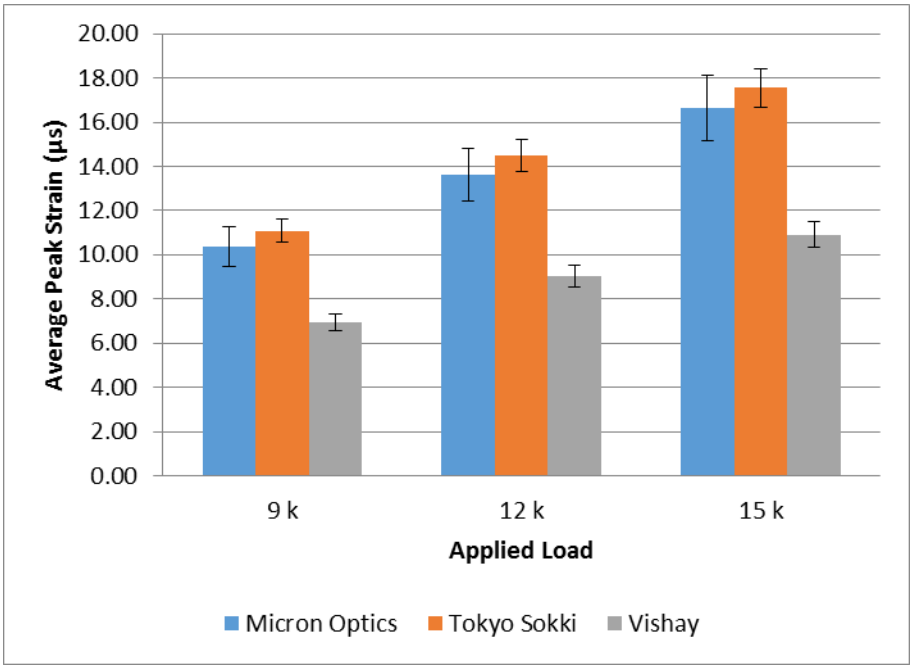

Figure 4-15. Sensory summary graph.

Table 4-3. Sensor analysis table.

Load	Value	Micron Optics	Tokyo Sokki	Vishay
	Average Noise (µs)	1.55	1.22	1.87
9 k	Average Peak (µs)	10.35	11.09	6.93
9 k	Std. Dev of Peak (µs)	0.85	0.50	0.35
9 k	Std. Dev of Peak (%)	8.21	4.54	5.00
12 k	Average Peak (µs)	13.64	14.48	9.04
12 k	Std. Dev of Peak (µs)	1.15	0.72	0.45
12 k	Std. Dev of Peak (%)	8.41	5.00	4.95
15 k	Average Peak (µs)	16.66	17.56	10.91
15 k	Std. Dev of Peak (µs)	1.64	0.92	0.63
15 k	Std. Dev of Peak (%)	9.83	5.25	5.81
	Average Sensor Std. Dev (%)	8.82	4.93	5.25

The peak strains were also analyzed to determine trends related to the time of day the test was recorded, the ambient temperature, and the slab temperature at the sensor depth. Since these three factors are correlated, with ambient temperature and slab temperature increasing

throughout the day, similar data trends result. All three sensor types measure increased peak strains as the temperatures increase. This behavior is expected since the peaks represent the bottom of the slab experiencing tension from the applied dynamic load in addition to tension from thermal expansion. Peak strains for the 15-kip load dynamic tests are shown vs. time of day, ambient temperature, and slab temperature in Figure 4-16, Figure 4-17, and Figure 4-18, respectively. These same plots for the 9- and 12-kip load cases can be found in Appendix A. The results of this analysis are summarized in Table 4-4, where the percent variation of the strain value is calculated over the change in ambient and slab temperatures, indicating the rate at which strain readings increase with temperature.

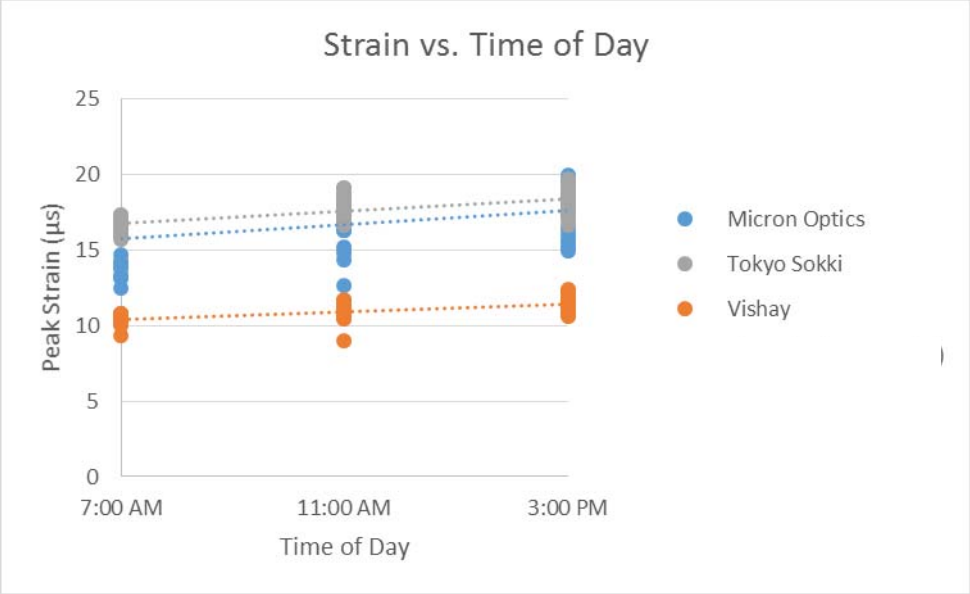

Figure 4-16. Strain vs. time of day – 15 kip.

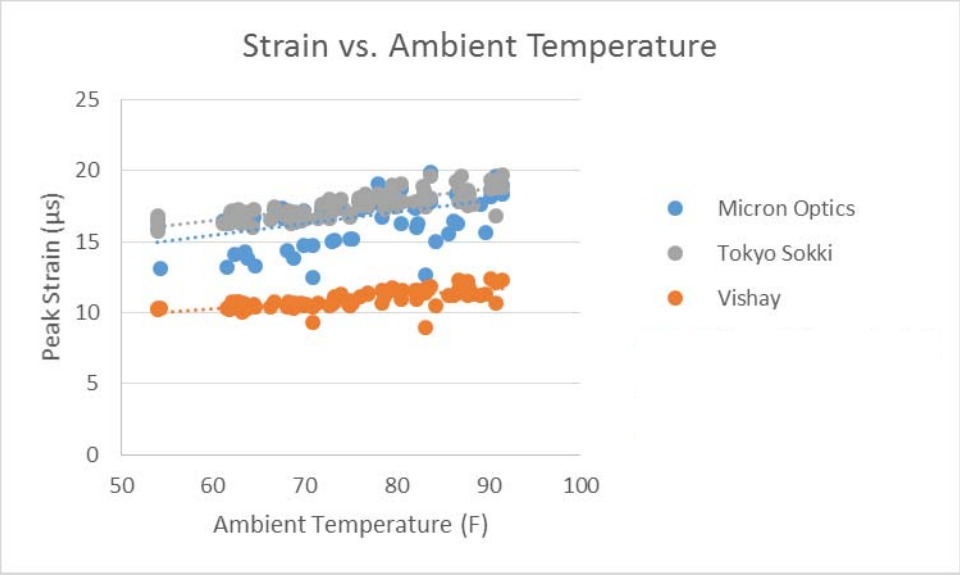

Figure 4-17. Strain vs. ambient temperature – 15 kip.

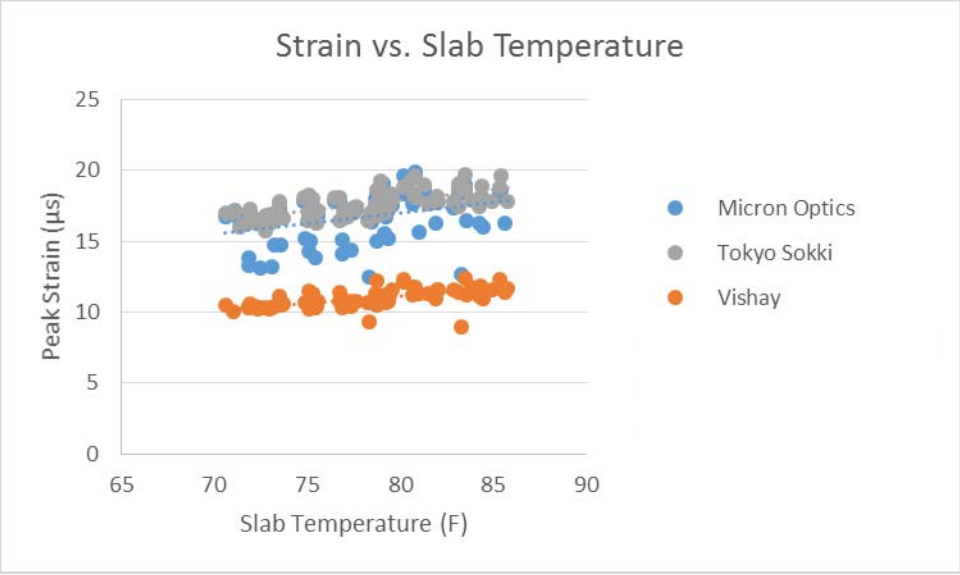

Figure 4-18. Peak strain vs. slab temperature – 15 kip.

Table 4-4. Peak strain variations due to ambient and slab temperatures.

Load	Strain Variation Relation	Micron Optics	Tokyo Sokki	Vishay
9 k	Ambient Temp.	0.63%	0.55%	0.53%
9 k	Slab Temp.	2.83%	1.78%	2.75%
12 k	Ambient Temp.	0.67%	0.53%	0.55%
12 k	Slab Temp.	2.96%	2.21%	2.45%
15 k	Ambient Temp.	0.79%	0.61%	0.60%
15 k	Slab Temp.	3.11%	2.58%	2.78%
Average	Ambient Temp.	0.70%	0.56%	0.56%
Average	Slab Temp.	2.97%	2.19%	2.66%

Data Repeatability Analysis – Peaks

To evaluate the measurement repeatability of the sensors over time, the average peak value of the sensor was taken for all tests at the given load for each day. The daily average value was then plotted across the various testing dates to observe the consistency of peak values throughout the dynamic testing period. Sample plots of all gauges for Micron Optics, Tokyo Sokki, and Vishay for the 15 kip load are shown in Figure 4-19, Figure 4-20, and Figure 4-21, respectively. The main variability seen is in Micron Optics gauge located at C3. This gauge consistently read lower than the other two Micron Optics gauges but did maintain the same variation pattern. For the same plots for the peaks of the 9 and 12 kip loads see Appendix B.

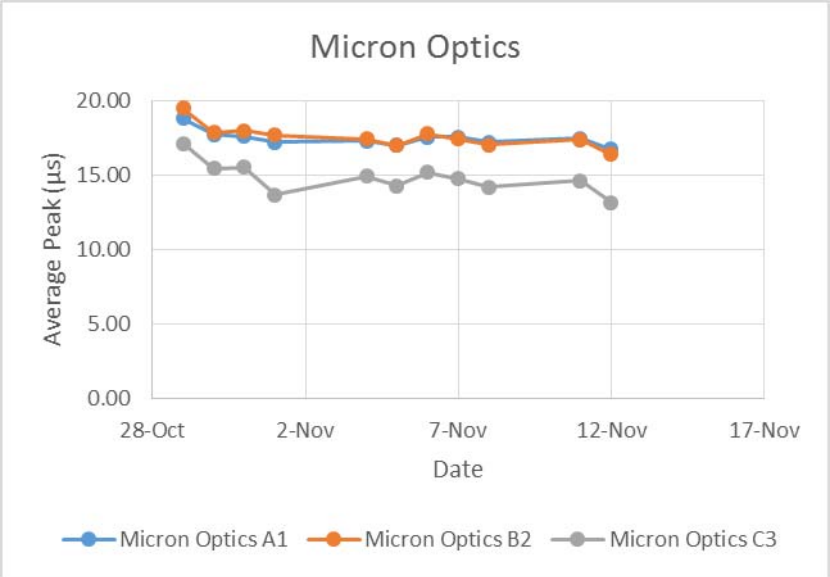

Figure 4-19. Micron Optics repeatability plot – 15 kip.

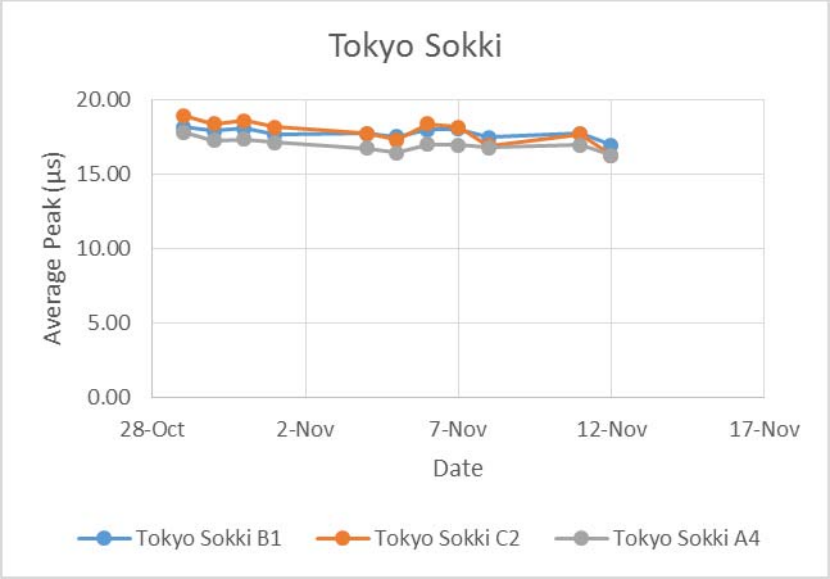

Figure 4-20. Tokyo Sokki repeatability plot – 15 kip.

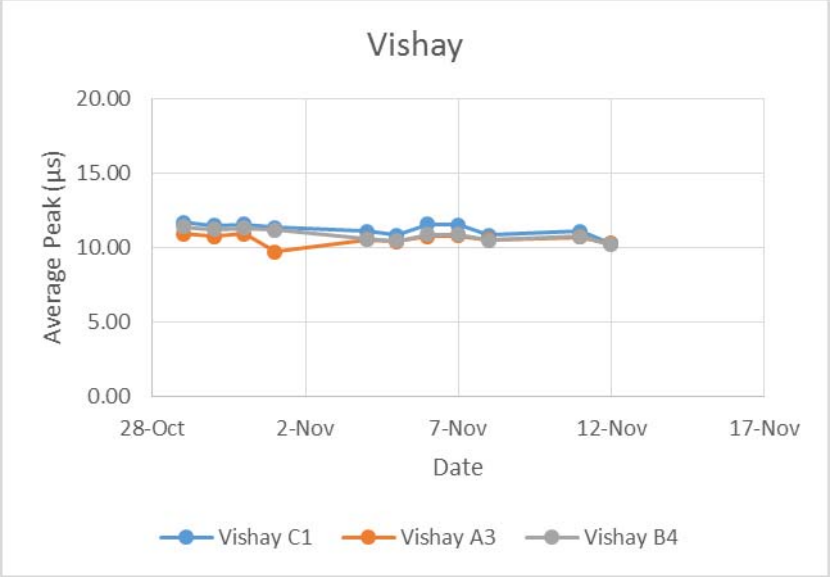

Figure 4-21. Vishay repeatability plot – 15 kip.

Data Repeatability Analysis – Noise

Similar plots were made for the noise levels observed in each sensor for each day of testing. For the noise plots, the average noise was taken regardless of the load for the given tests since there is no load applied during the noise measurements. The sensors all had very consistent

noise readings throughout the test dates, with the exception of the Vishay gauge at location A3, which had a spliced cable to add length in order to reach the DAQ unit. As a result of this alteration, the high noise of Vishay A3, which averaged 3.26 μs, was eliminated from this noise analysis. Plots of all gauges for Micron Optics, Tokyo Sokki, and Vishay are shown in Figure 4-22, Figure 4-23, and Figure 4-24, respectively. For reference, the noise for Vishay A3 is shown in the noise plots below.

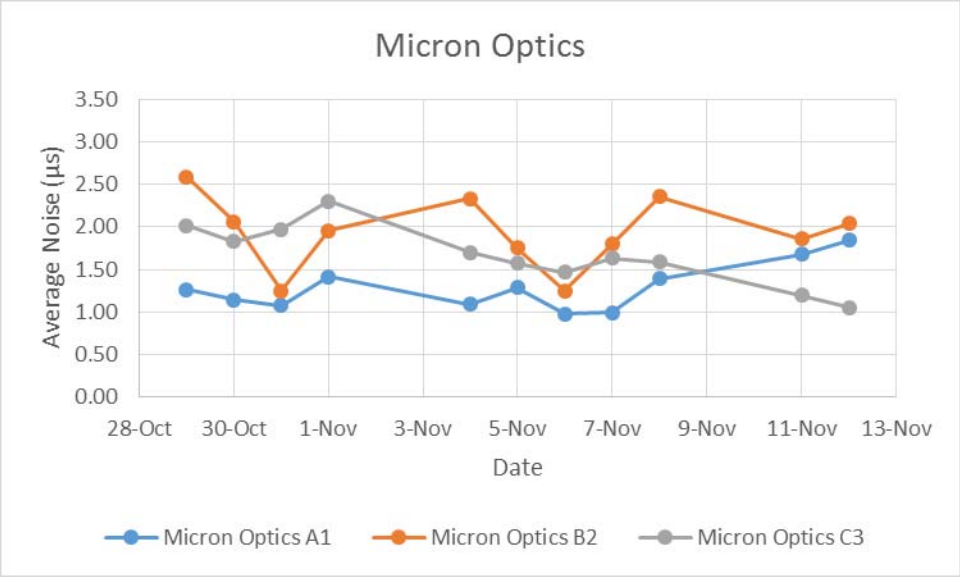

Figure 4-22. Micron Optics noise plot.

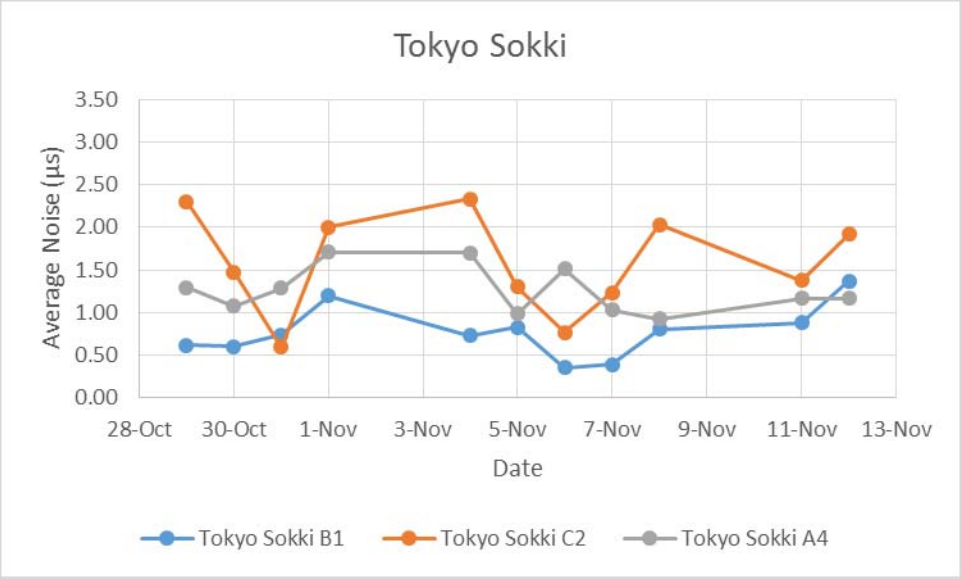

Figure 4-23. Tokyo Sokki noise plot.

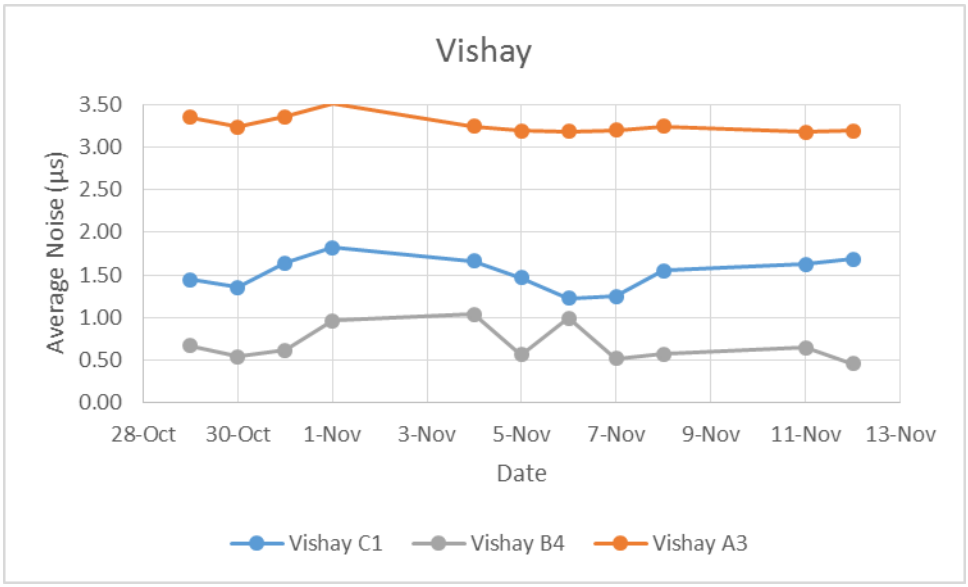

Figure 4-24. Vishay noise plot.

Strain Distribution

In addition to assessing the repeatability of the sensors, the dynamic tests were also used to evaluate the effect of distance of the sensor from the applied load on the measurement values. Sensors will not always be directly below the applied load of the wheel path. Thus, it is

beneficial to understand the sensitivity of the sensors to any load offset. Understanding the variation in strain readings based on the strain distribution of the slab allows for evaluation of the tolerance of sensor placement in relation to the applied load of the wheel path.

The strain distribution plots were constructed by considering the average peak value of each manufacturer's gauge that was placed in the longitudinal direction at the bottom depth of the sensor layout. The row spacing of 6 inches was used to note the location of the gauge with respect to the applied load of the wheel path. For example, if the load is running along row 2, then Micron Optics A1 is at a distance of 6 inches, Micron Optics B2 is at 0 inches, and Micron Optics C3 is at 6 inches as well. Sample plots of all gauges for Micron Optics, Tokyo Sokki, and Vishay for the 15 kip load are shown in Figure 4-25, Figure 4-26, and Figure 4-27, respectively. Similar to the calculation done in the peak analysis section, the percent dissipation of the strain can be found by determining the slope of the trend line and dividing it by the y-intercept which is the baseline value located directly at the load. This value gives the amount of strain lost as the sensor location moves away from the location of the applied load. For these plots, the percent losses in strain are 2.3%/inch, 2.7%/inch, and 2.1%/inch, respectively. These percentages are very similar to one another. It can be concluded that the percent deviation is relatively equivalent for the different sensor types. For the same plots for the peaks of the 9 and 12 kip loads see Appendix B.

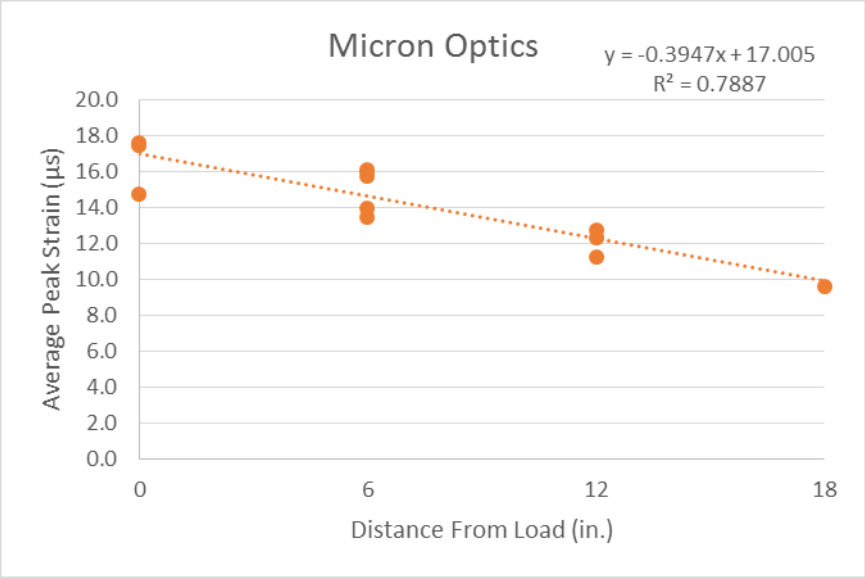

Figure 4-25. Micron Optics strain distribution – 15 kip.

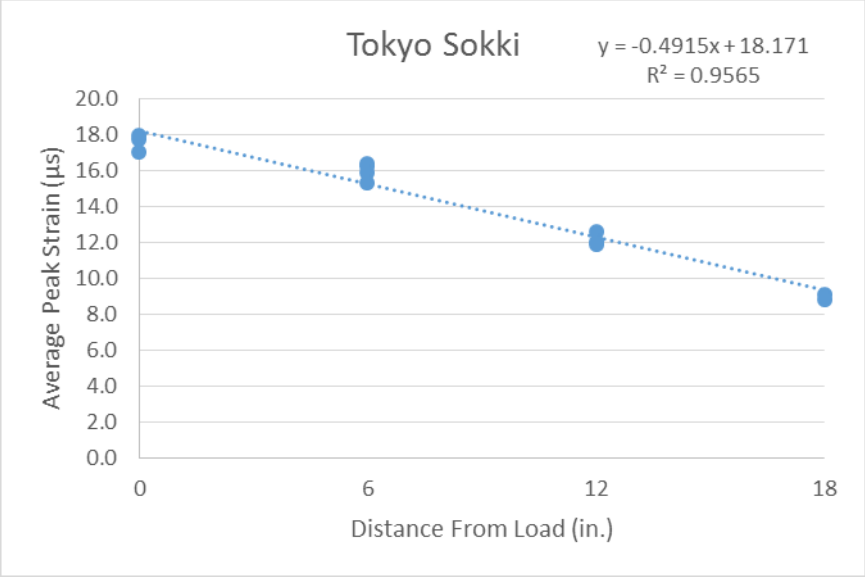

Figure 4-26. Tokyo Sokki strain distribution – 15 kip.

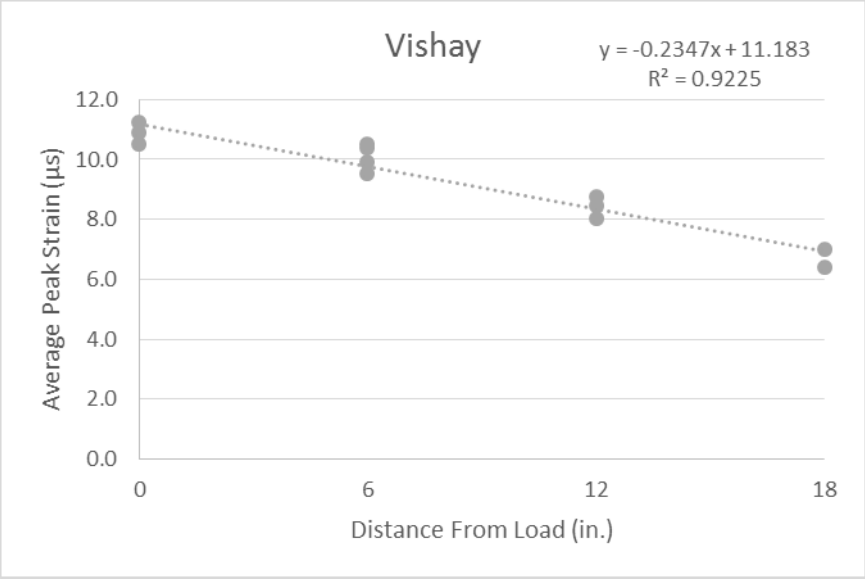

Figure 4-27. Vishay strain distribution – 15 kip.

4.3.3 National Instruments PXI Tests

As an alternative to the Micron Optics interrogator, National Instruments provides similar functionality in their PXIe-4844 interrogator (National Instruments, 2012). To assess the performance of the PXI interrogator, the same test pavement and embedded sensors were utilized. The purpose of these tests was to demonstrate the feasibility of the alternative hardware. For convenience of the test set up, the readings from some sensors were not collected for these data sets. It should be noted that the tests conducted using the National Instruments interrogator were performed five months after the tests using the Micron Optics interrogator. The primary difference between the NI PXI interrogator and the Micron Optics interrogator is the available sampling rates. The highest sampling rate provided by the NI PXI interrogator is ten samples per second (10 Hz). This sampling rate is adequate for environmental and static test cases but may not capture the effects of dynamic loads.

Environmental

To analyze the PXI interrogator setup for under the impact of environmental changes, data was collected at an effective sampling rate of one sample per minute, similar to the prior curing tests. Figure 4-28 shows the environmental data collected over a three day period

beginning on March 28, 2014 at 3:24 PM. For reference, the high and low ambient temperatures (°F) in the area for each day during this timeframe were 57/78, 62/75, and 47/73, respectively (Accuweather, 2014). The pattern of the temperature data is consistent with the expected daily fluctuations in ambient temperature. As expected, the top sensor produced higher temperature fluctuations than the bottom sensor. The PXIe-4844 interrogator shows an ability to acquire data from the Micron Optics sensors over a long test period.

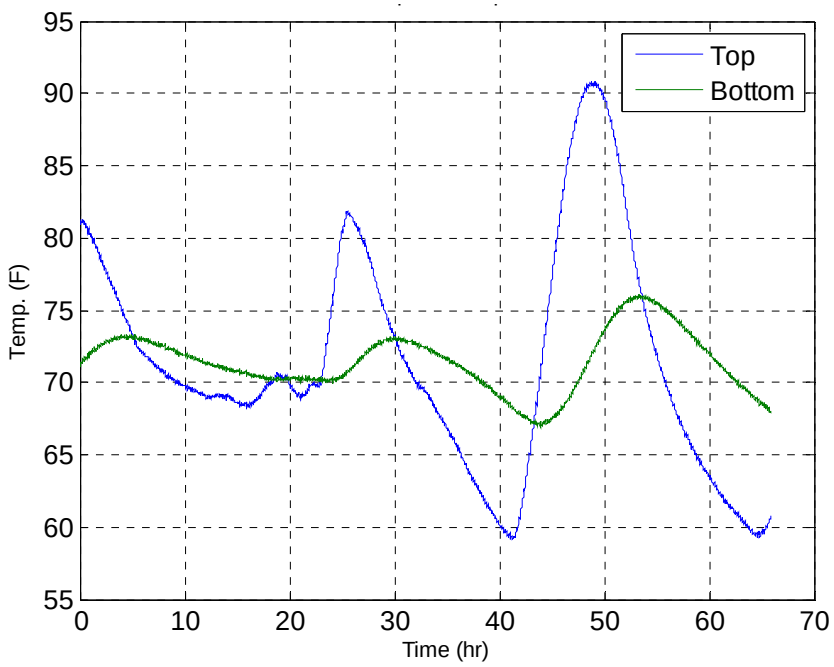

Figure 4-28. Micron Optics temperatures using PXIe-4844 interrogator.

Dynamic

The dynamic test set up was the same as described in Section 4.3.2, but with an effective sampling rate of 10 samples per second (the upper limit of the NI-PXI interrogator). A representative plot of the filtered and detrended dynamic data from one copper sensor and on Micron Optics sensor is shown in Figure 4-29. This data is from the test along row 1 with a 15-kip load. .

For a closer comparison of the data collected from the PXIe-4844 interrogator with that of the sm-130 interrogator from Micron Optics, Figure 4-30 and Figure 4-31 show two periods of the data from a test with a 15 kip load being applied across row 1 of sensors. These plots show markers for each data point acquired. The lower sampling rate of the PXIe-4844 interrogator is

evident in Figure 4-30, while the sampling rate of the Micron Optics sm-130 interrogator, illustrated in Figure 4-31, is 50 times that of the PXIe-4844 interrogator. It is noted that the peak strains captured from the NI PXI interrogator are less consistent than those captured by the Micron Optics interrogator. The lower sampling rate is not adequate to capture the true peak of the strain being measured. The NI-PXI interrogator is adequate for slowly evolving temperature and strain values; however, it is not recommend for dynamic load tests.

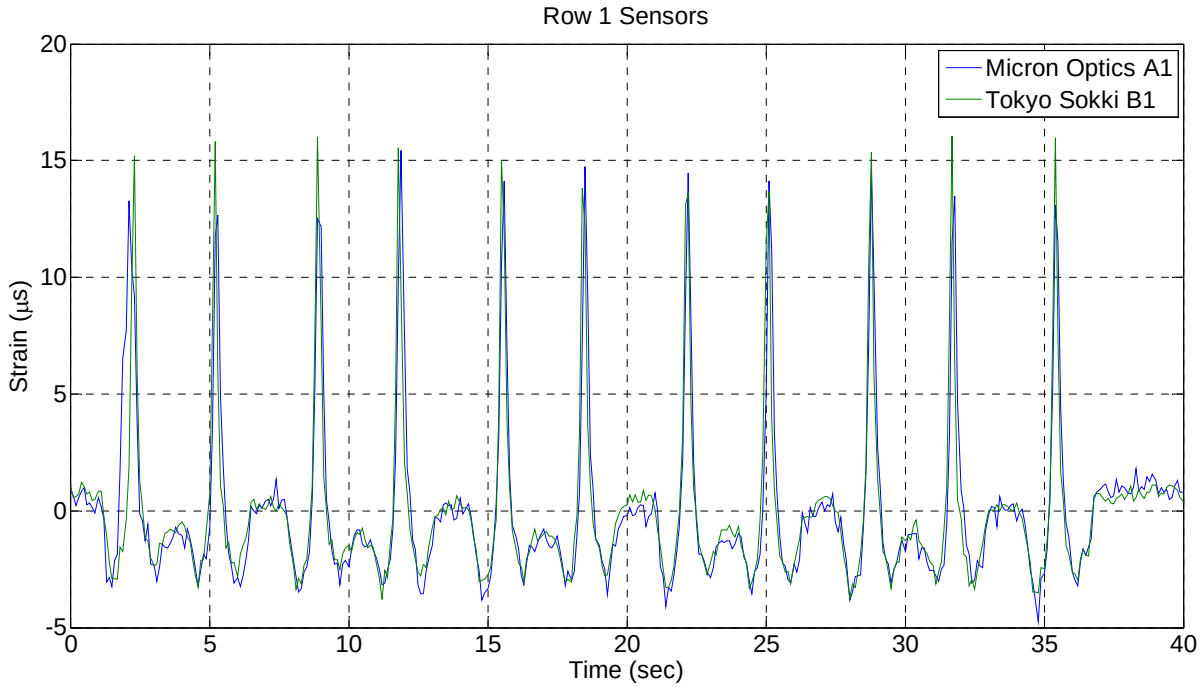

Figure 4-29. Representative dynamic plot.

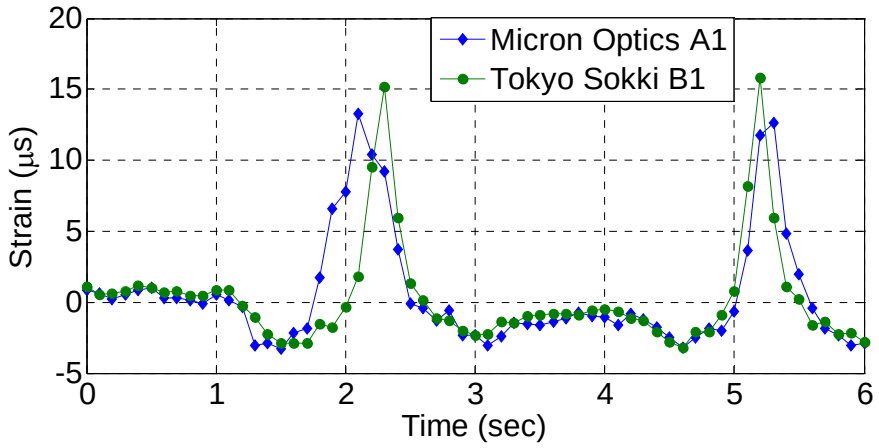

Figure 4-30. Dynamic data from the PXIe-4844 interrogator, sampled at 10 Hz.

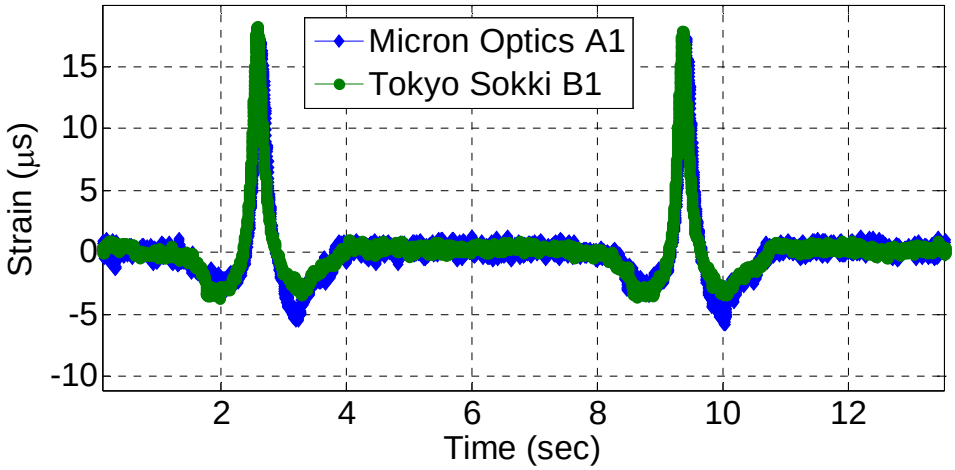

Figure 4-31. Dynamic data from the sm-130 interrogator, sampled at 500 Hz.

4.3.4 Geokon Data

The data from the Geokon 4200A-2 vibrating wire sensors was collected by a Geokon 8002-4-1 (LC-2x4) data logger (Geokon, 2011). The data was then compiled using its LogView software (Geokon, 2014). The sampling rate of vibrating wire technology only provided one sample per minute. In the previous section, the low sampling rate of the PXIe-4844 interrogator was shown to be inadequate for dynamic tests. Similarly, Geokon sensors were deemed unfit for

the dynamic tests on the test slab. However, the sensors were evaluated for their ability to sense the static influence of environmental effects over a 4-5 day period.

During this time period, the sensor strain measurements were simultaneously acquired with the sensor temperature. For analysis purposes, the information from the three Geokon sensors was averaged for each sample in the data stream to create an ensemble average of the temperature and strain. Figure 4-32 displays the ensemble temperature of the Geokon sensors over the testing period. Figure 4-33 shows the strain readings from each individual Geokon sensor over time which was then compiled to create the array of ensemble strain of the Geokon sensors throughout this timeframe in Figure 4-34.

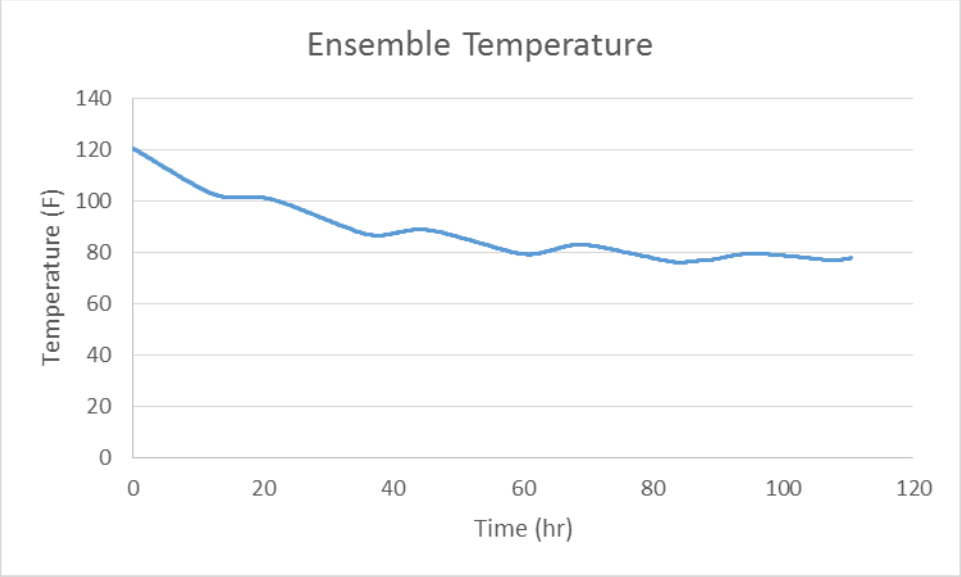

Figure 4-32. Geokon ensemble temperatures.

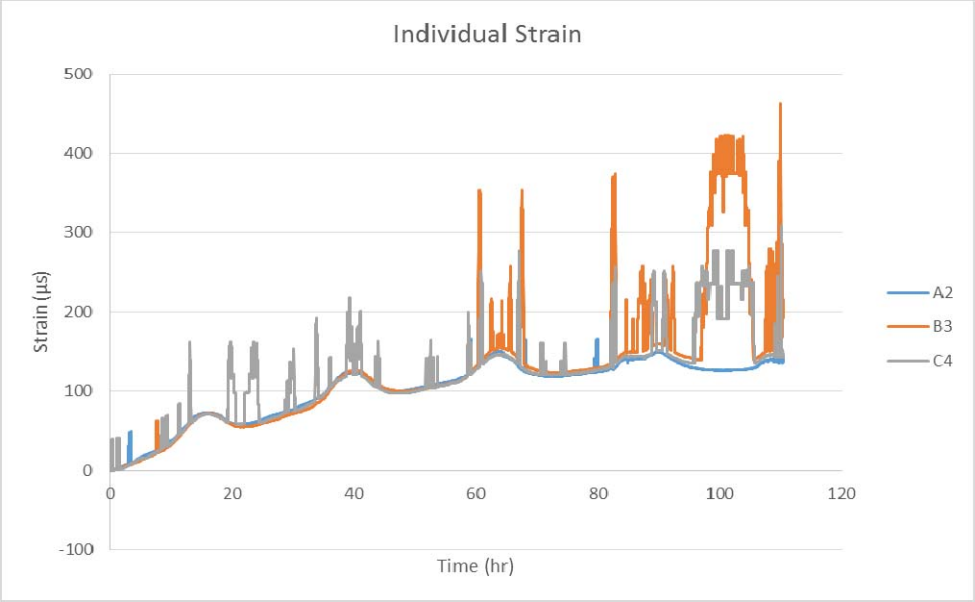

Figure 4-33. Geokon individual strain.

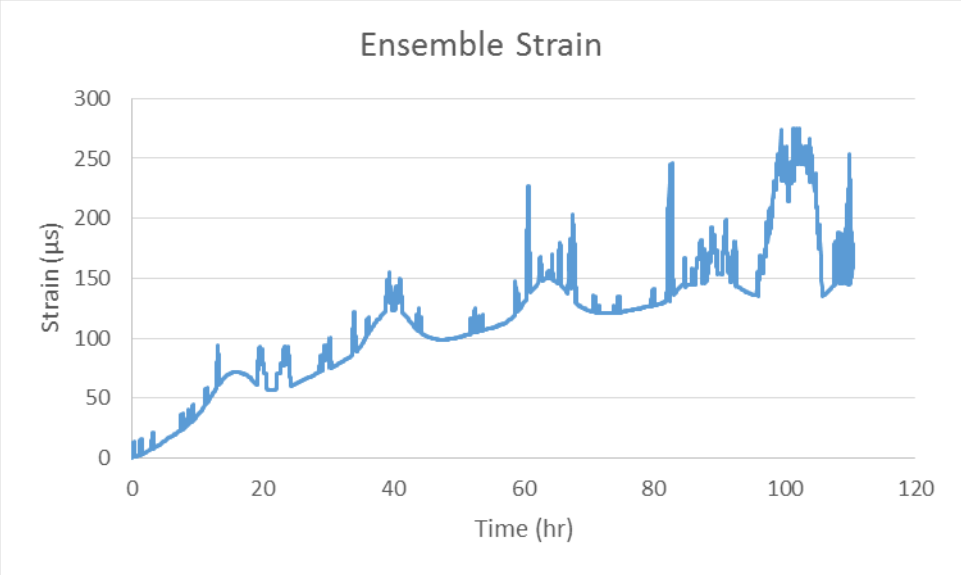

Figure 4-34. Geokon ensemble strain.

4.4 Embedded Testing Conclusions

This section presented results of experimental tests conducted to assess the performance of the candidate strain sensors embedded in a concrete slab. The tests enabled the evaluation of the installation and DAQ procedures for each sensor type and the sensors' responses during slab

curing and dynamic loading. The tests were carried out over a two-week period with over 280,000 HVS wheel load passes applied to simulate prolonged embedment and load exposure.

The performance of the fiber optic and copper sensors were analyzed for the two loading scenarios, providing comparison of their measurement noise, measurement repeatability, response to temperature changes, and response to dynamic loads. Each sensor type demonstrated repeatable results, though inconsistencies were observed between sensor types.

During the slab's curing period, the Micron Optics gauges showed the least temperature sensitivity as a result of their built-in temperature compensation. The Tokyo Sokki gauges were more susceptible to temperature effects than Vishay gauges. Additional analysis of the Tokyo Sokki gauges (due to their installation in the top and bottom regions of the slab) provided an assessment of the strain changes between the top and bottom of the slab resulting from slab temperature gradients. A minimal strain gradient was observed when the temperature gradient was zero, while a strain gradient of 502 με was observed when the temperature gradient was at its maximum. At this maximum gradient, the change in strain with temperature was 27.6 με/°F. The ambient temperatures were 65.1 °F and 54.1 °F for the minimum and maximum gradients, respectively.

Analysis of the measurement noise (prior to filtering applied during post-processing) revealed consistent levels across the sensor types, with average noise less than 2 με in all cases. The only exception was the Vishay gauge at location A3, which was eliminated from the noise study due to its spliced cable that was required to add adequate length to reach the DAQ unit. This result indicates that splices should be avoided to reduce measurement noise.

The results of the dynamic tests showed the ensemble averages of the measured peak strains were stable throughout the duration of the testing. The peak analysis revealed the Vishay strain gauges read consistently lower, approximately 36 percent lower, than the Tokyo Sokki and Micron Optics gauges. The reason for the lower readings of the Vishay sensors is unknown. The percent average standard deviation of the average peak values was consistent for both the Tokyo Sokki and Vishay gauges. While the standard deviations Micron Optics' peak strains were almost twice those of the electronic gauges, the peak data from all gauge types had reasonable standard deviations at less than 10 percent or the peak value.

Analysis of the strain variation as a function of the distance from the applied load showed that the percent loss in strain was approximately 2%/inch for each sensor type. This strain deviation was consistent for all sensor types.

In addition to the evaluation of sensor measurements in this section, the tests also presented an assessment opportunity for the data acquisition techniques and ease-of-use of the sensors. The installation procedures for the copper and fiber optic sensors at their slab locations were similar; however the connection to the DAQ hardware was simpler and less error prone for the Micron Optics sensors. The copper sensors' requirement of a soldered splice in the event of inadequate lead length and the challenge of connecting individual wires to the DAQ module are factors expected to result in longer installation times over the Micron Optics sensors. There are only marginal differences in the hardware setup of the different sensor types, but the configuration files necessary for the fiber optic DAQ software were rather advanced and constructed by Micron Optics support staff based on the parameters of the tests and the sensors to be used. The complexity of the configuration file increases with the complexity of the testing parameters. Once again, it is suggested that FDOT/UF researchers work to acquire the ability to create these files independently. The challenges related to alignment of data from two different data acquisition systems may not be present in future tests where the DAQ systems are integrated; however, the issue of data alignment should be kept in mind when designing a test plan with a hybrid sensor system.

The results of this testing phase indicate that the Micron Optics gauges are a viable alternative to traditional electronic sensors. Furthermore, with proper training, the ease of use of the Micron Optics sensors, both during installation and testing, was comparable to the traditional electronic sensors.

5 Conclusions and Recommendations

5.1 Summary

This report provides the results of comprehensive study to evaluate the availability and functionality of sensors for long-term deployment in a concrete test pavement. The selection and assessment of these sensors were driven by the specific constraints and challenges presented by the proposed US 301 test pavement. In particular, the sensors must provide accurate measurement data over long cable lengths in the presence of lightning strikes with an operational life of five to ten years. Maintaining reasonable sensor and data acquisition system costs was also factored in to the assessments provided in this report.

Prior to the initiation of this study, the SMO utilized copper-based strain and temperature sensors for small-scale, short-term pavement testing. Despite this history of use, it was determined that limitations of these traditional sensors, such as their noise and lightning strike susceptibility, may limit their suitability for the test pavement application. A preliminary evaluation of available sensors for measuring strain and temperature in concrete revealed that fiber optic sensors may be a viable option to meet the needs of the test pavement instrumentation. While fiber optic sensors are not a new technology, there are very few companies that provide off-the-shelf solutions with for embedded concrete instrumentation. It was determined that the sensors and instrumentation provided by Micron Optics would meet the needs of the project and were selected for further evaluation and testing.

A preliminary assessment of the overall system costs showed that the unit cost per sensor is significantly higher for fiber optic sensors than for copper-based sensors. However, the fiber optic sensor system will require much fewer DAQ cabinets; a single interrogator can support up to 80 sensors. Reducing the number of required DAQ cabinets will lower overall costs. A hybrid copper/fiber optic system that balances the unit sensor costs with the DAQ costs may provide the most cost-effective solution while meeting the instrumentation needs of the project.

Initial tests were conducted using copper and FOS strain gauges subjected to tension and compression. Additional tests evaluated the sensors sensitivity to temperature and noise. These tests indicated similar measurement results from both sensor types, with the FOS less sensitive to temperature changes due to their built-in temperature compensation.

Embedded tests also revealed similar measurement capabilities between the copper-based and fiber optic strain and temperature sensors. For temperature measurements, the thermocouples provided reasonable measurements at a fraction of the fiber optic temperature sensors. The strain measurements from both sensor types were similar, although the copper gauges were more sensitive to installation issues that introduce measurement noise. In general, the fiber optic sensors provided a more streamlined installation and setup process.

5.2 Recommendations

Based on the results of the background analysis and experimental tests, it is recommended that a hybrid instrumentation system be adopted for the US-301 test road. Copper thermocouples provide a cost-effective solution and can be densely distributed; redundancy will mitigate measurement loss due to lightning strike. The Micron Optics os3600 strain sensors are recommended for the primary strain measurements in the test pavement. For redundancy, and without significant additional cost, some copper based gauges (Tokyo Sokki) should be co-located with the os3600 gauges. To support data acquisition, a National Instruments DAQ system will provide the necessary interfaces for all copper sensors. Specifically, the NI CompactRIO may provide more options for the integration of a range of sensor types, including soil moisture sensors. Micron Optics' sm130-800 interrogator provides a streamlined interface and the necessary sampling rates (up to 1000 Hz) to support the fiber optic sensors for static and dynamic tests.

It is strongly recommended that adequate development time be dedicated to the creation of the DAQ software for the test road. A unified DAQ software interface in LabVIEW that simultaneously samples the sm130 interrogator and the NI-DAQ components will ensure alignment of the collected data in a consistent format for storage and processing. At least two software configurations should be developed: one to enable long-term environmental data collection, and one to support dynamic tests. Each configuration will identify the active sensors, the effective sampling rate, the test duration, and the file location and timestamp of the stored data. All strain data should be filtered upon collection to ensure that unwanted measurement noise is cancelled. Additional support from Micron Optics to create configuration files for the strain sensors will further ensure the quality, consistency, and accuracy of the strain measurements.

The development of training documents and procedures are recommended for the installation of the sensors in the test pavement. The large-scale and high sensor count of the test road requires systematic approaches to instrumentation installation. Sensor locating technology, such as RFID, may also be useful for identifying embedded sensors after the concrete has been placed.

References

Accuweather. (2014). Local weather: *Gainesville, FL 32609*. Retrieved from http://www.accuweather.com/en/us/gainesville-fl/32609/march-weather/14037_pc?monyr=3/1/2014

Annamdas, V. G. M. (2011). Review on developments in fiber optical sensors and applications. *International Journal of Materials Engineering 2011*, *1*(1), 1-16. doi: 10.5923/j.ijme.20110101.01

Ansari, F. (1997). State-of-the-art in the applications of fiber-optic sensors to cementitious composites. *Cement and Concrete Composites*, *19*(1), 3-9. doi: 10.1016/S0958-9465(96)00038-8

Ansari, F. (2007). Practical implementation of optical fiber sensors in civil structural health monitoring. *Journal of Intelligent Material Systems and Structures*, *18*(August), 879-889. doi: 10.1177/1045389X06075760

Blue M. (2011). Steady state / stability test chamber model CEO9: *Operation & maintenance manual* (reference no: M-013110302). New Columbia, Pennsylvania: TPS - thermal product solutions.

Bonfiglioli, B., & Pascale, G. (2003). Internal strain measurements in concrete elements by fiber optic sensors. *Journal of Materials in Civil Engineering*, *15*(2), 125-133. doi: 10.1061/(ASCE)0899-1561(2003)15:2(125)

Botsis, J., Humbert, L., Colpo, F., & Giaccari, P. (2005). Optics in Switzerland: Embedded fiber Bragg grating sensor for internal strain measurements in polymeric materials. *Optics and Lasers in Engineering*, *43*(3-5), 491-510. doi: 10.1016/j.optlaseng.2004.04.009

Geokon. (2011). *Model 8002 series* [data sheet]. Retrieved from http://www.geokon.com/content/datasheets/8002_Series_Dataloggers.pdf

Geokon. (2013a). *Model 4200 series vibrating wire strain gauges* [data sheet]. Retrieved from http://www.geokon.com/content/manuals/4200-4202-4204-4210_Strain_Gauges.pdf

Geokon. (2013b). *Model 3900 series embedment strain* gauge [data sheet]. Retrieved from http://www.geokon.com/content/datasheets/3900_Embedment_Strain_Gage.pdf

Geokon. (2014). *Model 8001-3 software* [data sheet]. Retrieved from http://www.geokon.com/content/datasheets/8001-3_LogView_Software.pdf

Greene, J., & Choubane, B. Florida Department of Transportation, (2012). *A ten year review of Florida's accelerated pavement testing program*. Retrieved from website: http://www.crcpress.com/product/isbn/9780415621380

Hammons, M. I., Timm, D., & Greene, J. Florida Department of Transportation, State Materials Office. (2007). *Instrumentation data interpretation* (PR490902). Retrieved from website: http://www.dot.state.fl.us/research-center/Completed_Proj/Summary_SMO/FDOT_PR490902_rpt.pdf

Instron. (2013). *ASTM E4-10 certificate of calibration* (certificate no: 270032713081359). Instron calibration laboratory.

Irrometer. (2010). *Watermark soil moisture sensor – model 200SS* [data sheet]. Retrieved from http://www.irrometer.com/pdf/sensors/403%20Sensor%20%20Web5.pdf

Jensen, M. Minnesota Department of Transportation, (2011). *Phase II overview brochure*. Retrieved from http://www.dot.state.mn.us/mnroad/New2011Brochure.pdf

Luna. (2012). *ODiSI B10* [data sheet]. Retrieved from http://www.alfaphotonics.com/dragon-media/oPTO/Instrumentation/ODiSI_B_data_sheet.pdf

Luna. (2013). *Luna sensing* brochure. Retrieved from http://lunainc.com/wp-content/uploads/2012/08/3567_Luna_Sensing_Brochure_FINAL_041713.pdf

Macro Sensors. (2010). *GHSD 750 series: spring-loaded DC-LVDT position sensors* [data sheet]. Retrieved from http://thesensorconnection.com/sites/default/files/product_files/datasheets/ghsd_750_datasheet.pdf

McMaster-Carr. (2013a). *Low-carbon steel tight-tolerance rectangle bar*. Retrieved from http://www.mcmaster.com/#9517k451/=plikva

McMaster-Carr. (2013b). *More about steel, iron, and tungsten* (document 88645KAC). Retrieved from http://www.mcmaster.com/#88645kac/=pivmwk

Micron Optics. (2009a). *Non-metallic temperature sensor os4300* [data sheet]. Retrieved from http://www.micronoptics.com/uploads/library/documents/Datasheets/Micron%20Optics%20-%20os4300.pdf

Micron Optics. (2009b). *Temperature compensation sensor os4100* [data sheet]. Retrieved from http://www.micronoptics.com/uploads/library/documents/datasheets/sensors/Micron_Optics_os4100.pdf

Micron Optics. (2010a). *Optical sensing interrogator sm130* [data sheet]. Retrieved from http://www.micronoptics.com/uploads/library/documents/Datasheets/Micron%20Optics%20sm130.pdf

Micron Optics. (2010b) *Optical sensing interrogator sm230* [data sheet]. Retrieved from http://www.micronoptics.com/uploads/library/documents/Datasheets/Micron%20Optics%20sm230.pdf

Micron Optics. (2010c). *Optical strain gauge os3110* [data sheet]. Retrieved from http://www.micronoptics.com/uploads/library/documents/datasheets/sensors/Micron_Optics_os3100.pdf

Micron Optics. (2011). *Displacement gauge os5100* [data sheet]. Retrieved from http://www.micronoptics.com/uploads/library/documents/Datasheets/Micron%20Optics%20-%20os5100.pdf

Micron Optics. (2012a). *Surface mount strain sensor os3610* [data sheet]. Retrieved from http://www.micronoptics.com/uploads/library/documents/Datasheets/Micron%20Optics%20-%20os3610.pdf

Micron Optics. (2012b). *Embeddable strain sensor os3600* [data sheet]. Retrieved from http://www.micronoptics.com/uploads/library/documents/datasheets/sensors/Micron_Optics_os3600.pdf

Micron Optics. (2012c). *Optical sensing instrumentation & software ENLIGHT* [manual]. Retrieved from http://www.micronoptics.com/support_downloads/Manual.pdf#page=161

Micron Optics. (2013). *Applications: Civil structures*. Retrieved from www.micronoptics.com/civil_structures.php

Moore, E. D. (2011). *Advances in swept-wavelength interferometry for precision measurements*. (Doctoral dissertation), Available from ProQuest LLC. (3453762).

Moyo, P., Brownjohn, J. M. W., Suresh, R., & Tjin, S. C. (2005). Development of fiber Bragg grating sensors for monitoring civil infrastructure. *Engineering Structures*, *27*(12), 1828-1834. doi: 10.1016/j.engstruct.2005.04.023

National Instruments. (2012). *NI PXIe-4844: Optical sensor interrogator for fiber bragg gratings* [data sheet]. Retrieved from http://sine.ni.com/nips/cds/print/p/lang/en/nid/209012

National Instruments. (2013a). *What is data acquisition*. Retrieved from http://www.ni.com/data-acquisition/what-is/

National Instruments. (2013b). *All products and services: DAQ modules*. Retrieved from http://sine.ni.com/np/app/main/p/ap/daq/lang/en/pg/1/sn/n17:daq,n21:35/

National Instruments. (2013c). *NI compactDAQ USB chassis*. Retrieved from http://sine.ni.com/nips/cds/view/p/lang/en/nid/208988

NCAT. (2010). *NCAT pavement test track research findings 2000-2010*. Retrieved from http://www.eng.auburn.edu/files/centers/ncat/test-track-findings-2-14.pdf

NCAT. (2013). *GAVLAB resources*. Retrieved from http://www.eng.auburn.edu/~dmbevly/gavlab/resources-03.htm

Noise. (2013). In *Merriam-Webster online*. Retrieved from http://www.merriam-webster.com/dictionary /noise

Omega. (2013). *Thermocouple wire: Duplex insulated* [data sheet]. Retrieved from http://www.omega.com/Temperature/pdf/XC_K_TC_WIRE.pdf

Rice, J. A. (2009). *Flexible smart sensor framework for autonomous full-scale structural health monitoring*. (Doctoral dissertation), Available from Newmark Structural Engineering Laboratory Report Series. (ISSN: 1940-9826) Retrieved from https://www.ideals.illinois.edu/bitstream/handle/2142/13635/NSEL.Report.018.pdf?sequence=4

Tokyo Sokki. (2013a). *KM strain transducer* [data sheet]. Retrieved from https://www.tml.jp/e/product/transducers/catalog_pdf/KM.pdf

Tokyo Sokki. (2013b). *PM mold strain gauge* [data sheet]. Retrieved from http://www.tml.jp/e/product/strain_gauge/catalog_pdf/PM_PMF_PMFLSseries.pdf

Tokyo Sokki. (2013c). *PF series polyester foil strain gauge* [data sheet]. Retrieved from http://www.tml.jp/e/product/strain_gauge/catalog_pdf/PFseries.pdf

Udd, E. (1995). *Fiber optic smart structures*. (1st ed., p. 203). Hoboken, NJ: John Wiley & Sons, Inc.

Udd, E., & Spillman Jr., W. B. (2011). *Fiber optic sensors: An introduction for engineers and scientists*. (2nd ed., p. 9). Hoboken, NJ: John Wiley & Sons, Inc.

Crisp, Betsy. (2013). When Lightning Strikes. Dade City, FL: Pasco County Cooperative Extension Service. Retrieved from http://pasco.ifas.ufl.edu/fcs/Lightning.shtml, accessed August 1, 2013.

Vishay. (2011). *Special use sensors: Concrete embedment strain gauge* [data sheet]. Retrieved from http://www.vishaypg.com/docs/11526/emgauges.pdf

Worel, B. Minnesota Department of Transportation, (2006). *MnROAD lessons learned - December 2006: Overview of MnROAD reports*. Retrieved from http://www.dot.state.mn.us/mnroad/reports/PDF's/overview.pdf

Yu, F. T. S., & Yin, S. (2002). *Fiber optic sensors*. (1st ed., pp. 124-125). New York, NY: Marcel Dekker, Inc.

Appendix A: Out of Pavement Raw Data

Cylinder Compression Data

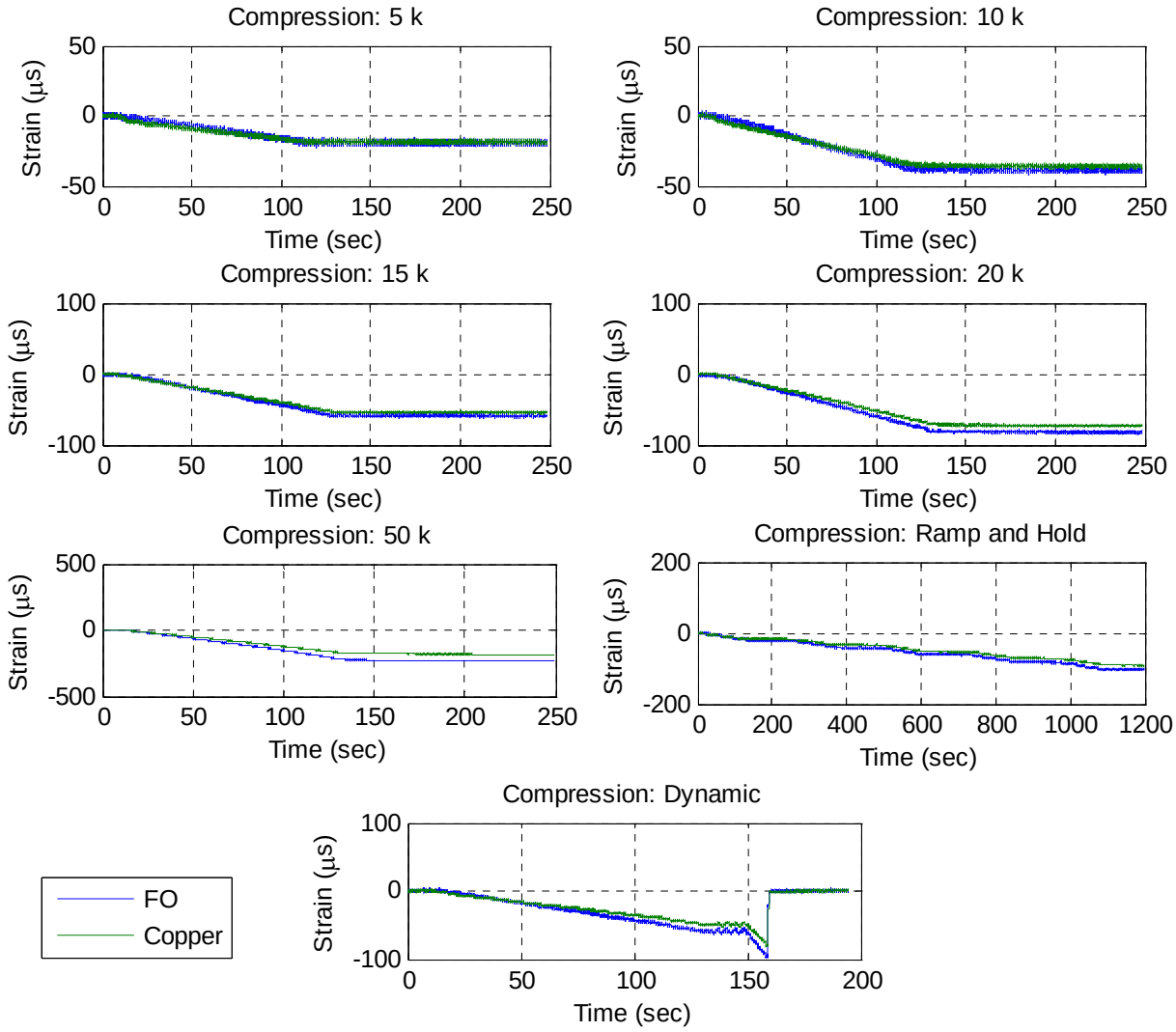

Figure A-1. Compression strain results.

Tension Data

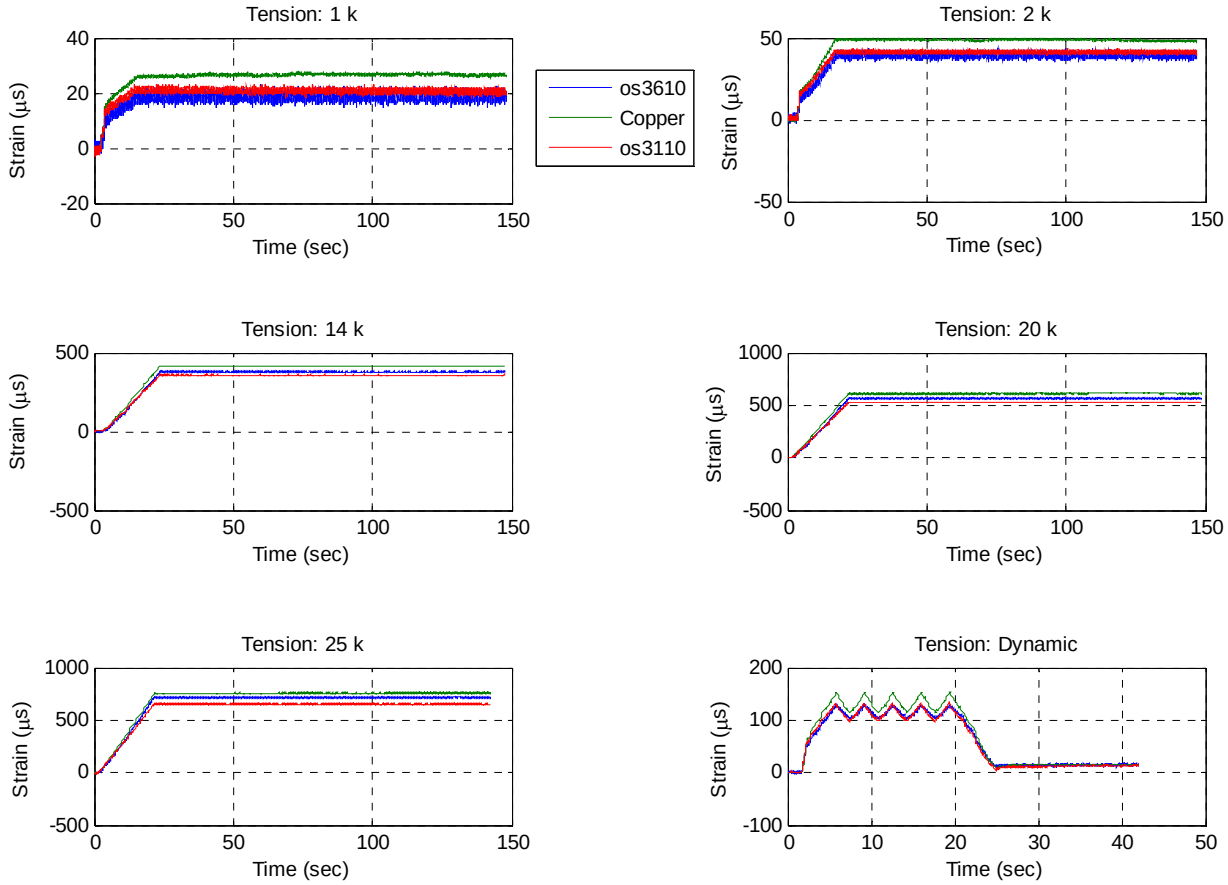

Figure A-2. Tension strain results.

Temperature Data

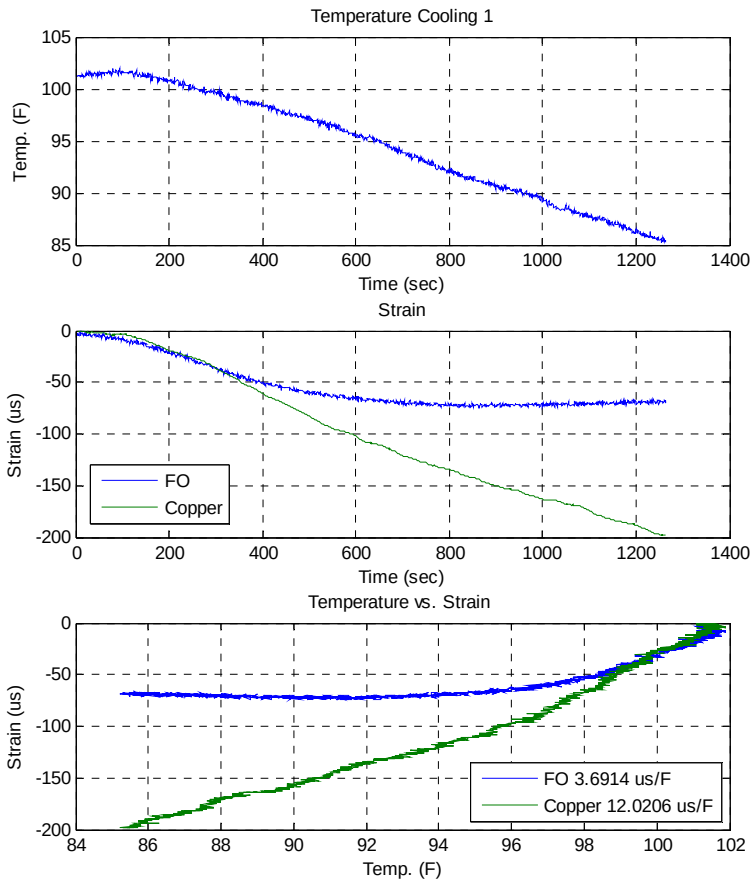

Figure A-3. Cooling strain readings

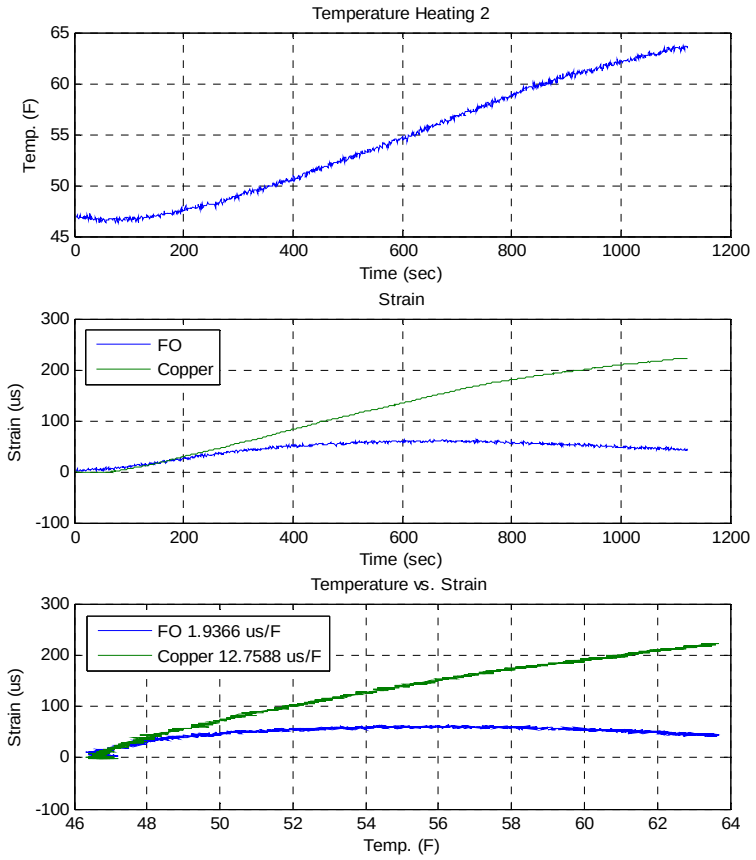

Figure A-4. Heating strain readings

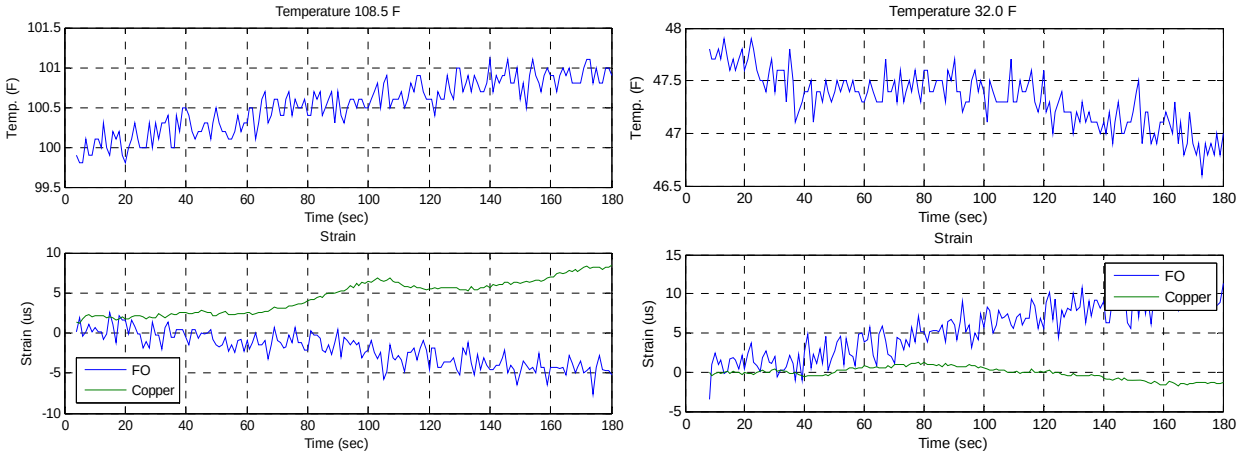

Figure A-5. Hot (left) and cold (right) strain readings.

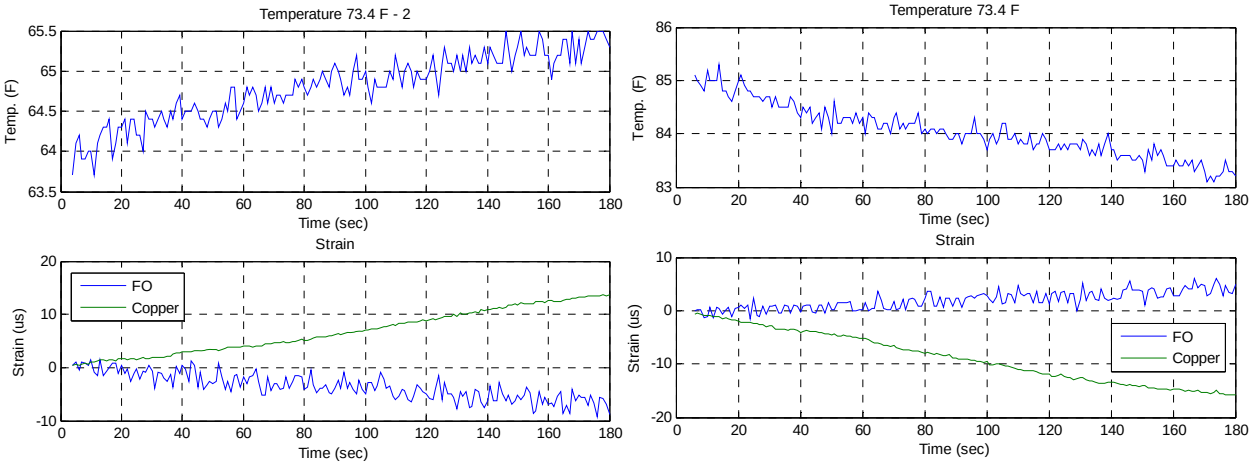

Figure A-6. Room temperature strain readings.

Appendix B: Additional Embedded Dynamic Analysis

Raw Data

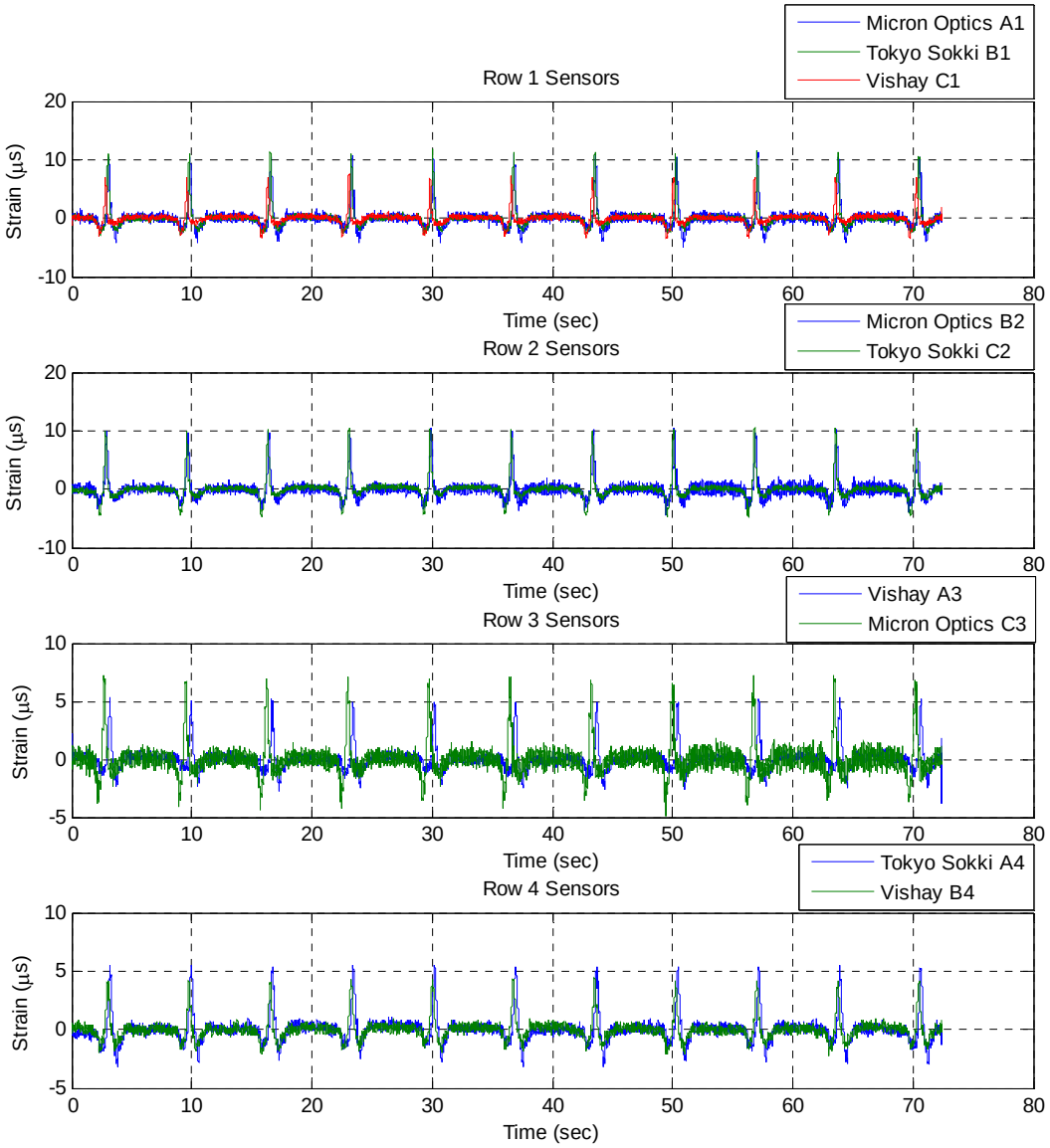

Figure B-1. November 4th 3:00 PM 9-kip dynamic test along row 1, separate plot for each row of sensors.

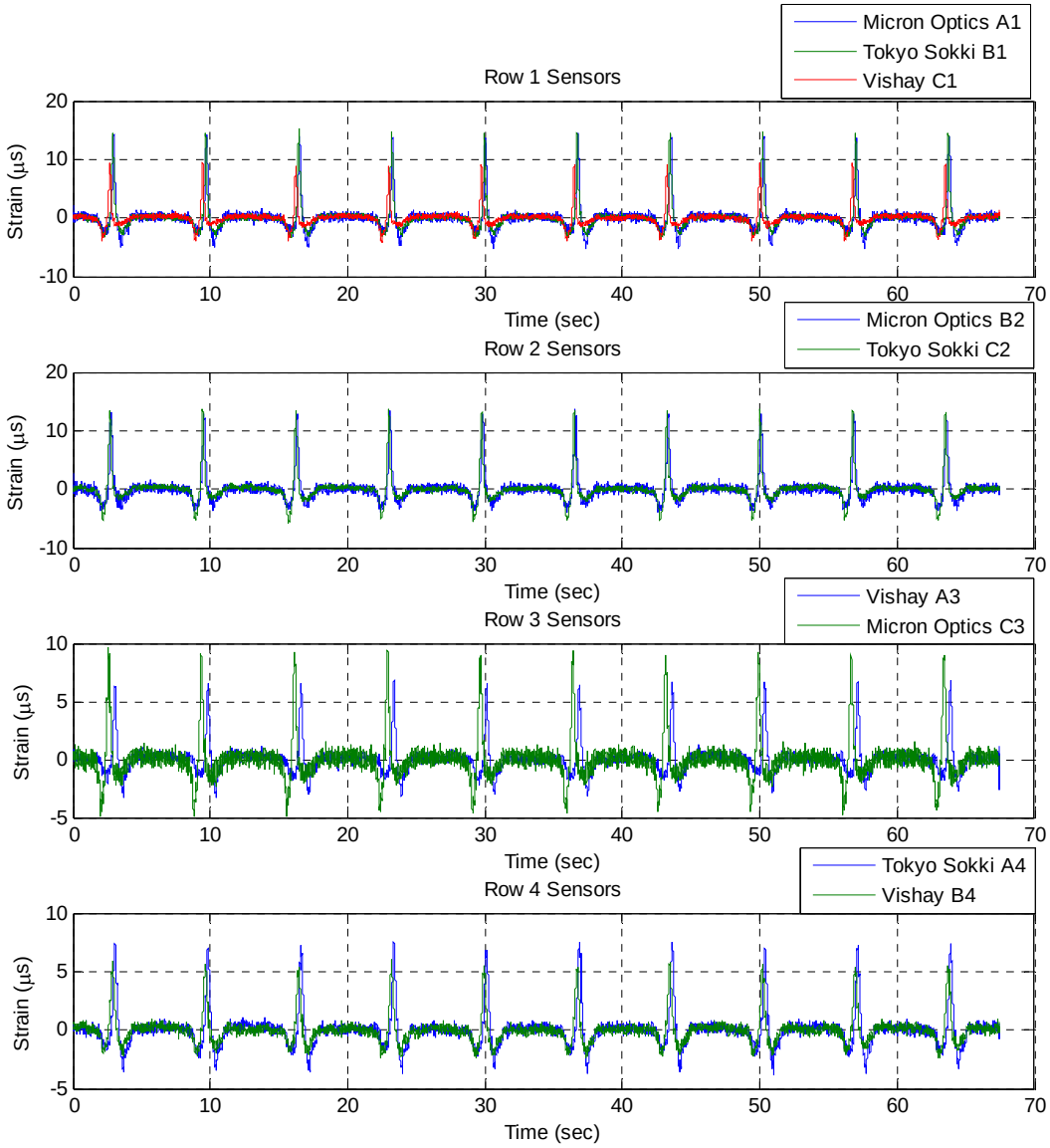

Figure B-2. November 4th 3:00 PM 12-kip dynamic test along row 1, separate plot for each row of sensors.

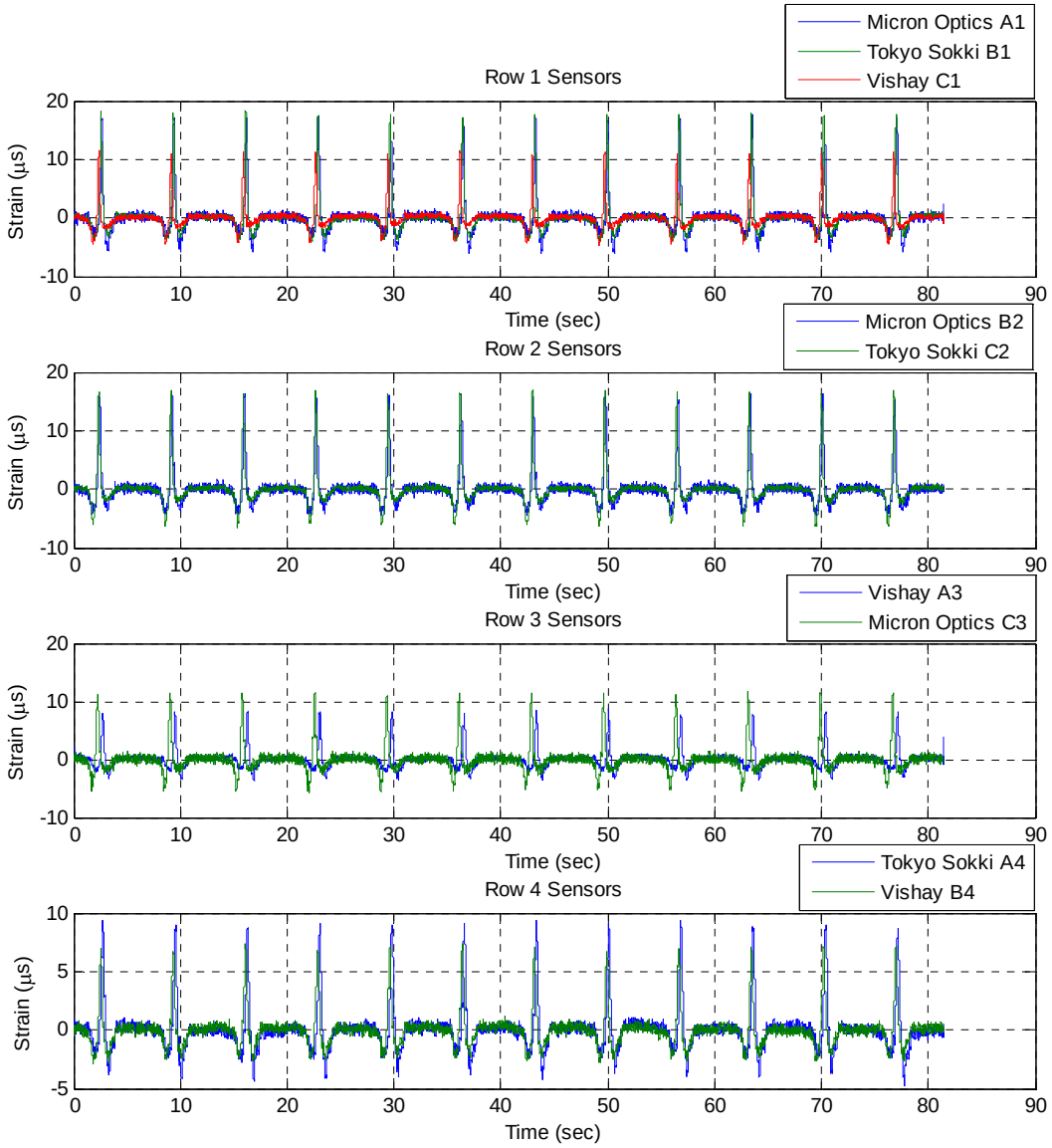

Figure B-3. November 4th 3:00 PM 15-kip dynamic test along row 1, separate plot for each row of sensors.

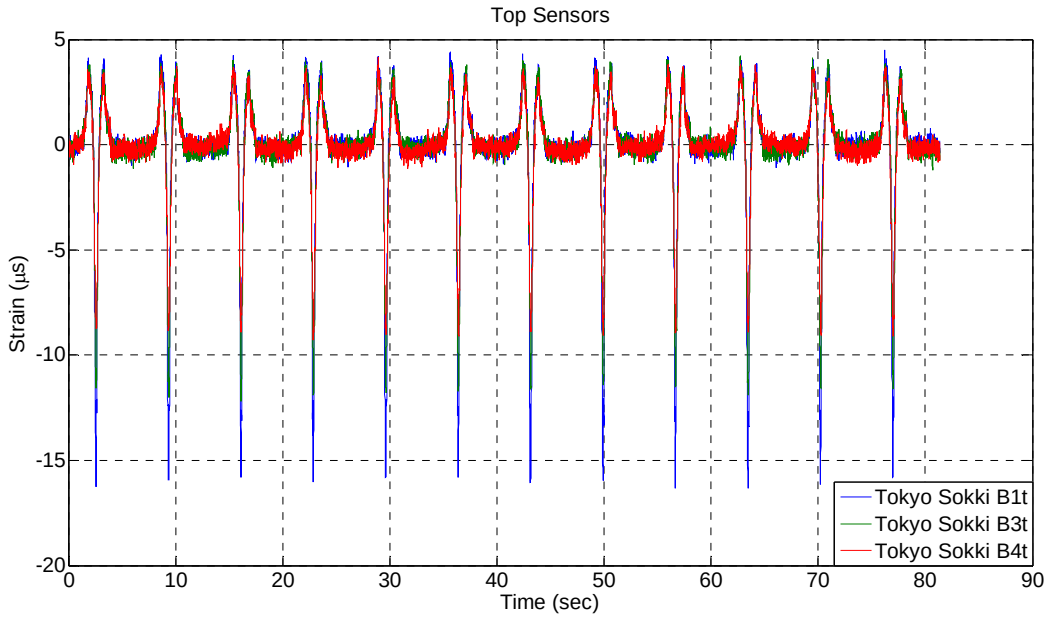

Figure B-4. November 4th 3:00 PM 15-kip dynamic test along row 1, top sensors.

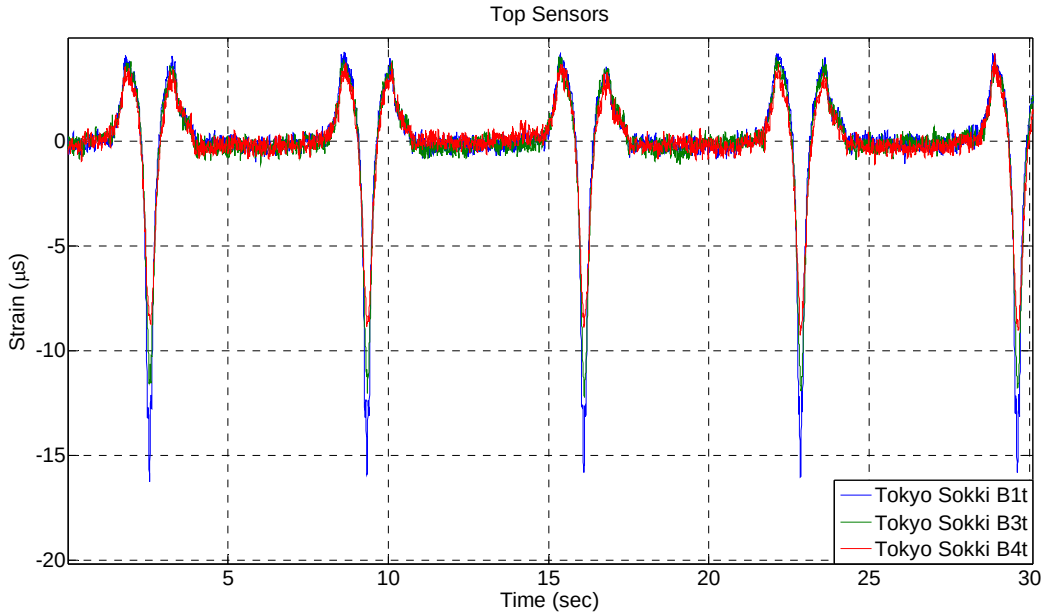

Figure B-5. November 4th 3:00 PM 15-kip dynamic test along row 1, top sensors – zoomed view.

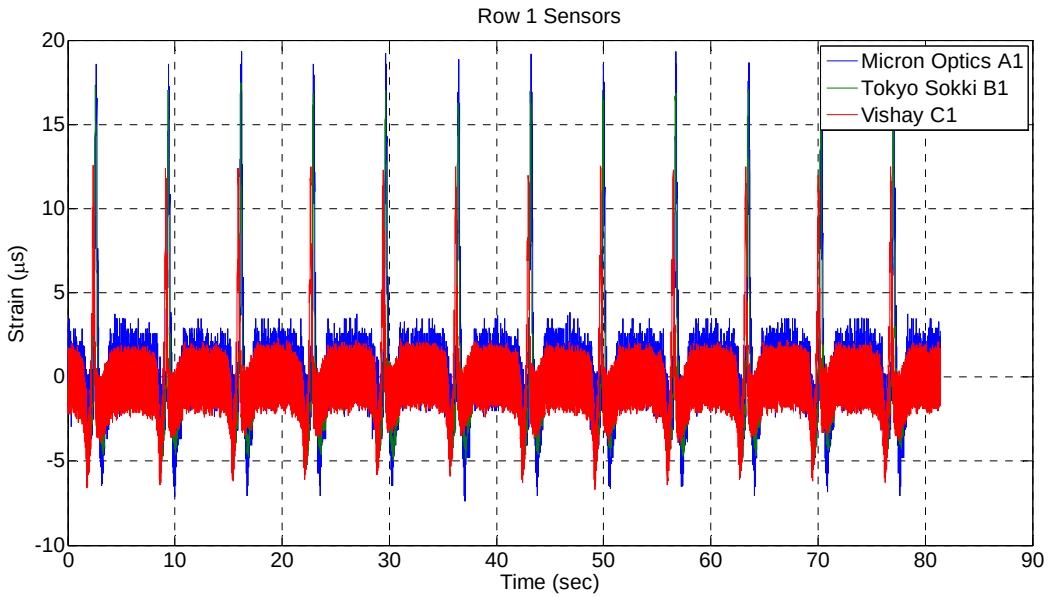

Figure B-6. November 4th 3:00 PM 15-kip dynamic test along row 1, unfiltered data without detrending.

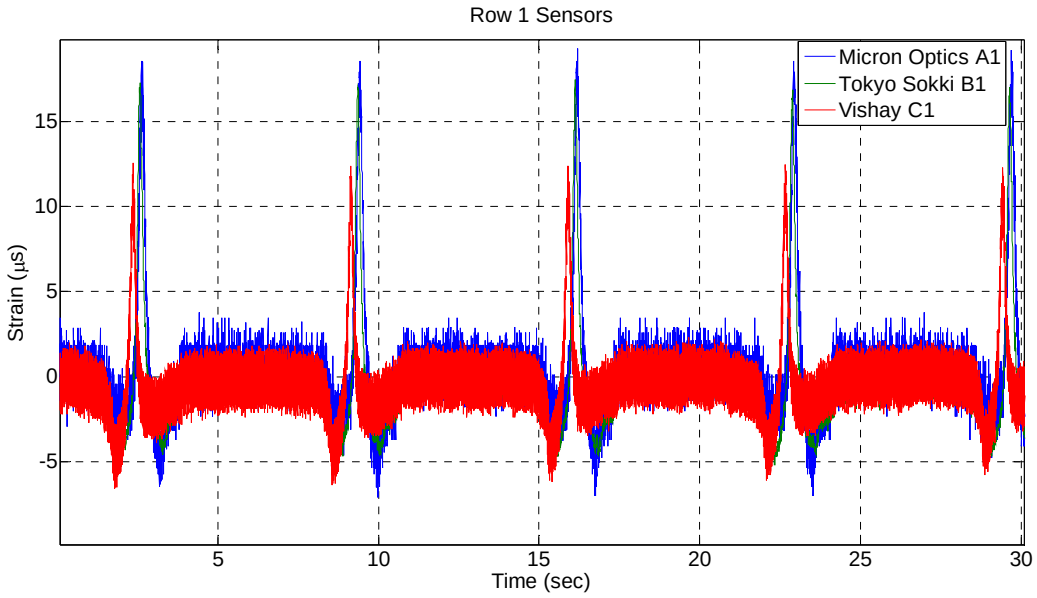

Figure B-7. November 4th 3:00 PM 15-kip dynamic test along row 1, unfiltered data without detrending – zoomed view.

Peak Analysis

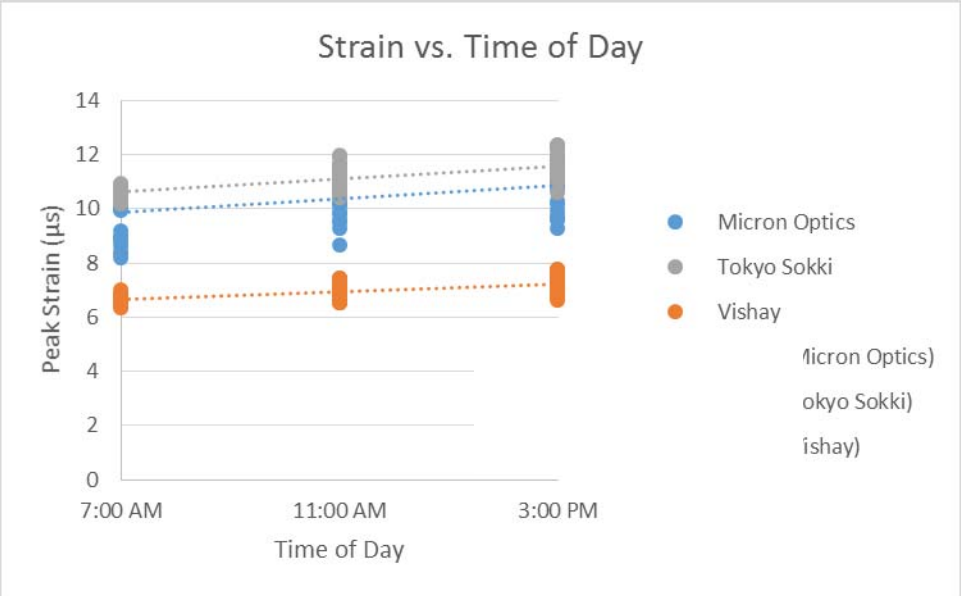

Figure B-8. Strain vs. time of day – 9 kip.

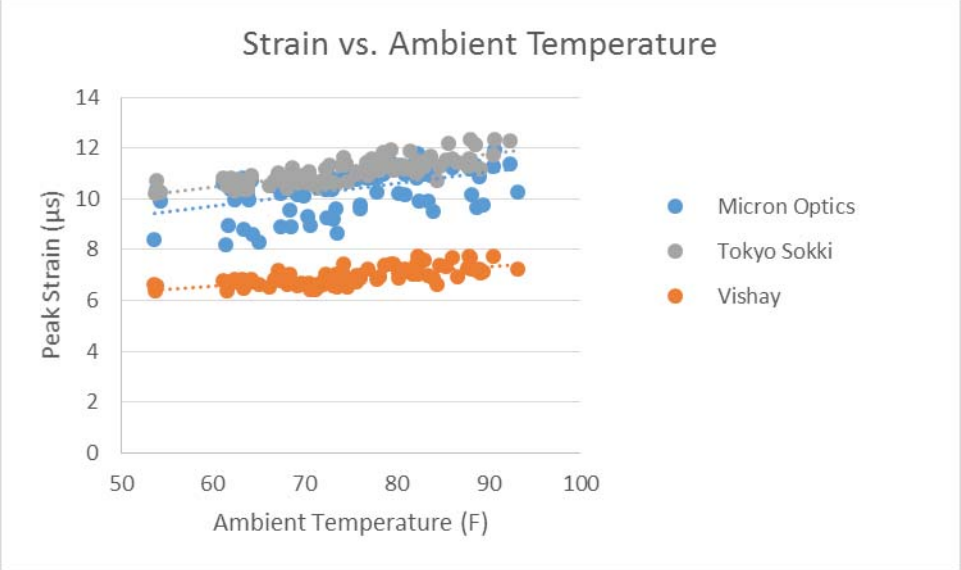

Figure B-9. Strain vs. ambient temperature – 9 kip.

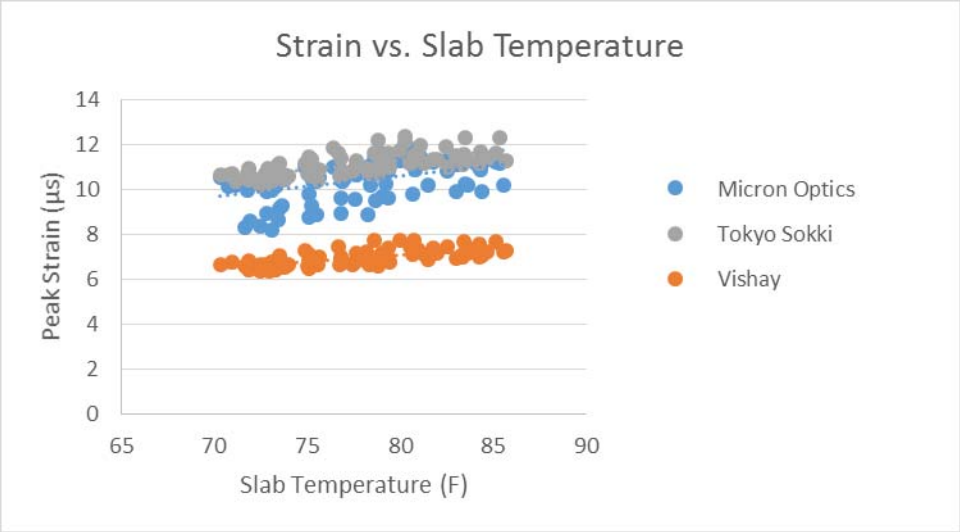

Figure B-10. Strain vs. slab temperature – 9 kip.

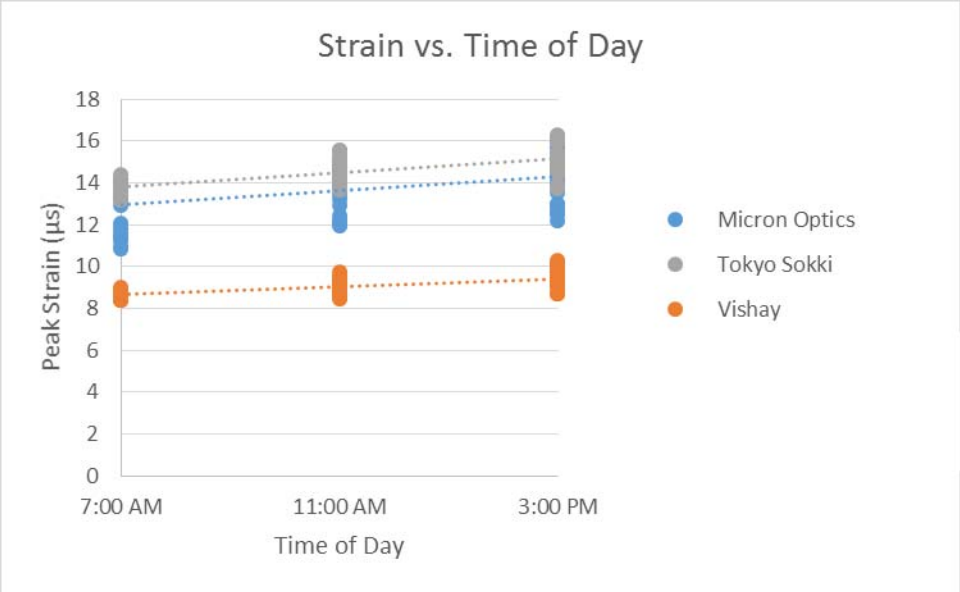

Figure B-11. Strain vs. time of day – 12 kip.

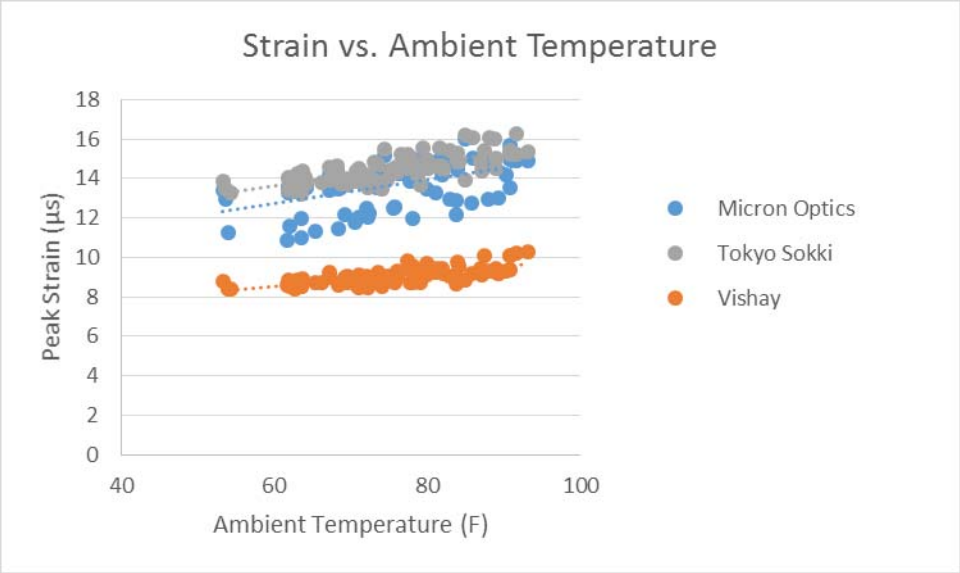

Figure B-12. Strain vs. ambient temperature – 12 kip.

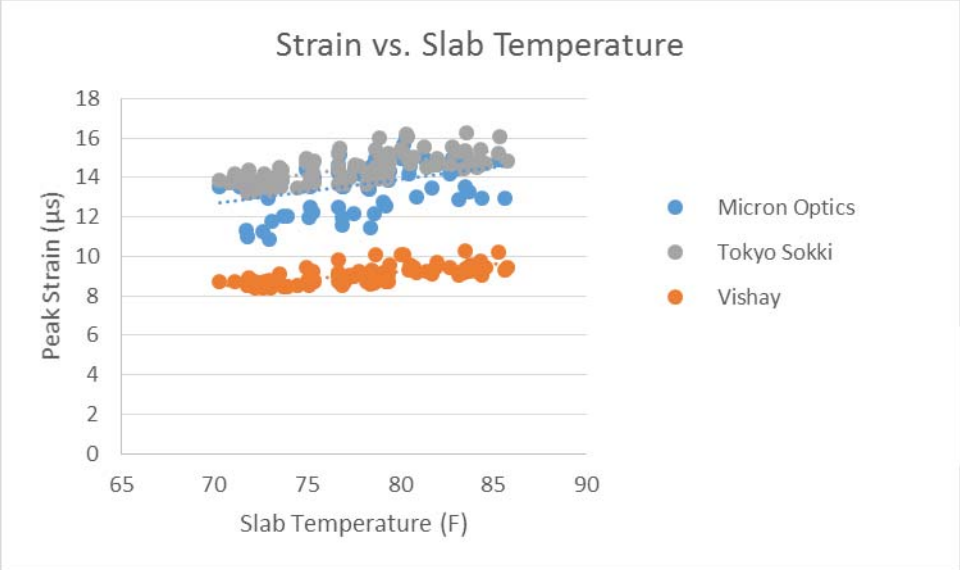

Figure B-13. Strain vs. slab temperature – 12 kip.

Data Repeatability Analysis – Peaks

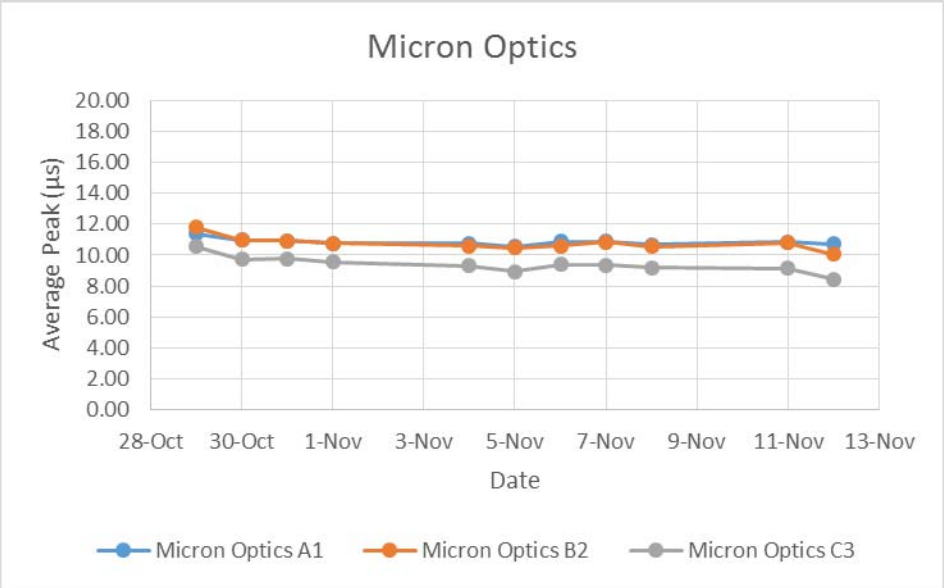

Figure B-14. Micron Optics repeatability plot – 9 kip.

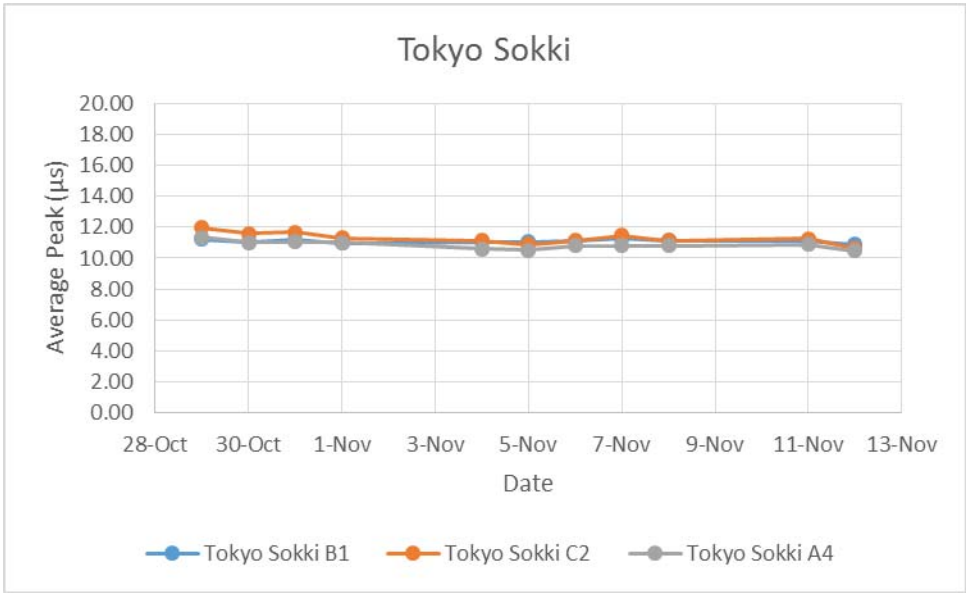

Figure B-15. Tokyo Sokki repeatability plot – 9 kip.

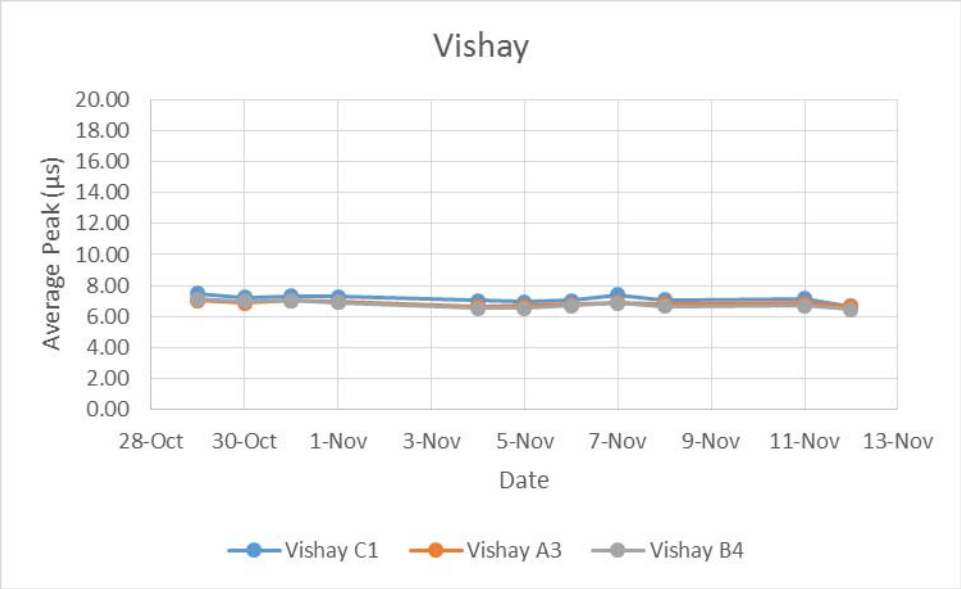

Figure B-16. Vishay repeatability plot – 9 kip.

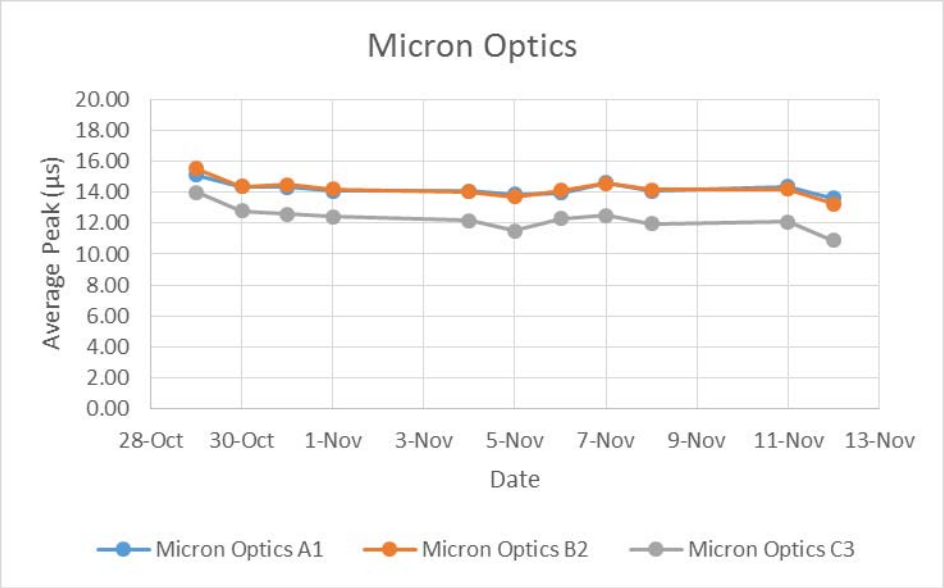

Figure B-17. Micron Optics repeatability plot – 12 kip.

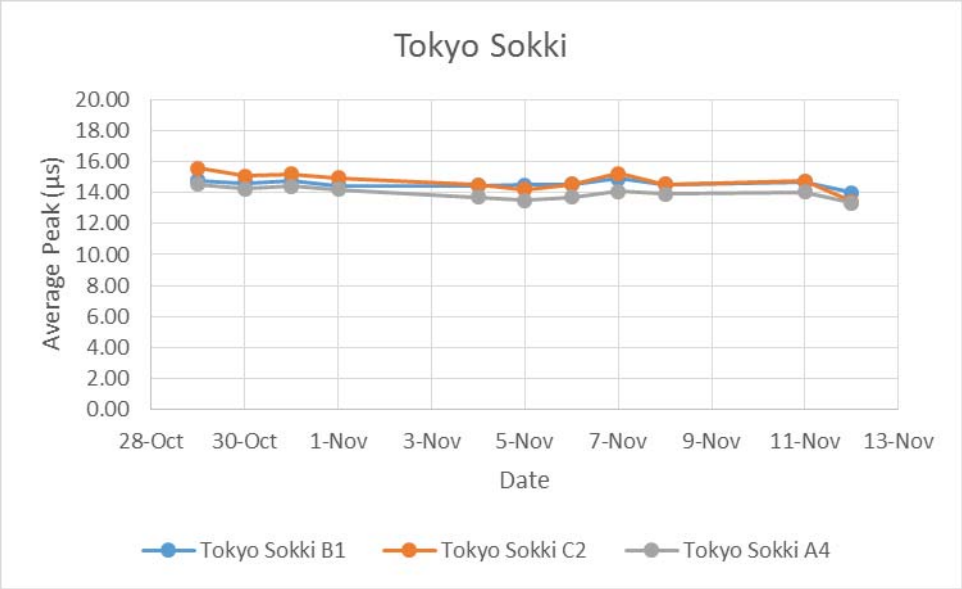

Figure B-18. Tokyo Sokki repeatability plot – 12 kip.

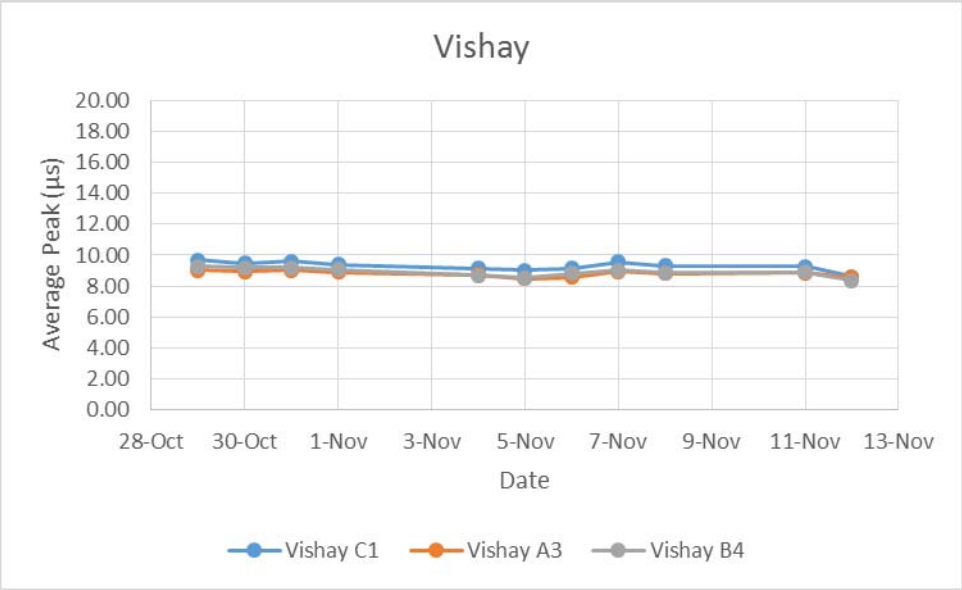

Figure B-19. Vishay repeatability plot – 12 kip.

Strain Distribution

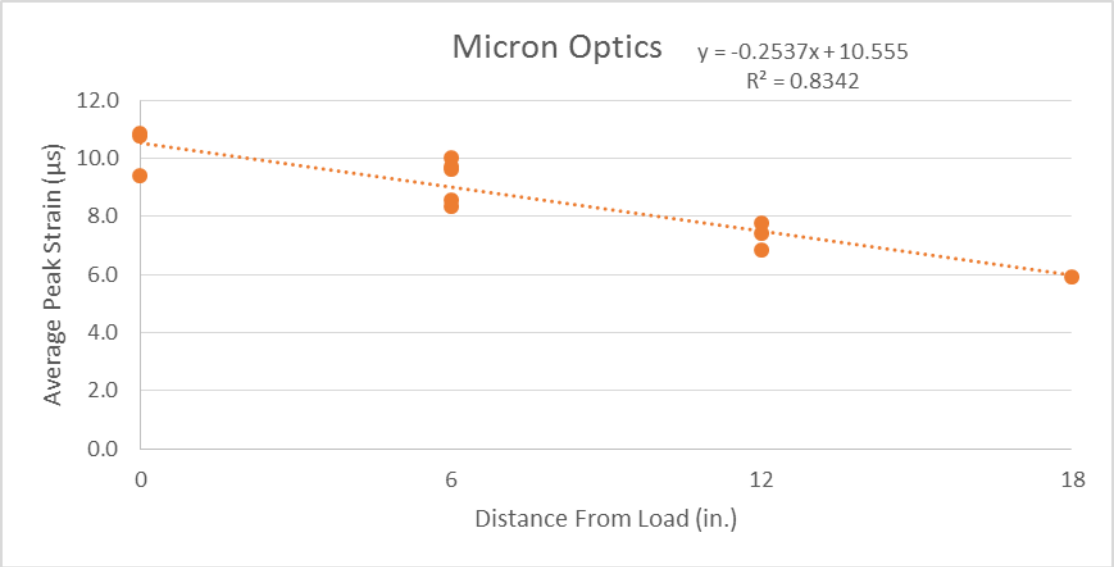

Figure B-20. Micron Optics strain distribution – 9 kip.

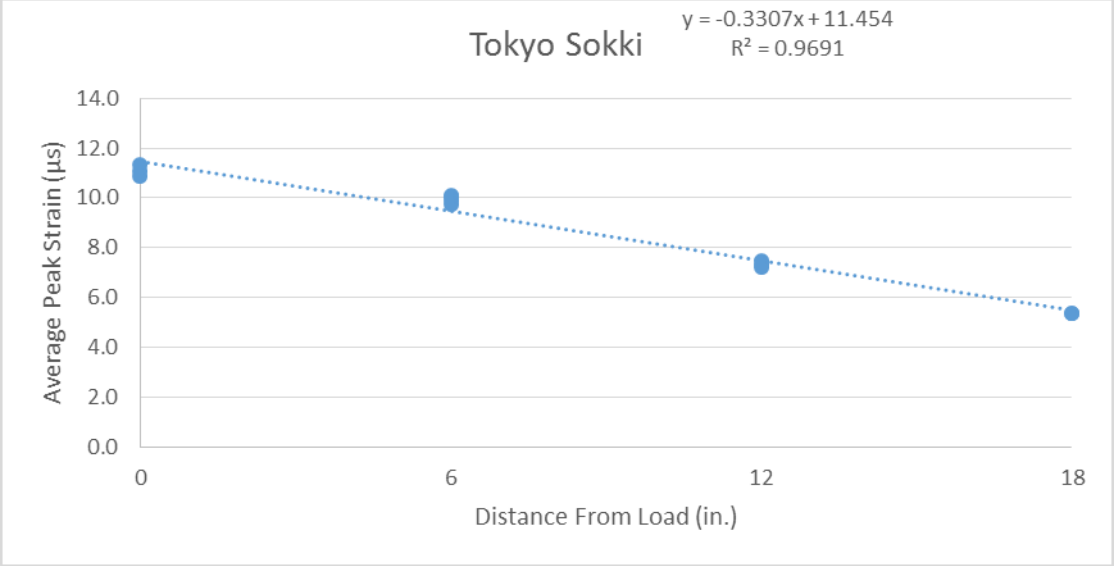

Figure B-21. Tokyo Sokki strain distribution – 9 kip.

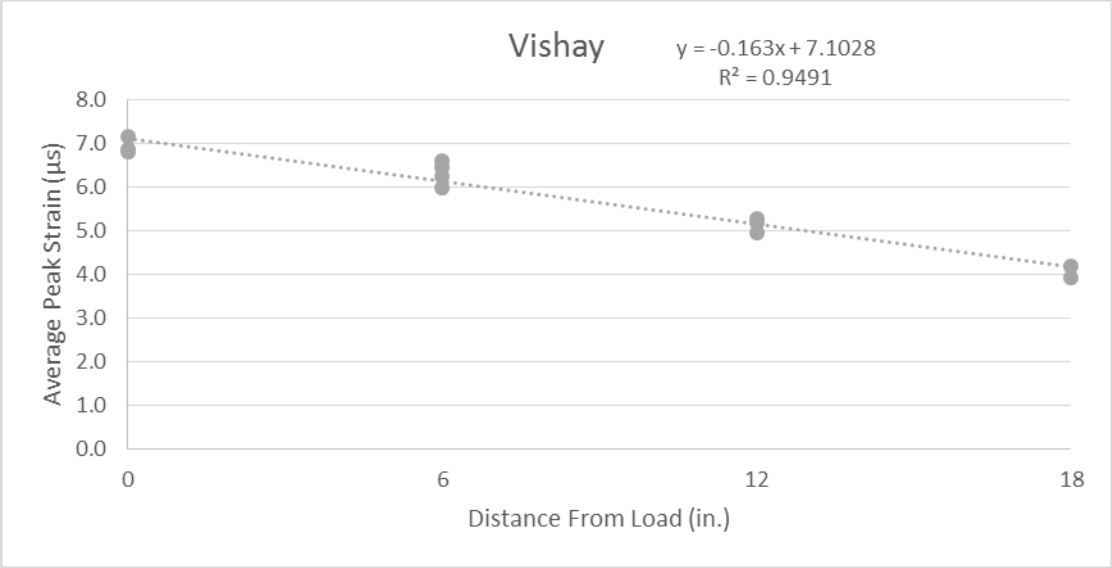

Figure B-22. Vishay strain distribution – 9 kip.

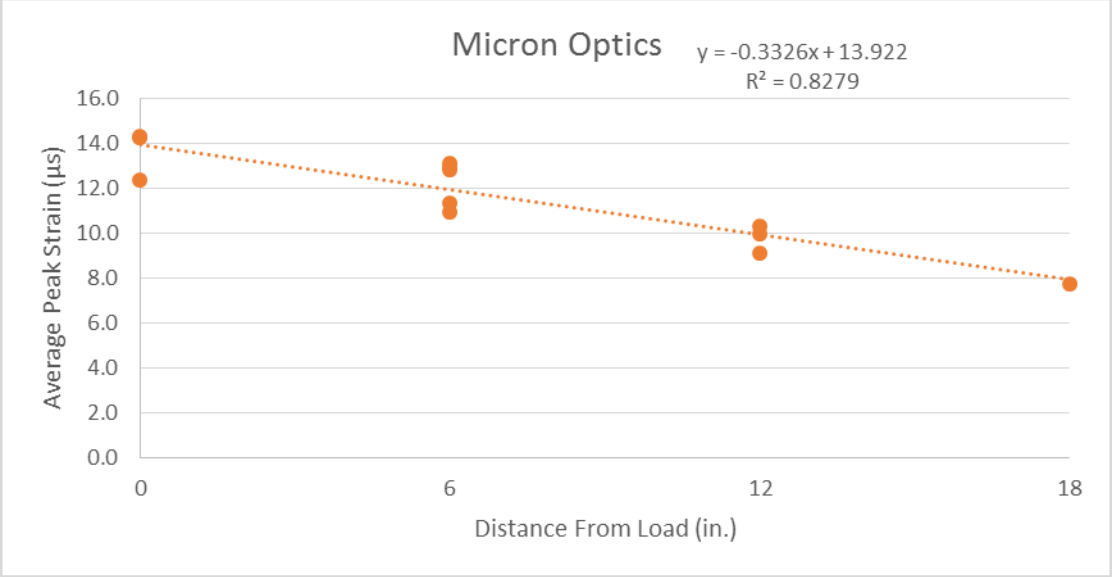

Figure B-23. Micron Optics strain distribution – 12 kip.

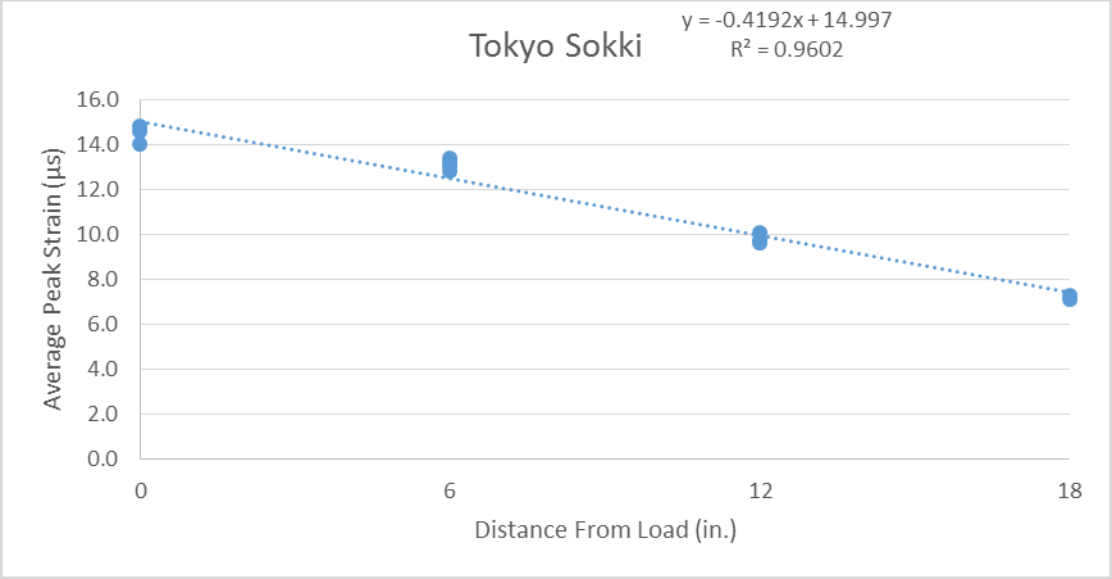

Figure B-24. Tokyo Sokki strain distribution – 12 kip.

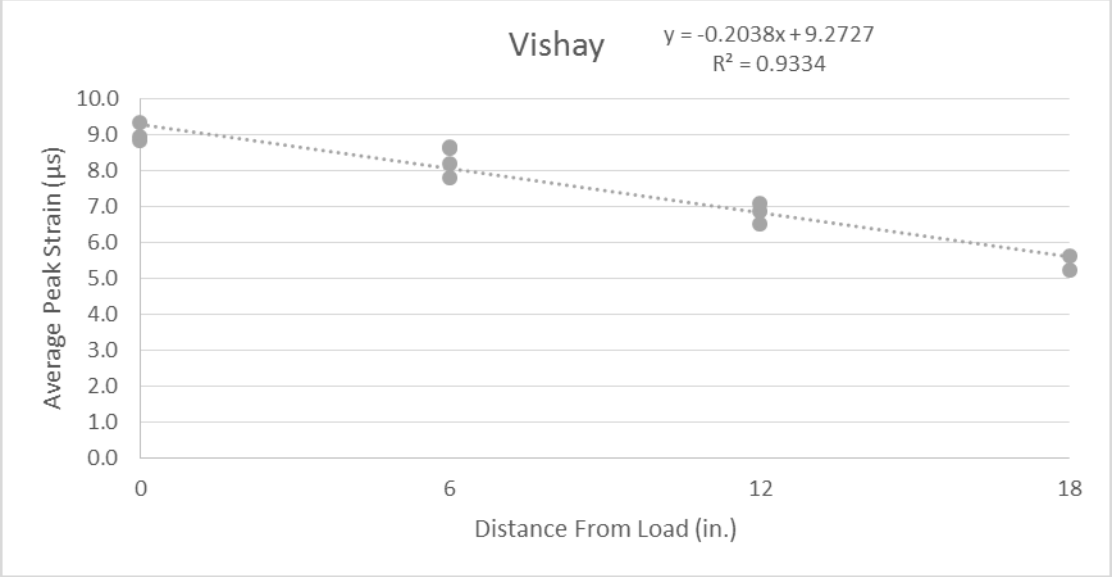

Figure B-25. Vishay strain distribution – 12 kip.